NASA CR 73,231

AVAILABLE TO THE PUBLIC

NEW FUNCTIONAL REDUNDANCY APPROACHES FOR ATTITUDE CONTROL THRUSTER SYSTEMS

By C. E. Hallum and P. W. Webster

July 1968

Prepared Under Contract No. NAS2-3664 by
Aeronutronic Division, Philco-Ford Corporation,
Newport Beach, California

for

AMES RESEARCH CENTER
NATIONAL AERONAUTICS AND SPACE ADMINISTRATION

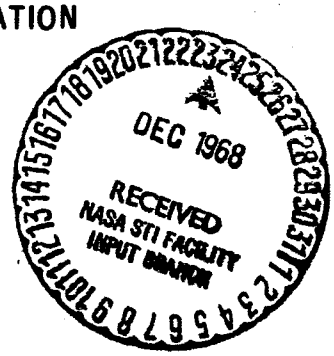

PHILCO
PHILCO-FORD CORPORATION
Aeronutronic Division
Newport Beach, Calif. • 92663

NASA CR 73,231

NEW FUNCTIONAL REDUNDANCY APPROACHES FOR ATTITUDE CONTROL THRUSTER SYSTEMS

By C. E. Hallum and P. W. Webster

July 1968

Prepared Under Contract No. NAS2-3664 by
Aeronutronic Division, Philco-Ford Corporation,
Newport Beach, California

for

AMES RESEARCH CENTER
NATIONAL AERONAUTICS AND SPACE ADMINISTRATION

PHILCO-FORD CORPORATION
Aeronutronic Division
Newport Beach, Calif. • 92663

ABSTRACT

The Inert Gas Thruster System Study Program reported here has been conducted by the Aeronutronic Division of the Philco-Ford Corporation for NASA Ames Research Center under Contract NAS 2-3664. The objective of the study program was to survey, study, conceive, investigate and demonstrate new components and systems which would provide improved system reliability and have potential performance improvements. The detail program requirements are contained in Statement of Work A-11070 dated 16 November 1965 as modified by Supplemental Agreement dated 8 May 1967.

The program was initially directed to study improved thruster valve concepts. Task I of the study program entailed a survey of existing thruster valves to establish the most likely failure modes and associated design features and shortcomings. During Task II new thruster valve concepts were proposed and evaluated. Some of these concepts could offer improved reliability if other system components were also included. It was also considered desirable for the proposed improvements to be applicable to either of two specific spacecraft (Bios and Pioneer). Subsequently the program was redirected to study new approaches to inert gas thruster systems (reflected in Statement of Work dated 8 May 1967). Task III, Improved Thruster Valve Fabrication and Test, of the initial program was eliminated. New component and thruster system functional approaches were studied in Task IV. Preliminary designs of two systems for both the Biosatellite and Pioneer were prepared and presented to NASA ARC. The Pioneer multi-tank thruster system was selected for further evaluation in Task V. Critical elements of the selected system were designed, fabricated and tested in Task V.

CONTENTS

FIGURES

FIGURE PAGE

TABLES

SECTION 1

INTRODUCTION

In the majority of inert gas attitude control systems the pneumatic portion of the system (as distinguished from the electrical) is the only portion of the system which is not redundant. Even with the long development time which has been put into the active pneumatic components they are usually the least reliable of the complete attitude control system. Since redundancy is not provided, a single pneumatic component malfunction can cause a mission failure.

The object of this program was the investigation of design methods and concepts to provide redundancy safeguards at a minimum cost of weight, volume and power. The program encompassed both component and system considerations. Only inert gas was considered for the working fluid. The items of primary concern were those with the lowest reliability. In the typical system the functioning elements, regulator, relief valves and shutoff valves, are the lowest reliability components. However, the study program was not limited to these items. Any component, or combination, or system variation that would improve reliability could be considered. As the study developed, two primary areas of improvement were concentrated on: 1) shutoff or valving devices, and 2) system approaches, including combining functions and storage methods which would eliminate the need for a regulator or relief valve.

Contractually the work was performed under five task assignments which were varied or adjusted from time to time as the study progressed. Section 2 of the report summarizes component considerations covered in Tasks I and II and a portion of Task IV. The valve concepts studied are applicable to current thruster systems. Some new types of shutoff devices are presented. Efficient methods of providing component function redundancy was also studied. Section 3 presents integrated system approaches including new functional concepts and a new component (for

a specific application) which were developed under Task IV. The system designs proposed were tailored around the possible application for the Pioneer and Biosatellite programs. Section 4 discusses the fabrication and test demonstration of new components proposed for a multitank Pioneer system. Overall program conclusions and discussion are contained in Section 5. The Appendix presents technical support data for the system selected at the Task IV design review meeting and subsequently simulated and tested in Task V.

SECTION 2

COMPONENT CONSIDERATIONS

Components which can be used on existing type thruster systems are covered in this section. Thruster valve concepts were studied and investigated in Task I and Task II of the program. Thruster valve concepts, methods of obtaining redundancy and a comparative evaluation are presented. A diversion valve, studied during Task IV, can improve system performance and specific weight and volume for applications where redundant shut-off valves are required.

A limited survey of performance and reliability of existing thruster valve designs was conducted in Task I. Probable failure modes and causes were tentatively established. The valve concepts considered in Task II were based on the preliminary survey as well as data contained in References* 1-4 containing pertinent design information on valves. Results of the studies on valve components are presented in the following paragraphs. Only components for thruster systems in the range of 0.02 to 0.5 pounds force were considered during this program.

2.1 THRUSTER VALVES

Thruster valve redundancy is continually mentioned as a method of improving inert gas attitude control system reliability. In inert gas systems the thruster valve (solenoid actuated shut-off valve) is one of the lowest reliability elements. Typical methods of providing valve redundancy are to use a "quad" valve arrangement or provide a duplicate system capable of fulfilling the mission. Both the "quad" valve and duplicate system solution to the problem are rather prohibitive when weight, power and volume are considered.

---

*Numbers in superscript denote references listed in a separate section.

A portion of the study covered characterization of normal valve failure modes and new, or improved, concepts which could protect against the normal, or predominant, failure modes. (The actual study was directed only for mission durations of over a year.) However because of recent experience, (valve failed to close and leaking regulator) protection against any single valve failure is considered to be necessary.

2.1.1 FAILURE MODES

The solution of the problem depends upon the failure modes of the valve and the probability of their occurrence. During the initial portion of the program four spacecraft manufacturers were contact; Jet Propulsion Laboratory, TRW Inc., Hughes and Lockheed Missiles and Space Company. The spacecraft fabricators usually do the testing of the subsystems and had considerably more information on valve reliability than did the valve manufacturers.

Each of the companies contacted expressed the opinion that on a long mission (1 year or more) leakage was critical and was the most likely factor to cause a mission failure. Data from Apollo Product Information Center (APIC) of NASA indicates that the order of functional failure for solenoid valves is leakage (most likely), then failure to open and finally failure to close. A report on Spacecraft Attitude Control Gas Systems Analysis[5] (for a 400-day mission) prepared for NASA Jet Propulsion Laboratory also indicates the same general trend of solenoid valve failures. The approximate failures distribution is summarized below

	APIC	Ref. 5
Leakage	50%	A
Fail to Open	30%	B
Fail to Close	20%	D

The letter connotation shows a considerable decrease in the probability of a valve failure to close.

Personnel contacted at three of the four spacecraft manufacturers stated that wear particles were probably the cause of many failures. The contaminants in the gas do not themselves cause the problems, but rather these contaminants get into close fitting areas or places were parts are sliding. Two such locations (the alignment bore and seat) are illustrated schematically in Figure 2-1. If particles are in these areas for a number of cycles, wear particles are generated and can cause galling, binding, sticking and damage the seat surfaces. No matter how perfectly the valve is built the shaft-armature-poppet will always be misaligned since some clearance must be provided and there will be some unsymmetrical forces acting. The shaft will slide against the sleeve and cause wear particles to be generated, particularly if any contaminant is introduced. The misaligned seat-poppet will cause the poppet to strike the seat off center and slide into place. Again wear will occur, particularly if any contaminants are present.

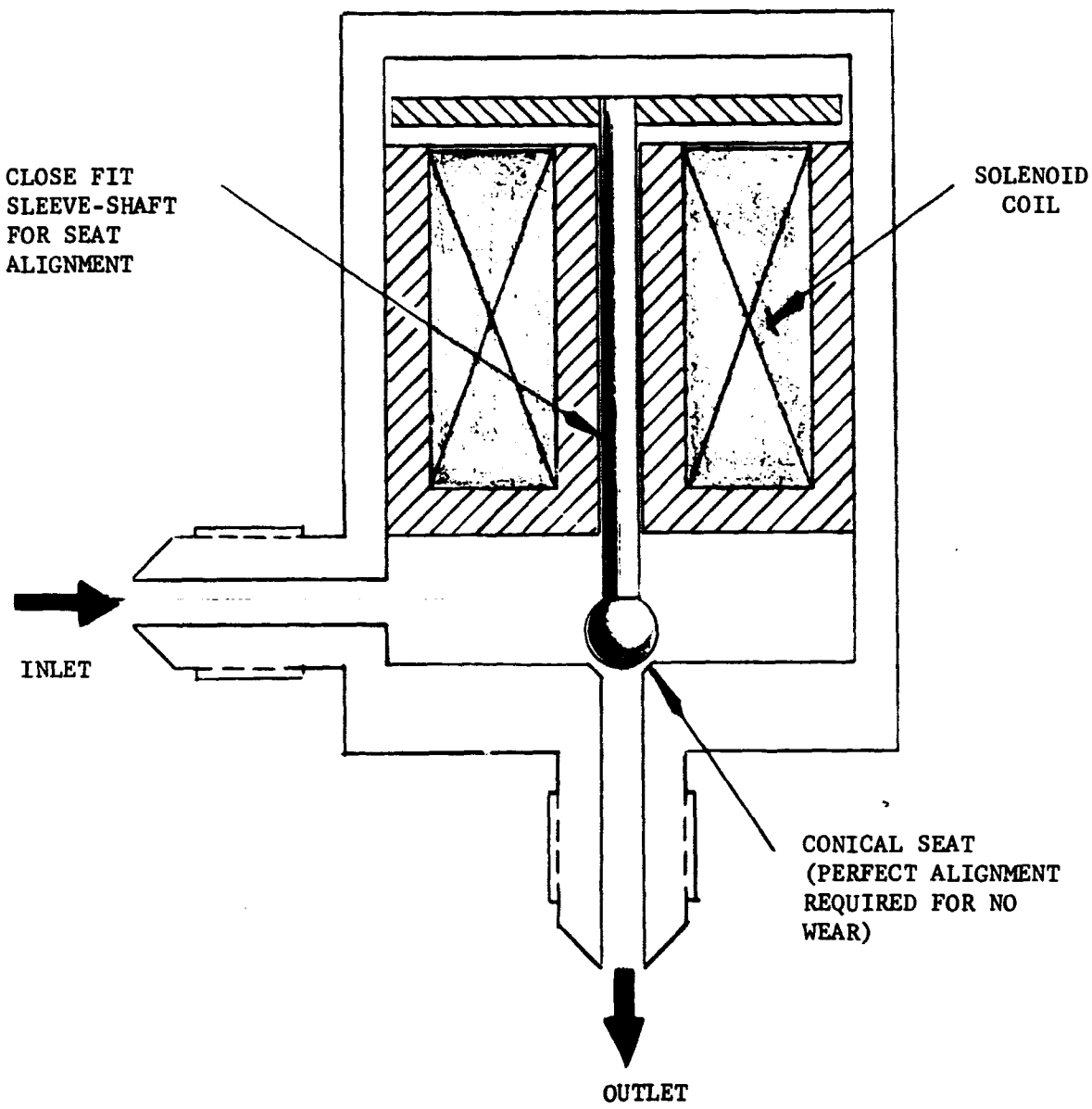

FIGURE 2-1. CONVENTIONAL SOLENOID VALVE SCHEMATIC

On short duration satellites the leakage failure mode is essentially eliminated, or at least unlikely to cause a mission failure. The typical leak rate on thruster valves is 1 scch. For a thirty day mission leakages over an order of magnitude greater can be tolerated with little system effect. Consequently on short duration missions only protection against failures to open and failures to close need to be provided. The table below summarizes the valve failure protection required for long missions such as for the Pioneer spacecraft and short missions such as the Biosatellite.

FAILURE PROTECTION REQUIREMENTS

MISSION DURATION	FAILURE PROTECTION FOR	
One Year	Leakage	(60)
	Fail to open	(30)
	Fail to close	(10)
Thirty Days	Fail to open	(75)
	Fail to close	(25)

2.1.2 METHODS OF PROTECTION

There are two general methods of providing control thruster redundancy: 1) provide valve element redundancy and 2) provide thruster reaction thrust control duplication.

a. Valve Element Redundancy. Included in this section are numerous methods of providing redundant valve action and statements as to what failure modes the arrangements protect against, or their proposed advantages.

(1) Quad Valve. A quad valve is normally two series valves in parallel as below:

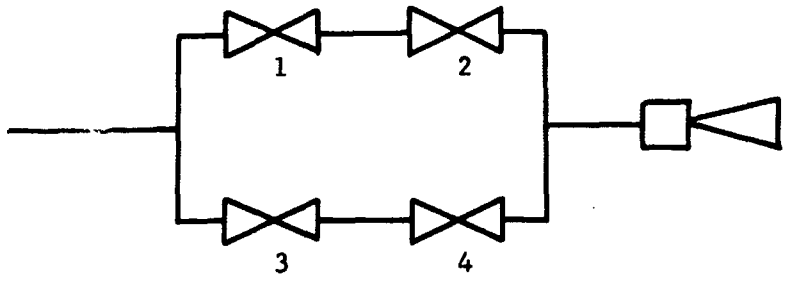

Without going into detail this arrangement protects against leakage, failure to open and failure to close. Protection against multiple failure occurrence (two of one type) would be in the order: failure to close (least probable failure), leakage and failure to open. What is meant here is that if valve 1 failed to open, failure of either valve 3 or valve 4 (two to one odds) to open would cause a quad failure. Whereas if valve 1 leaked or failed open the next failure must be in valve 2 (one to two odds) to cause quad failure, but either valve 3 or valve 4 can fail with no effect.

An alternate quad valve arrangement is parallel valves in series as below:

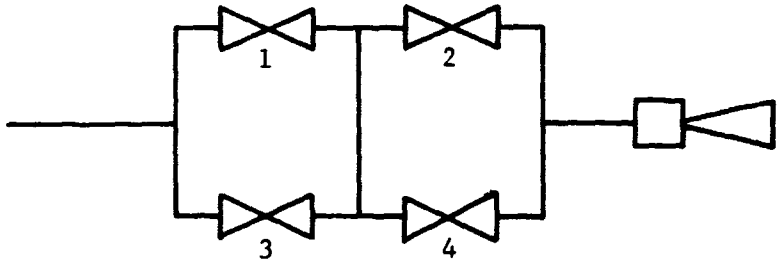

The only difference from the series valves in parallel configuration is the crossover leg. The alternate quad valve arrangement still protects against leakage failures, failure to open and failure to close. However, the multiple failure protection order (decreasing) changes to: failure to open, leakage and failure to close. If valve 1 fails to open, failure of valve 2 or valve 4 will not cause a quad valve failure (one failure to two successes odds). So we see all that happened is a shift in the order of multiple failure protection.

The alternate (parallel valves in series) quad arrangement is best for shorter duration missions since the more likely failure mode (fail to open) is best protected by this quad arrangement. Also on multi-control thruster systems deviations of this configuration can be used. For example one parallel valve can provide leakage and fail to close protection for (possibly) three to four other parallel thruster valves. The proposed improved systems for the Bios and Pioneer covered in the Task IV Design Report utilized this configuration.

(2) Series Valves. This arrangement is simply two valves in series as below.

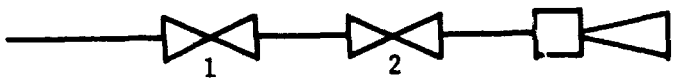

The series valves protects against single failures of leakage and failure to close. No redundancy is provided for failure to open (in fact failure to open is now twice as likely to occur).

(3) Parallel Valves. Schematically the valve arrangement is

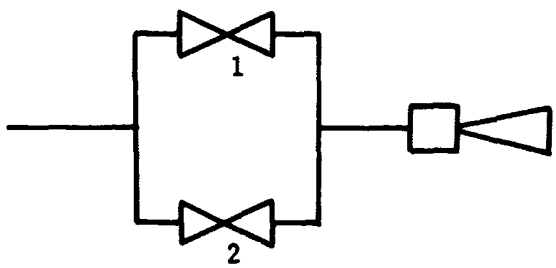

The parallel valve arrangement only protects against failure to open. Two leak paths are possible so both leakage and failure to close are more likely occur.

(4) Specialty Valves. Several valve configurations have been developed which offer protection against single failure modes. Some of the valve concepts, including some generated in the initial phases of this program, are covered below.

(a) Series Seat Valve. Series seat type valves are presently being produced by valve companies. Energizing a solenoid normally initiates motion of an armature which first opens one seat and then the other. The active element is common to both seats. Hence if armature motion is restricted, either in the closed or open position, the seats will not open or close.

The series seat valve only protects against leakage and provides no redundancy for protection against failure to open or failure to close. To provide redundant protection against these failure modes a quad valve arrangement of valves must be provided. Since the series seat valve is more complicated than a single seat valve, probability of fail to open or close is increased.

(b) Flexure Valves. In general the moving element of a flexure valve is supported by a flexure type element so that close fits for bearings

or guides are eliminated. Since generous (at least with respect to the contamination present) clearances are provided, contaminants in the gas do not cause wear particles to be generated, which are normally the cause of the majority of the valve failures (sticking open-or close, and excess leakage due to seat damage).

Flexure valves decrease the probability of sticking or binding and improve valve seat life. Coil, or solenoid, failures and possible cold welding and sticking on the seat are not changed hence fail to open probability is not changed appreciably. The order of probability of failure for the flexure mounted valve is probably: 1) fail to open; 2) leak and 3) fail to close. Leakage and fail to close are probably reduced by almost an order of magnitude. The actual numbers have yet to be demonstrated over a period of time.

References 3 and 4, on valve design, present information which shows that flat, or perpendicular, seats have much better long term sealing characteristics than conical seats. The reason for the poor long term seal characteristics of the conical seats is that a slight misalignment of the poppet causes improper seat contact, skidding and wear. Seat condition degrades and leakage occurs. On the other hand perpendicular seats do not slip if there is a slight axial misalignment, however the initial leakage may be a little higher than the conical seat.

Flexure valves can use two flexure elements (See Figure A-8 in Appendix) to provide consistent and nearly absolute perpendicular alignment. A combination of flexure valve moving element supports and a seat perpendicular to the poppet motion is an attractive valve design.

(c) Delayed Series Seat. The delayed closing series seat is considered an improvement over the standard series seat if the supply contamination causes seat wear or the closing poppet acts like a filter during closing. A critical part of this concept is the time delay of the second seat closing and the response time of the volume downstream of the seat. The following schematic illustrates the delayed closing series seat valve.

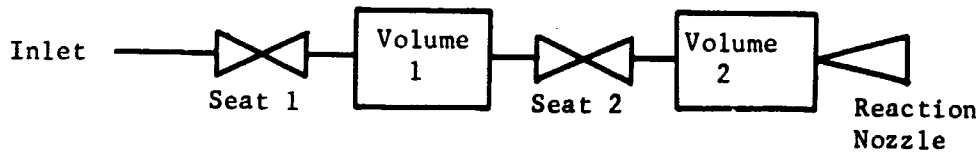

In the closing sequence, seat one closes first and the second seat closing is delayed (pneumatically, mechanically, or electrically). Seat two is delayed about four time constants of the downstream volume ($V_1 + V_2$). This delay allows the pressure in the downstream portion of the system to decay to about 1 percent of the normal flowing pressure. If V_1 is

small no appreciable impulse is added to the tail off. The principle of imposing the pressure decay before closure is twofold: 1) contaminants in the supply gas within the valve is approximately proportional to density and 2) flow through the second seat has decreased hence fewer particles, including wear particles, will pass through the seat during closing. These two factors should extend the life of the second seat considerably. Seat one leakage probability will not change.

A preliminary layout design of a series seat valve with a pneumatic delay was made during Phase I of the current program and is presented as Figure 2-2. The volume between the seats has been held to a minimum. Seat one is part of the armature and during the opening cycle when it moves a short distance seat two is picked up and opened. On the closing sequence seat one closes when the coil is de-energized but seat two remains open by means of a pneumatic delay. When the pressure at seat two drops to a few psi, the second poppet begins to close. A restriction in the volume below the lower diaphragm support, the balance diaphragm, introduces the delay in the closing motion of the second seat.

The moving elements are flexure supported and the two seats improve the leakage characteristics. The order of probability of failure is estimated to be: 1) fail to open, 2) fail to close and 3) leakage.

(d) Impulse Bit Valve. The impulse bit valve delivers a specified amount of gas on command independent of valve response. Schematically, the valve is similar to the figure below.

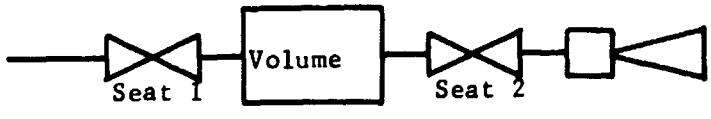

The normal, no command, position of Seat 1 is open and Seat 2 closed. On command Seat 1 closes first and then Seat 2 opens. The gas in the fixed volume exhausts and delivers a fixed amount of impulse. When power is removed, Seat 2 closes first and then Seat 1 opens.

By exhausting a fixed volume of gas, the valve response deviation is eliminated and operation variation with command voltage and soak temperature is eliminated from the impulse accuracy. With this type valve, impulse bits equivalent to 1 millisecond of operation can be reproduced to less than $\pm 5\%$ assuming the regulated pressure is maintained constant.

A preliminary layout of an impulse bit is given in Figure 2-3. The design incorporates flexural suspension of the armature. Since diaphragm

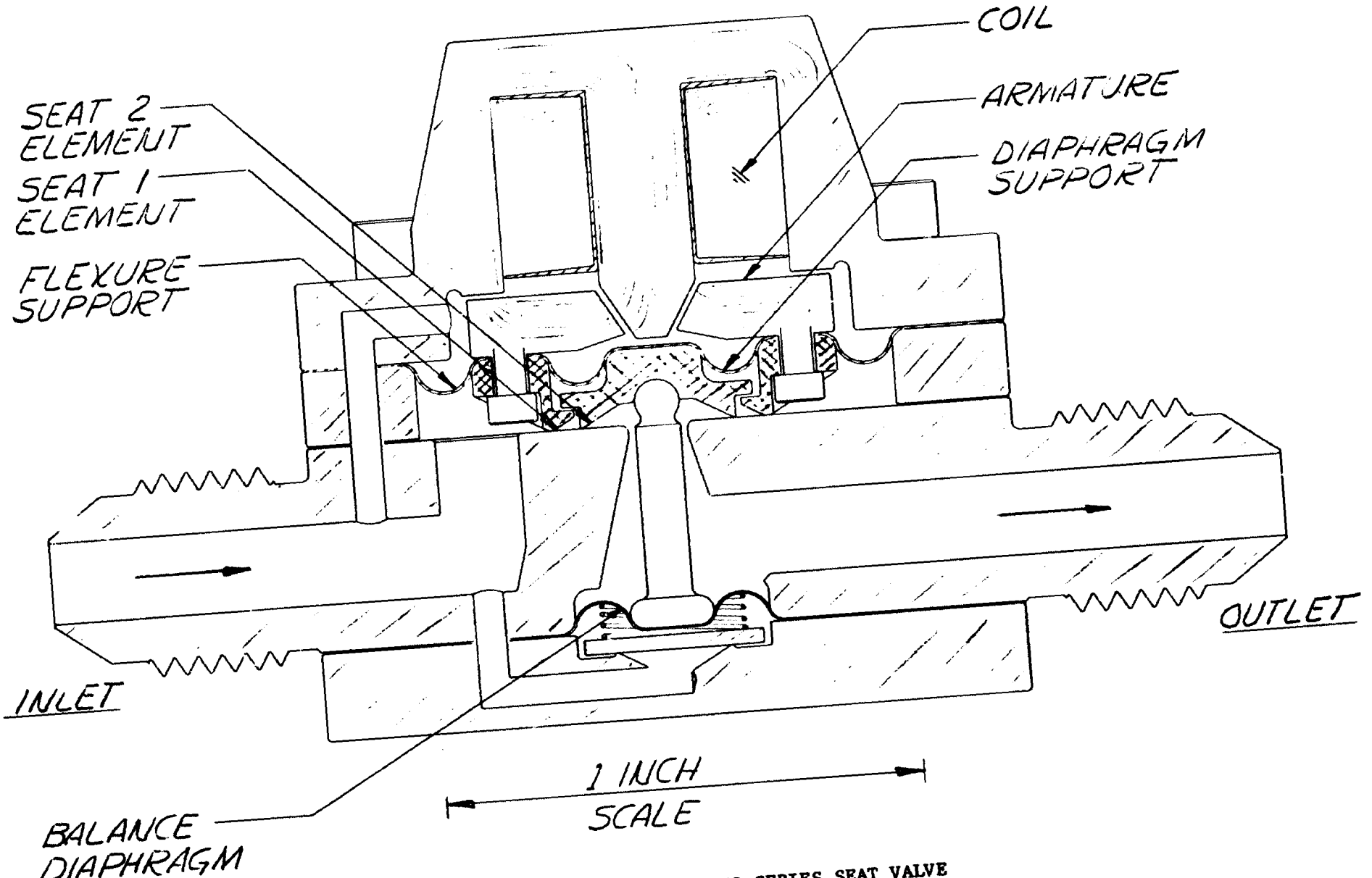

FIGURE 2-2. DELAYED CLOSING SERIES SEAT VALVE

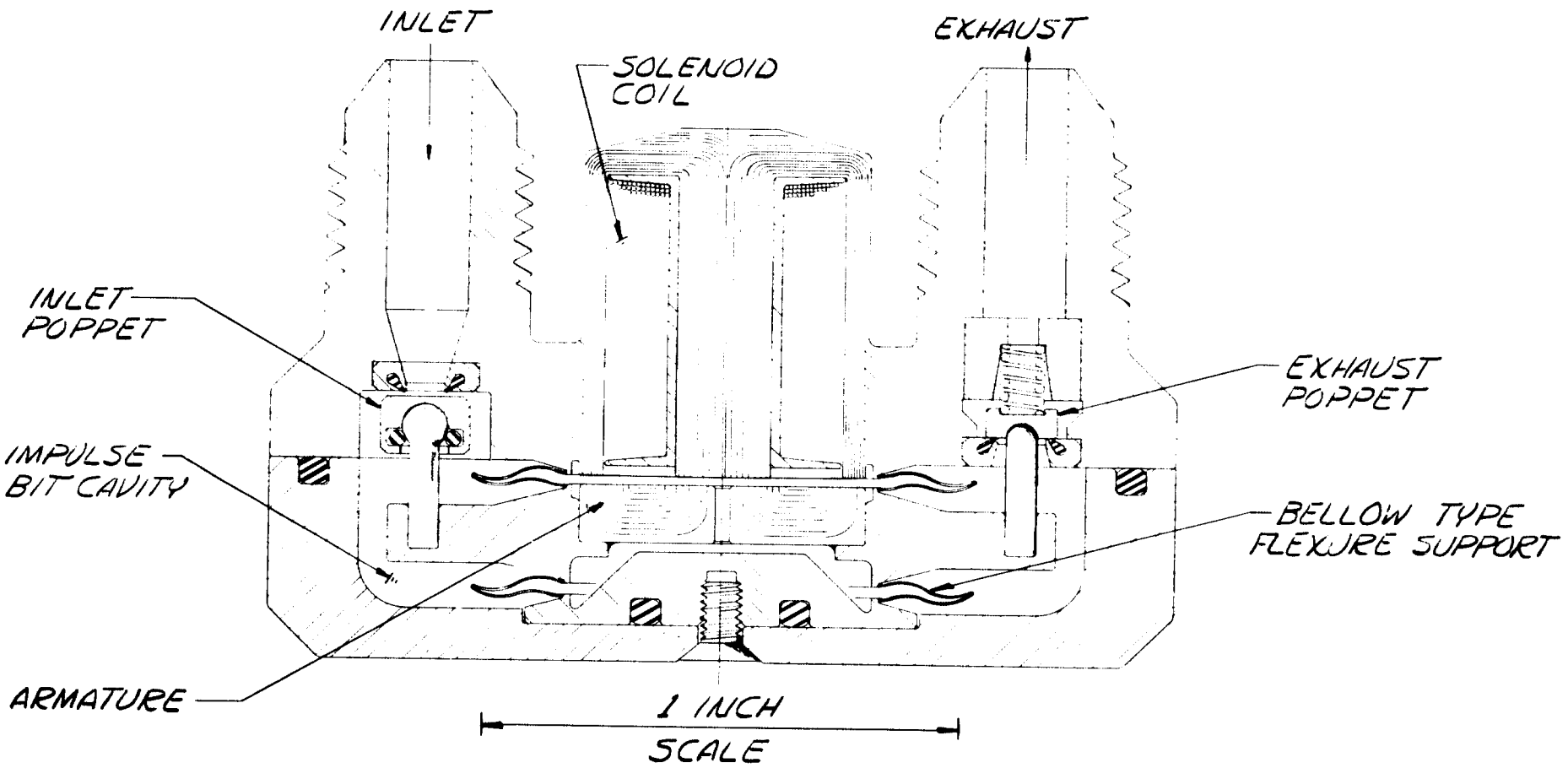

FIGURE 2-3. IMPULSE BIT VALVE

or single convolution bellows elements are used, the magnetic materials are isolated or hermetically sealed from the working fluid and flow passages. Normally the magnetic material is the first to corrode or have surface reactions. Spacing and poppet forces are designed such that on a command the inlet seat closes first (no pressure forces) and the outlet seat opens second, since excess spring force must be overcome. In the energized position the downstream poppet pressure force is relieved so there is a high closing spring force. When power is removed for the closing cycle, seat two initiates motion first.

If one pulse bit for each command can be used through the duty cycle (as for precessing the axis on spinning spacecraft) the preliminary valve design is sufficient. For continuous impulse delivery an electronic pulse generator is required.

The basic design of the valve design can be changed so that either steady-state or pulse operation can be attained; Figure 2-4 presents such a design. The valve utilizes two electromagnetic coils. Either coil will close the fill orifice, which is seat one and open the second seat (see schematic above). When both coils are energized seat one is also opened and steady-state action is attained. When only the second, or downstream, seat is opened, the valve operates in the "impulse bit" mode. Redundancy of coil actuation is provided since either of the two coils will actuate the valve.

In both designs the moving element is flexurally supported and the action of the two seats improves the leakage characteristics. The order of probability of failure is estimated to be 1) fail to open, 2) fail to close and 3) leakage.

(e) Magnetic Particle Seal. A magnetic particle seal concept was investigated experimentally during Task II. In this concept the magnetic particles are the moving element. Porous metal with pores below the powder size are located at the inlet and outlet of the valve cavity to contain the powder. A function schematic of the valve is shown in Figure 2-5.

The advantages of simplicity, toleration of contaminants and reliability are obvious. The sealing characteristics of the particles were questionable and tests were run to evaluate this property.

In the functional schematic energizing the coil at the inlet end of valve pulls the magnetic particles to that end and compaction by the magnetic field provides sealing. Energizing the coil at opposite end, and de-energizing inlet coil, allows the particles to uncover the inlet and collect at the opposite pole so that gas flows through the outlet filter. After long term storage, particle compaction may resist breakup, therefore pressure aiding the opening cycle was used.

Reversal of operation could easily be attained and a permanent magnet field could be used for the shutoff condition.

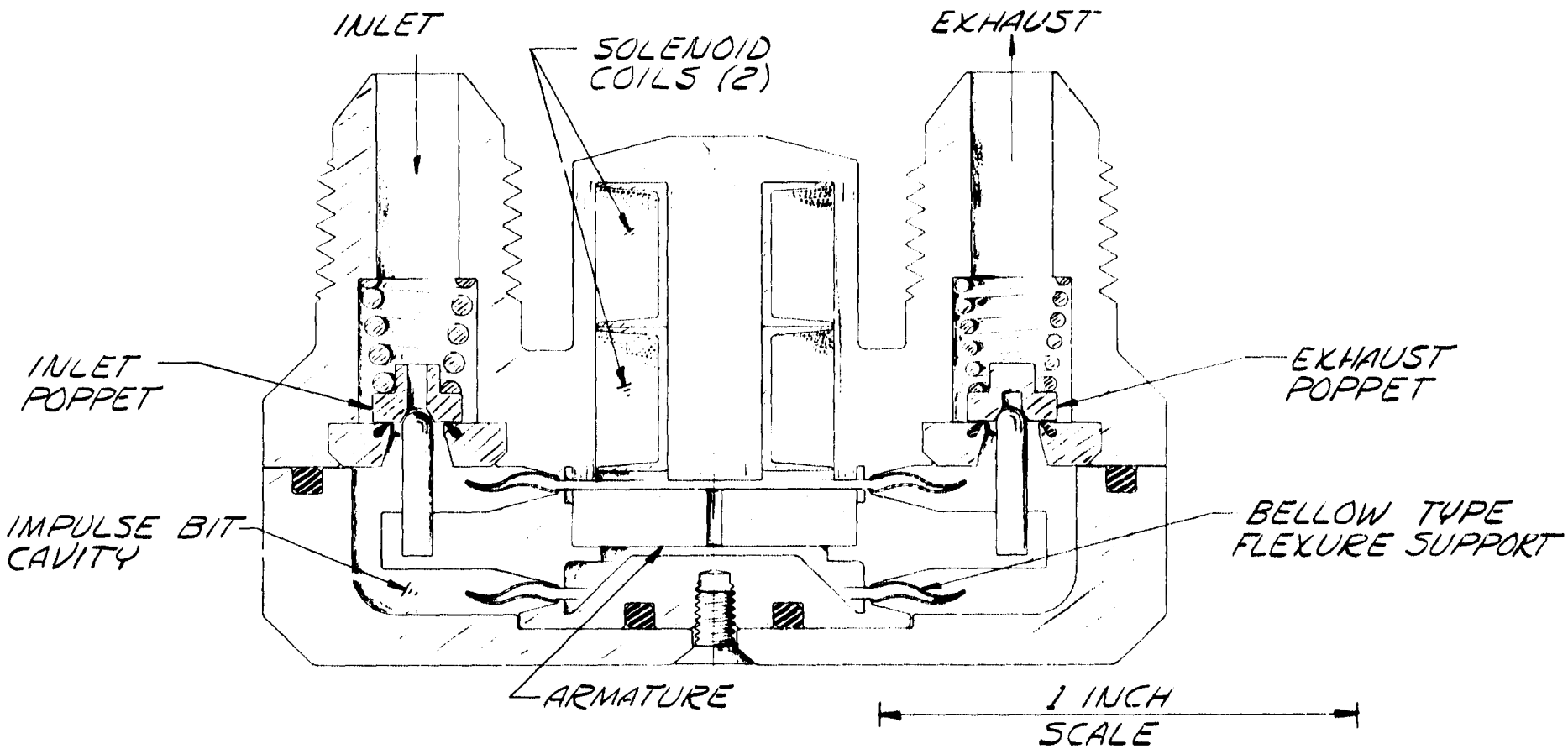

FIGURE 2-4. IMPULSE BIT AND CONTINUOUS FLOW VALVE

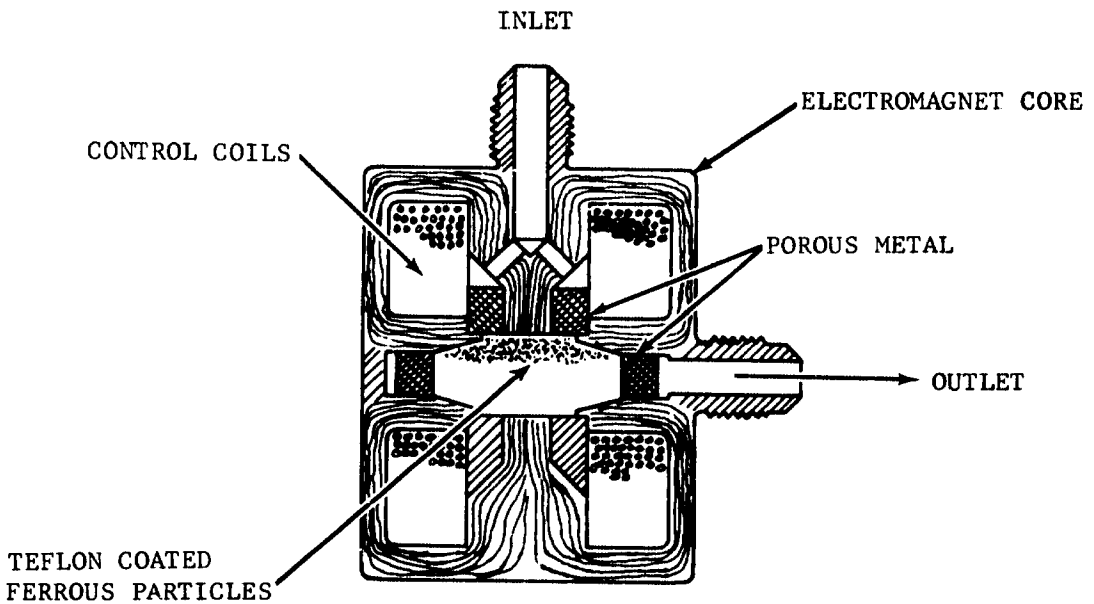

FIGURE 2-5. MAGNETIC PARTICLE SEAL - VALVE

Several tests were conducted using magnetic particles. Both uncoated and coated type (with silicone) were tested to see if elastomeric deformation would improve sealing. A test fixture with adjustable poles was fabricated. The two poles formed a slit type opening of the appropriate area with a concentrated magnetic field.

The initial tests with several sizes of soft iron particles resulted in leakage of about 1 to 2 sccs. After this the several sizes of particles were precipitation coated with silicone. Aeronutronic's Plastics Research group coated the particles using a process developed for coating beryllium solid propellant additives. The coated particles were tested and the average leakage was reduced to about 0.5 to 1 sccs. However, this was still over three orders of magnitude above the requirement.

Containing the particles, or a magnetic fluid, in a plastic bag or pancake had been considered. The smooth surfaces of the capsule would provide a compliant seal. Some particles were enclosed in flat capsule mode with .002 thick teflon and placed in the test fixture. The leakage improved only slight, to a value below 0.2 sccs.

At this point the flux density capability was questioned. A disc of soft iron was placed above the capsule and leakage measured again. Leakage improved to about 0.03 sccs. A flux permeability test showed that the flux carrying capability of the powder was about 30 percent of that of soft iron. Investigation revealed that the manufacturers quoted permeability was related to powder under a compressive load of 2000 psi.

Since plastic coated soft iron was considered to be in the realm of conventional soft seated valves the magnetic particle seal valve was terminated.

b. Reaction Thrust Control Duplication. Redundancy of control action can possibly be provided without adding a complete set of redundant valves. Consider the two axis control systems below

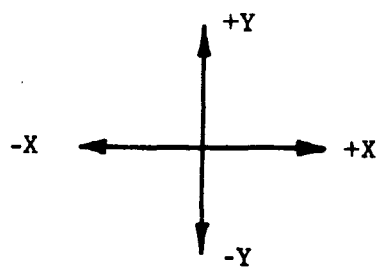

Partial duplication of commands and redundancy can be provided by adding only two more control thrusters as below

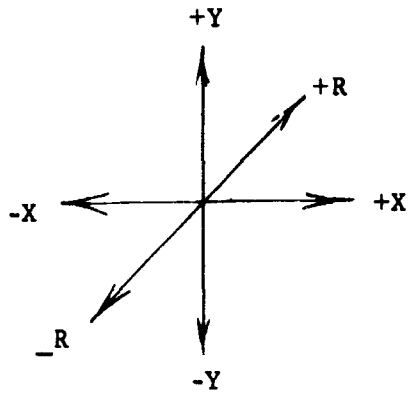

If the +X thruster fails the command can be executed by +R with occasional unstabilizing force corrections in the y plane handled by -Y. The payment for fewer valves is inefficient gas use. The +R unit also protects against the +Y failure.

The foregoing example is primarily applicable to systems which use valve elements which have a higher probability of failure to open. Hence configurations in this section are pointed toward the series valves or flexure type valves used in each leg.

Only a few of the more obvious and most efficient configurations to provide duplication of control forces, and hence protection against the most likely failure mode of fail to open, are presented herein.

(1) Three Axis Control Systems. The normal three axis stabilization system uses two pitch, two yaw and two roll valves for a total of six valves. No control redundancy is provided.

(a) Single Valve System. One possible configuration which provides control action redundancy is shown in Figure 2-6. The configuration uses opposed valves in each quadrant pointed in the tangential direction. Valves 1 and 6 provide plus yaw, 2 and 5 minus yaw, 4 and 7 plus pitch, 3 and 8 minus pitch,plus roll is provided by all clockwise jets and minus roll by all counter clockwise jets. The roll command is mixed with the pitch and yaw. The jets may be positioned closer to the roll axis so that excessive torques are not exerted.

All control actions are duplicated with eight valves; to provide protection against fail to open. If valve 1 fails valve 6 still provides plus yaw. The roll induced is taken out by a 33% 'on time' command to valves 3, 5 and 7 (valve 1 has failed). Hence we see all control functions are duplicated. Again the payment for this redundancy is possibly a slight loss of roll jet efficiency and poorer pitch and yaw gas usage once there has been a failure.

(b) Redundant Parallel Valve System. A configuration which provides complete redundancy for a three axis control system is depicted in Figure 2-7. Any single valve failure can be tolerated and only 16 valves are used. The normal control system layout would require 24 valves (quad valves on six channels) to provide equivalent redundancy.

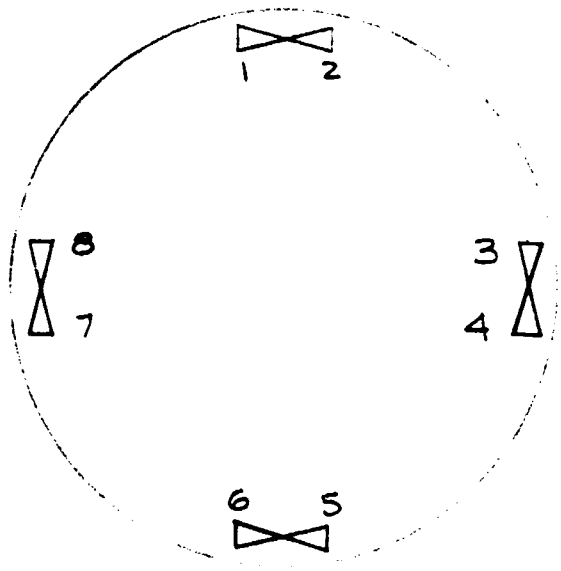

EACH NUMBERED JET
HAS A CONTROL VALVE

FIGURE 2-6 THREE AXIS SECTOR SYSTEM FOR ATTITUDE CONTROL

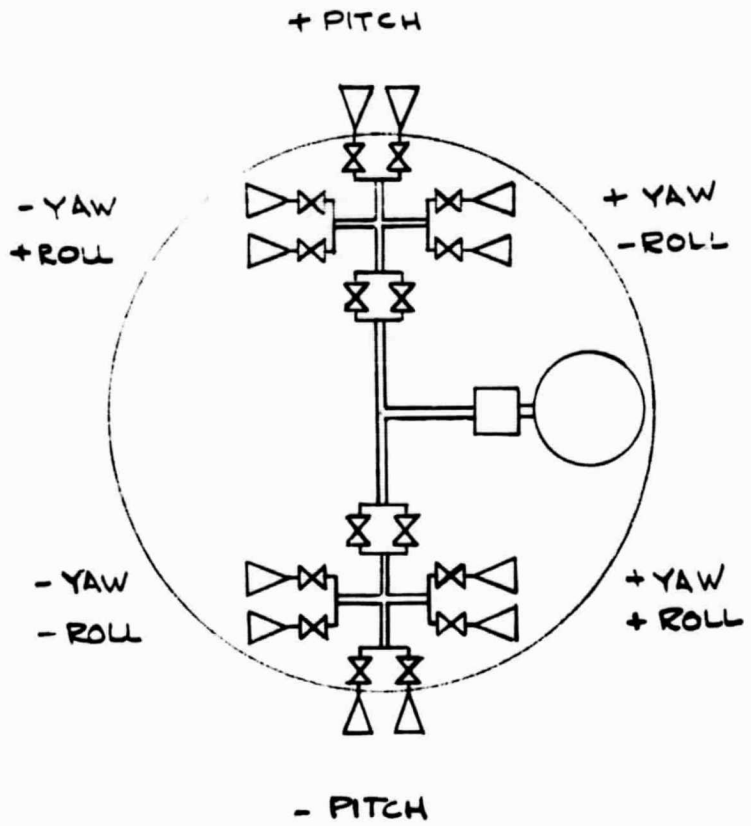

FIGURE 2-7 THREE AXIS PARALLEL REDUNDANT CONTROL SYSTEM

Very little, or possibly no, measurable degradation of performance occurs when there is a valve leak or failure to open. If the final parallel valves feed a common nozzle the thrust may only drop a few percent when one valve fails closed.

(2) Spin Stabilized System. For spin axis control systems where only a precess jet is required there is little beyond the quad valve configurations (series in parallel or parallel in series) that can provide any real improvement in reliability.

For fuily spin stabilized satellites where spin jets for replenishment and retarding as well as a precess jet is required control duplication can be used to provide redundancy to protect against failure to open. One near optimum system is shown in Figure 2-8. Several other configurations, as well as the one depicted, are fully covered in Reference 6.

The configuration provides complete functional redundancy for any single-jet failure and for most combinations of double failures. Normal spin replenishment and despin operations is efficient. The increment of hardware over the minimum configuration are, (1) latching relay and four command channels, (2) canted jets with OR gates. The configuration failure compensation accommodates any single jet failure and 4 out of 6 two-jet failures. The possible function losses due to two failures are despin and spin replenishment. The additional command channels and hardware can be eliminated by simply sending the spin command to both the spin jet and the appropriate canted jet. The payment for the dual signal command is a slightly higher gas consumption.

As can be seen from the figure, the principal cost of redundancy is the added jets (including valves), some additional command channels and an additional latching relay. The payoff is that the probability of compromise of mission success (i.e., degradation of any function) is approximately squared when going from the two-jet to the four-jet configuration.

A parallel redundant spin control system can also be used. The system is half of that pictured in Figure 2-7. One parallel valve arrangement is used in series with parallel valves for plus spin, minus spin and precess. Eight valves are required and protection against any single failure is provided.

2.1.3 THRUSTER REDUNDANCY SUMMARY

Two methods of providing thruster redundancy have been described. The pertinent valve configurations with failure modes and approximate probabilities are summarized in Table 2.1. The probabilities are normalized by the approximate order and percentages of a typical current state-of-the-art solenoid valve. The probabilities are only estimates in some instances but the relative comparison of different choices is expected to be in the correct direction.

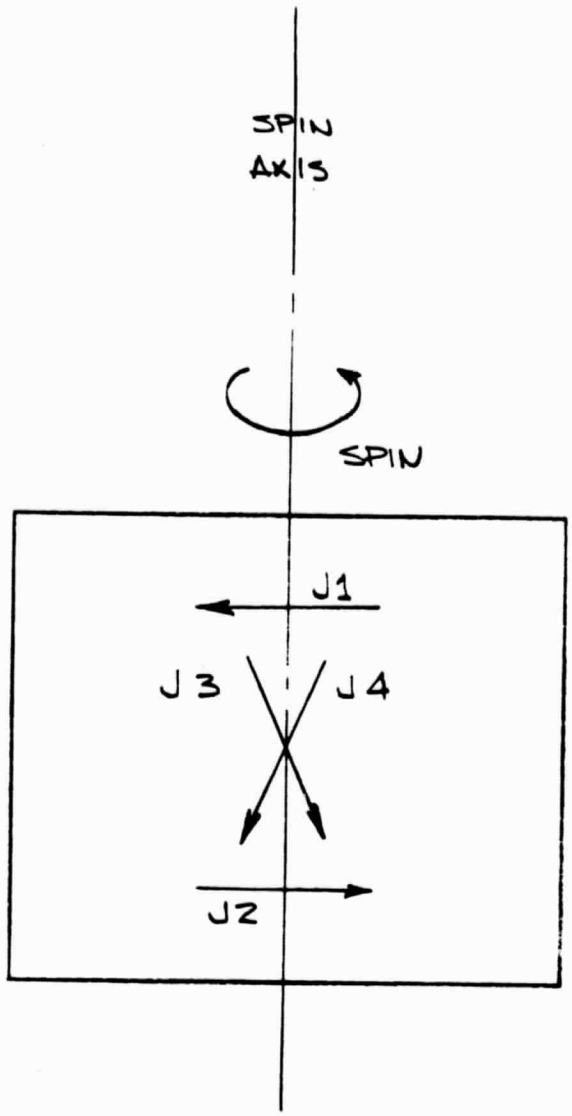

FIGURE 2-8 OFFSET AND ANGLED JET SPIN CONTROL SYSTEM

TABLE 2.1

VALVE FAILURE PROBABILITY AND PROTECTION

Valve Configuration	Number of Valves	Moving Elements	Failure Probability(1)			Failure Protection Against		
			Leakage(2)	Fail to Open	Fail to Close	Leak	Fail to Open	Fail to Close
Standard Solenoid	1	1	60	30	10	No	No	No
Quad - Series in Parallel	4	4	6	8	2	Yes	Yes	Yes
Quad - Parallel in Series	4	4	15	3	4	Yes	Yes	Yes
Series Valves	2	2	6	60	2	Yes	No	Yes
Parallel Valves	2	2	120	2	20	No	Yes	No
Series Seat	1	2	6	45	15	Yes	No	No
Flexure Supported	1	1	15	25	1	Partial	No	Qualified Yes
Delayed Series Seat	1	2	3	40	12	Yes	No	Partial
Impulse Bit	1	3	20	45	8	Partial	No	Partial

(1) Estimate in percent, normalized by failure probability of standard solenoid valves.

(2) Leakage failure mode applicable only to long duration missions, nominal limit 1 scch

Comparison of several control thruster systems appears in Table 2.2. Control action redundancy to protect against the most likely failure mode (fail to open) of series valves or flexure type valves can be accomplished with fewer valves than the application of quad valves to standard thruster layouts. The table also reflects the fact that a parallel redundant system (one parallel valve in series with several others) provides protection against any single failure with fewer valves than the application of quad valves.

For the present time, to provide the highest reliability, Aeronutronic recommends using complete redundant valve action such as three-axis parallel redundant or spin parallel redundant systems. Once (if) the most likely failure mode of the flexure type valves has been demonstrated and documented, systems such as the three-axis sector or spin-offset and angled jet systems could be used. To provide protection against any single failure, by definition, includes all possible failure modes and, necessarily requires a quad type valve arrangement or a common parallel valve in series with several of these parallel valves.

2.2 DIVERSION VALVES

The use of diversion valves in the thruster system allows one shutoff valve (redundant or nonredundant) to accomplish two or more functions. By proper use of the diversion valves both the leakage and the effects of leakage are reduced or eliminated.

2.2.1 DIVERSION VALVE THRUSTER SYSTEMS

Figure 2-9 shows a typical three-axis stabilization system. The number of shutoff valves has been reduced from 6, in the equivalent system without diversion valves, to 3, by the use of diversion valves. The leak paths have been decreased from six to three, hence the potential leakage problem has been decreased.

An additional advantage of the diversion valve is that if there is leakage the reaction torque is eliminated. The diversion valve normally assumes a central position such that both ports are opened equally. In the normal 6-valve system if one valve leaks there is a torque generated. Occasionally the opposing valve has to be opened to counteract the leakage torque. Hence the 6-valve system can magnify the leakage by a factor of two, whereas the diversion valve system eliminates the leakage torque.

The diversion valve cuts the leak paths in half and does not magnify the leakage because of torques generated. Hence the diversion valve can improve the leakage characteristics by a factor of 4. If redundant shutoff valves are used weight can be saved at the same time since the total number of valves is decreased ($4 \times 6 = 24 > 4 \times 3 = 15$).

Diversion valves can be used also in spin stabilization systems as shown in Figure 2-10. In the illustration there is only one (1) leak patch as

TABLE 2.2

CONTROL SYSTEM PROTECTION
BY
THRUSTER TORQUE DUPLICATION

System Configuration	Number	Efficiency After Failure	Failure Protection Against		
			Leakage	Fail to Open	Fail to Close
3-Axis Standard (Ref.)	6	None	No	No	No
3-Axis Quad Valve (Ref.)	24	Excellent	Yes	Yes	Yes
3-Axis Sector System					
Flexure	8	Fair	No	Yes	No
Series	16	Good	Yes	Yes	Yes
3-Axis Parallel Redundant	16	Excellent	Yes	Yes	Yes
Spin(1) - Standard (Ref.)	3	None	No	No	No
Spin(1) - Quad Valve (Ref.)	12	Excellent	Yes	Yes	Yes
Spin(1) - Parallel Redundant	8	Excellent	Yes	Yes	Yes
Spin(1) - Offset and Angled Jets					
Flexure	4	Fair	No	Yes	No
Series	8	Good	Yes	Yes	Yes

(1) Precess and plus and minus spin control functions

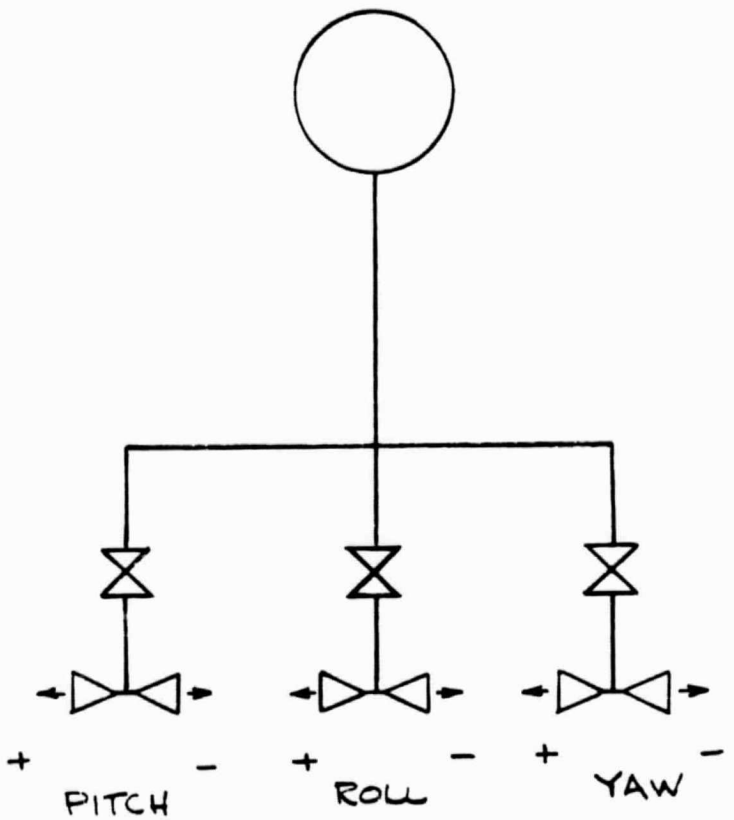

FIGURE 2-9 THREE AXIS STABILIZED SYSTEM WITH DIVERSION VALVES

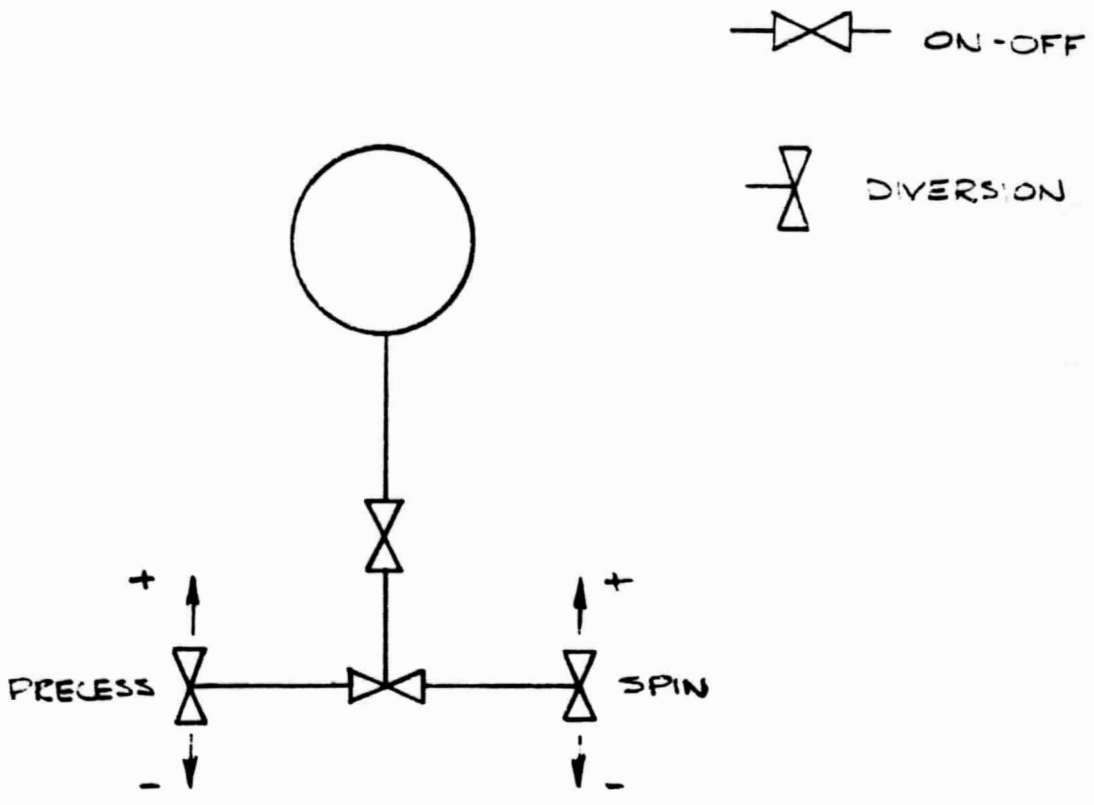

FIGURE 2-10 SPIN STABILIZED SYSTEM WITH DIVERSION VALVES

opposed to four (4) leak paths in the nondiversion valve system. Again leakage torques would be eliminated. The schematic in Figure 2-10 is a limiting configuration using one shutoff valve and three diversion valves. For the single shutoff valve if a 'quad' shutoff valve configuration is used 7 valves are required rather than 16 valves on the equivalent non-diversion valve system.

The systems illustrated in Figures 2-9 and 2-10 are only typical. Actual systems are dependent upon the required vehicle characteristics and envelope and space available. However the discussion above does point out the potential improvements on leakage and system weight when diversion valves can be utilized.

2.2.2 PERFORMANCE AND RELIABILITY

Performance of the diversion valve is not critical. The diversion valve only directs gas and is not required to shut off for long periods of time. Hence a leakage of one-half of one percent (very easily obtainable) only means that slightly more gas must be stored. Normally leakage is the most difficult valve requirement. The diversion valves' moving element is normally positioned in the center, or null position, so that the valve does not remain closed for long periods of time. Sticking closed problems are thereby essentially eliminated or at least reduced to being no greater than the fail to close probability. In standard valves fail to open, or stick closed, is the second most likely mode of failure. Both the first and second most likely failure modes of standard valves have been drastically reduced with diversion valves, and unreliability is decreased by one or two orders or magnitude.

Aeronutronic experience with diversion valves substantiates the improved reliability. Based upon typical acceptance test criteria the probability of successful operation of the diversion valves is 0.99955 as compared to 0.99461 for standard solenoid valves. On the diversion valves, the majority (over 66 percent) of the failures were for leakage in excess of about 1/4 of one percent of full flow. If acceptable leakage was increased to 1/2 of one percent or 1 percent practically all valves would be acceptable.

2.2.3 DIVERSION VALVE DESIGNS

a. Mechanical Diversion Valve. Figure 2-11 shows a preliminary layout of a mechanical diversion valve. The armature-flapper is flexure mounted with its null position between the two outlet nozzles. With no power the inlet gas would flow equally out the two valve ports. The electromagnet coils are located on either side of the armature. Energizing one side or the other attracts the armature and causes the flapper to seat the outlet port on the corresponding side.

The required power for a 0.2 lbf thrust valve at about 50 psi would be near 1 watt. The clearances are 0.002 in. to 0.004 in. minimum, increasing to about 0.010 in. maximum, hence there should be no contamination problems.

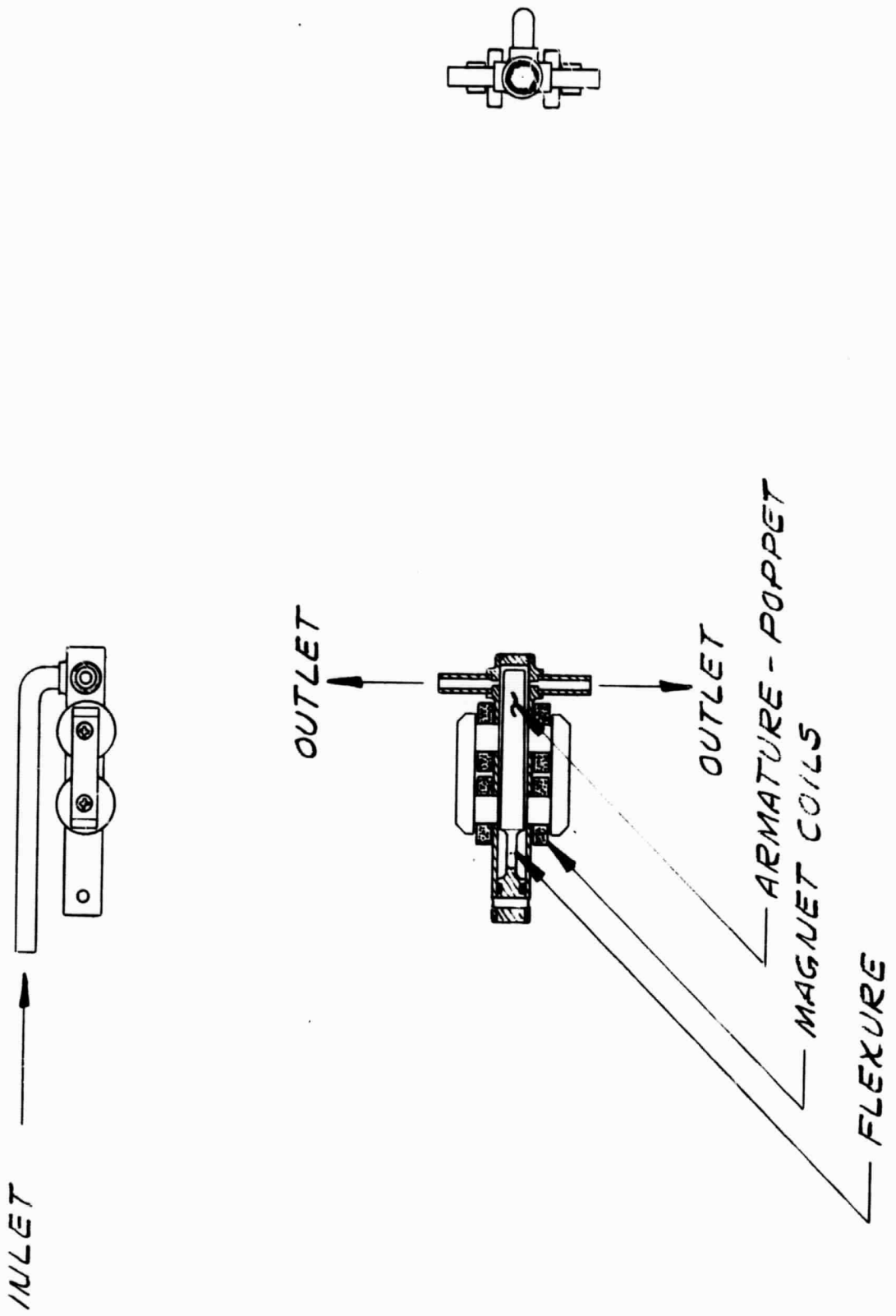

FIGURE 2-11. MECHANICAL DIVERSION VALVE DESIGN

Off side leakage can easily be maintained below 0.2 percent. Performance will probably improve for some period of time while the seat 'breaks in.'

b. Flueric Diversion Valve. A flueric diversion valve can be used to allow a single on-off valve to provide both precess and spin replenishment control on a spin stabilized vehicle. A typical system schematic is shown in Figure 2-12.

The shutoff valve provides positive shut off and minimum leakage over long term periods. The flueric diversion valve directs flow out the precess jet (for a steady inlet flow). The time delay of switching from precess to spin is set slightly longer than the period of time to cover the angular position in which the precess jet is to be on. Hence for short command pulses precess control is provided and for long steady pulses spin control is provided.

The command input and control output for different commands for the system are illustrated in Figure 2-13. A spin replenishment function is accomplished by sending a continuous command, as in Figure 2-13a. For the first several milliseconds a precess thrust is produced, but then the thrust is switched to spin replenishment and remains on for the remainder of the command duration.

Spin axis precession is normally accomplished by commanding the precess jet to thrust while it is in a given sector, typically about 45 degrees. At spin rates between 60 rpm and 120 rpm the command duration would be 0.125 second to 0.062 second during each revolution. Figure 2-13b illustrates this command. The resulting output is all precess since the time delay to switch, to spin, is greater than 0.125 second or 0.062 second, whichever is applicable.

The flueric diversion valve is a pure pneumatic control device with no moving parts and is shown in Figure 2-14.

A pilot stage was inserted to get clean switching of the power stage. The low flow initial pilot set circuit and delay circuit might be placed directly on power stage.

When flow is initially introduced to this valve the low flow set circuit stabilizes the primary pilot flow in the upper leg. In turn the pilot flow directs the primary power stage flow in the lower leg. At this time the lower leg total pressure is more than twice the upper leg total pressure. The main power flow exhausts directly out the lower vortex valve and provides thrust to precess. Flow goes from the lower vortex valve to the upper vortex valve because of the pressure drop and injects tangentially to shut off the flow to the spin jet. The power stage valve is identical to the valve described in warm gas bi-stable aerodynamic valve study final report.[7] After a selected time the high flow from the delay circuit comes on, overpowers the set circuit low flow and diverts the pilot flow to the lower leg of the pilot fluid amplifier. The switched

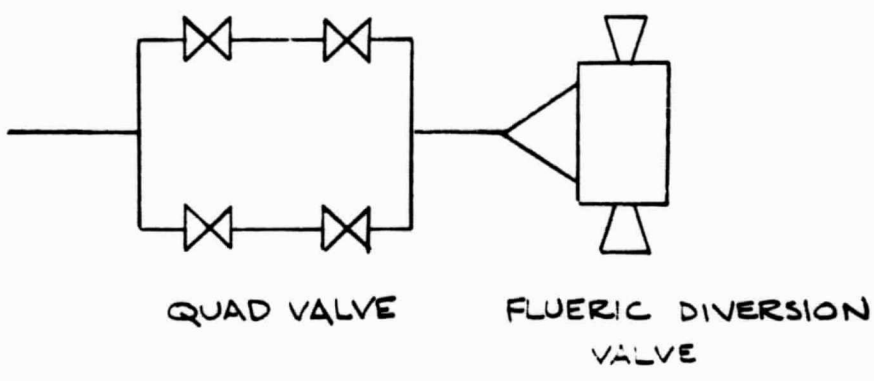

FIGURE 2-12 FLUERIC DIVERSION VALVE SYSTEM SCHEMATIC

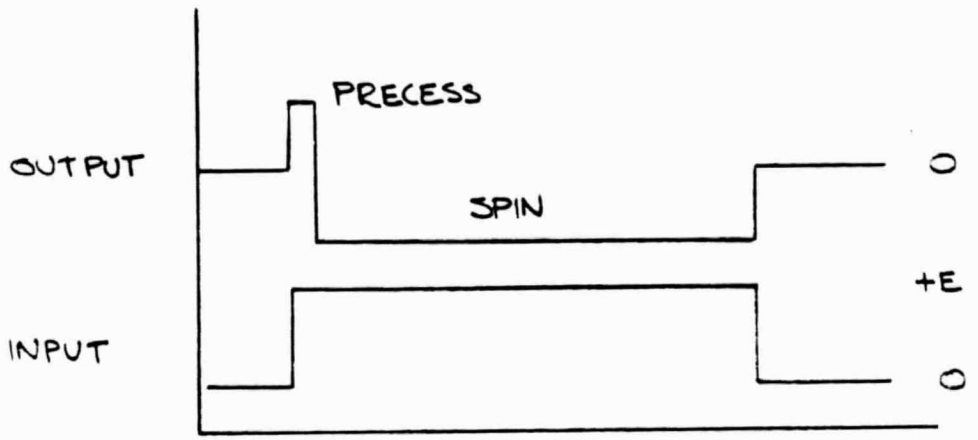

SPIN COMMAND
(2-8a)

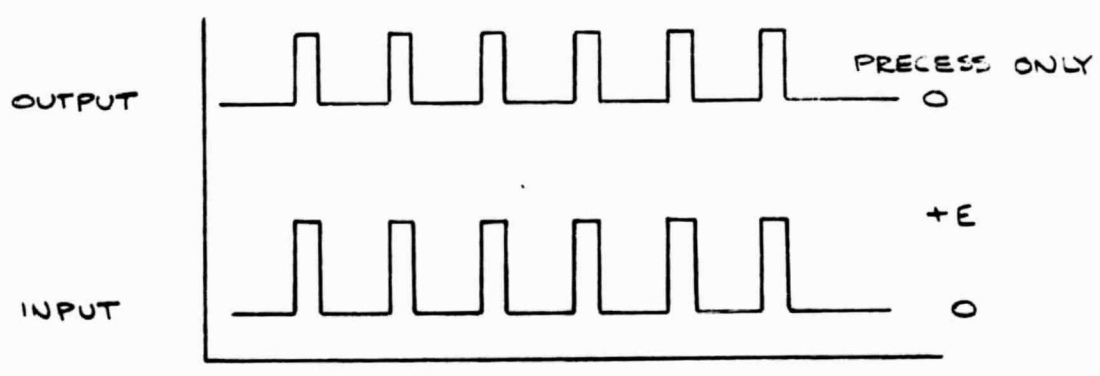

PRECESS COMMAND
(2-8b)

FIGURE 2-13 FLUERIC DIVERSION VALVE COMMAND LOGIC

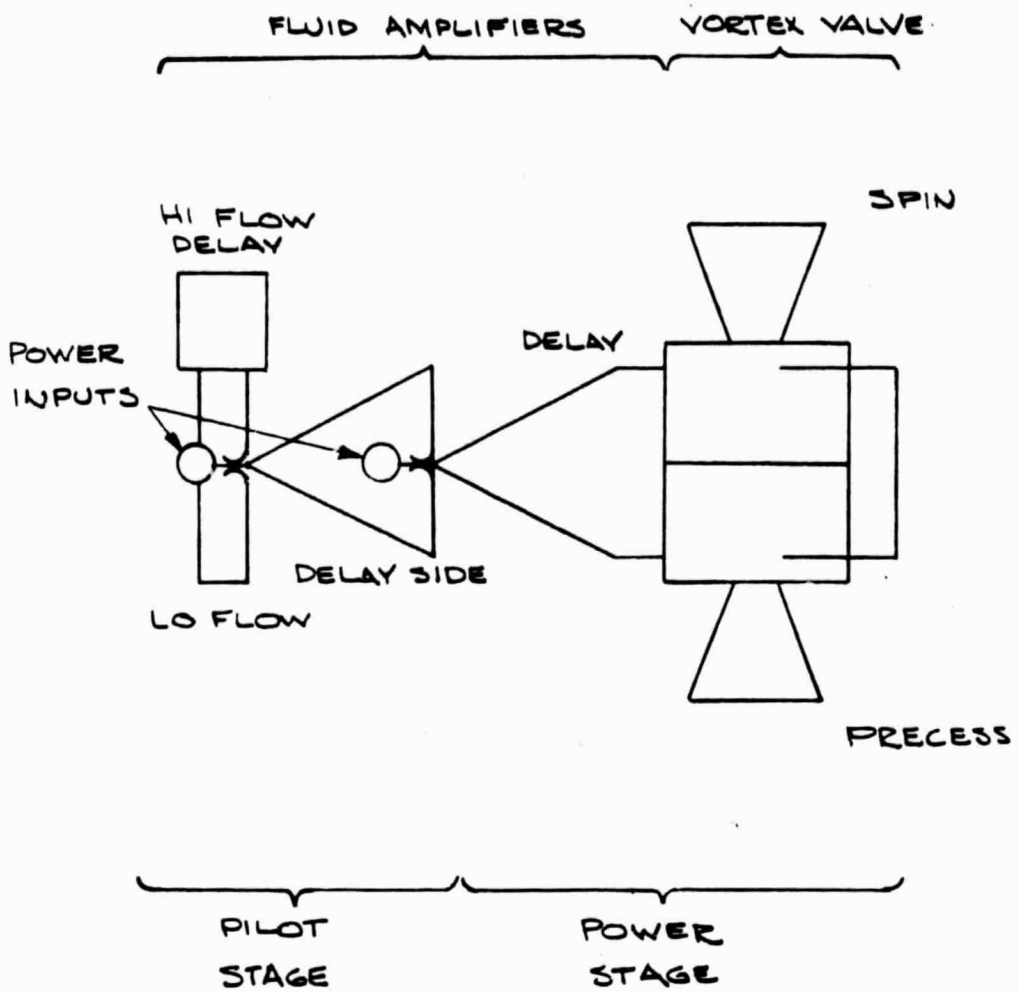

FIGURE 2-14 FLUERIC DIVERSION VALVE SCHEMATIC

pilot flow then diverts the main power flow into the upper leg of the power fluid amplifier. The pressure in the spin vortex valve increases while that in the precess vortex valve is decreased and the cross bleed changes flow direction and shuts off the precess jet.

Typical off jet leakage would be below 5 percent. When precess is commanded 5 percent of the gas would leak out of the spin jet and vice versa.

If the leakage out the spin jet is too great an additional vortex diversion valve can be added on the spin jet to null the leakage thrust. When the precess jet is on spin jet flow is split and no spin thrust produced. When the spin jet is on some pilot flow from the spin vortex valve is bled to the minus spin jet on the spin nullifier vortex diversion valve and only plus spin is provided.

SECTION 3

INTEGRATED SYSTEM DESIGNS

Task IV considered non-standard system mechanizations which would improve system reliability. Improvements in system reliability can be obtained at the component level or with the overall system. By combining functions and tailoring the system toward the specific application it may be possible to simplify the system, change the system operation, eliminate components or obtain redundance with no increase in parts thus improving reliability.

3.1 APPROACHES

The design approaches covered are for application to the Pioneer or Biosatellite vehicles. The basic design concepts can be applied to other vehicles. Combining functions of active pneumatic elements and methods of eliminating the regulator and/or relief valve were investigated.

3.1.1 MULTIPLE FUNCTION ELEMENTS

a. Solenoid Activated Regulator - Thrustor. A solenoid activated (or pilot actuated) regulator-thruster was proposed as a combined function element. The basis of original selection was that one seal would provide better leakage control than a regulator (including a relief valve) in series with a shut off valve. For the Pioneer application where one regulator and one valve is required the concept appeared to be applicable. On multi-thruster applications, such as the Biosatellite, the concept feasibility is not as high.

Preliminary design considerations for the Pioneer brought out two pertinent facts: 1) high design complexity and 2) potential instability problems. A regulator can be solenoid activated either mechanically or pneumatically. A pneumatically actuated regulator requires an additional seat and valve, hence is as complex as a regulator and valve. The mechanically actuated

version, to have fast action, requires more power and is more complex than a simple regulator. Also in order to attain good thrust response the volume between the regulating element and the reaction nozzle must be small. The small ullage volume and the normal operating inlet pressure range (20:1) can lead to severe instability problems, at some inlet pressure conditions. A detail design of a regulator-valve was not pursued because of these potential problems.

b. Diversion Valves. Diversion valves and their advantages are covered in Section 2.2. The work was actually accomplished in Task IV but more logically fit in Section 2. Diversion valve elements allow one shut off valve to perform that of several shut off valves in a system that does not employ diversion valves.

c. Parallel Path Capillary Restrictors. The regulator can be eliminated if a thrust variation, typically 2:1, can be tolerated. Stepped restrictors to be used to accomplish this as illustrated in Figure 3-1. In Figure 3-1 the valves at the restrictor inlets are actuated by either pressure difference or very low power (1/2 to 1 watt). In the schematic the series valves are provided to obtain leakage redundancy and the volume between the restrictors and the solenoid valves should be small. The thruster solenoid valves obviously must operate to full supply pressure. There is an initial thrust spike which decreases as the gas downstream of the restrictors is exhausted. The spike is not severe if volumes are low or non-existent if the upstream valve does not leak. For a four-path system, as illustrated, a supply source variation of 16:1 will only produce a thrust variation of 2:1.

If the restirctor inlet valves are low powered solenoid valves they are normally closed. As the pressure differential across the valves decrease the valves are opened. The valves progressively open lower resistance passages as the supply pressure decreases. If spring loaded-pressure actuated valves are used they are normally open. When the solenoid shut off valves are operated the pressure differential actuated valves close and open progressively as the inlet pressure decays.

A flow metering element similar to that described above was proposed as part of the Pioneer Multi Tank System [Section 3.2.1 a. (1)]. The flow metering element is a spring loaded pressure differential actuated device which used multiple clearance areas rather than capillary restrictors. The device developed is described in Section 4.1.

3.1.2 SYSTEM APPROACHES

The basic concepts investigated were two different methods of propellant storage which would elminate the regulator; one would also eliminate the relief valve. The systems conceived were liquid nitrogen storage and a multi-tank storage system. The liquid storage system provides a much higher density for storage and offers improved specific system weight. For the applications considered, thermal protection is required but is

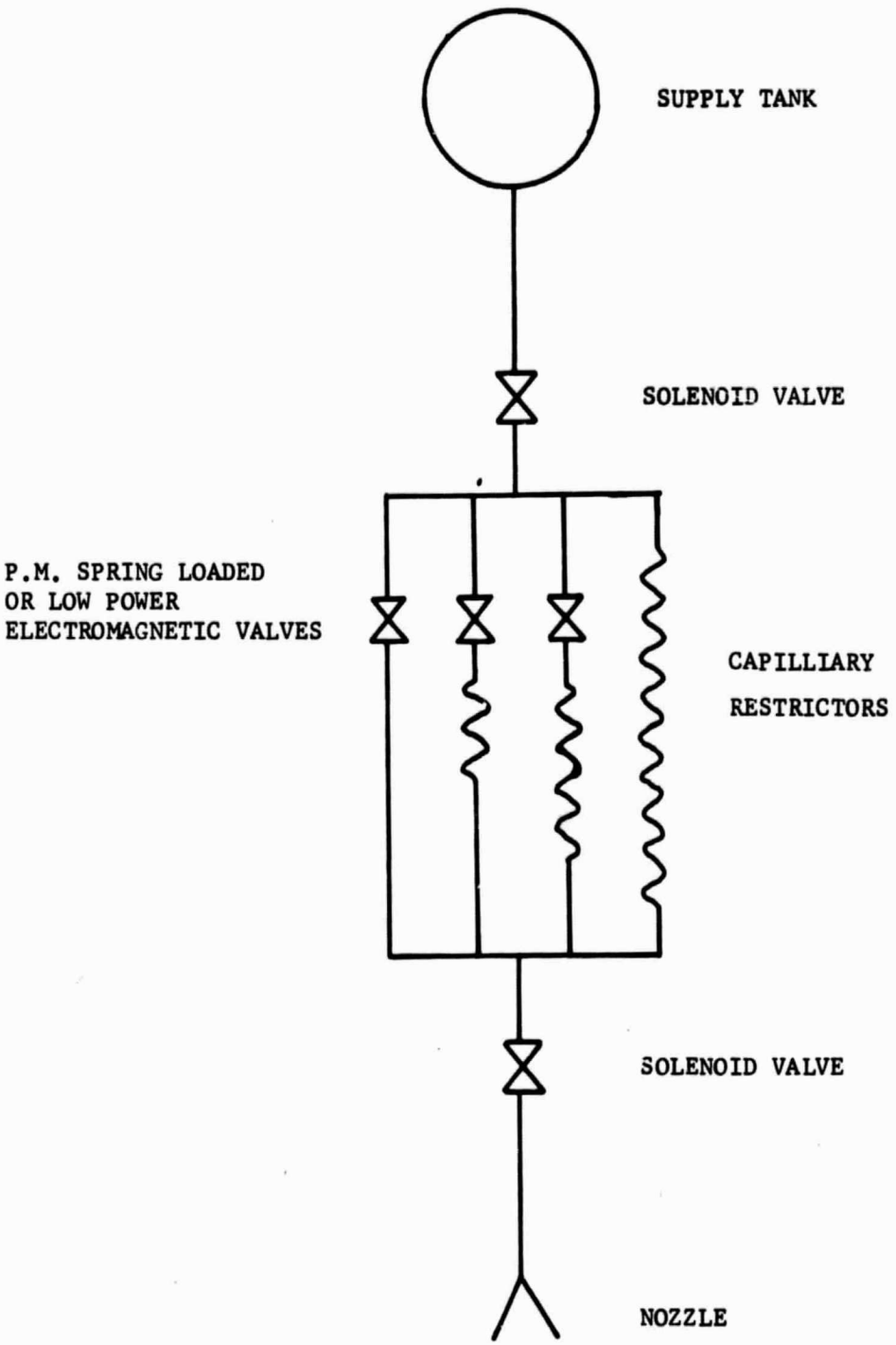

FIGURE 3-1 STEPPED PRESSURE REGULATION
BY MULTIPLE RESTRICTORS

not cirtical. Liquid storage requires a relief valve but eliminates the regulator. In some systems (such as the Pioneer) the relief valve is inactive and can be backed up by a burst disc to completely eliminate leakage.

The multi-tank storage method depends upon discs rupturing at predetermined pressure differences to maintain the system plenum between crude (2:1 to 4:1) pressure limits. The burst discs are extremely reliable and the system eliminates both the regulator and relief valve. In many systems the resultant thrust variation, proportional to pressure variation, is acceptable. If the thrust variation is not acceptable a simple pressure sensitive metering element can reduce thrust variation to a tolerable limit. Failure of the metering element, or any portions thereof; normally will not cause a catastrophic system failure.

The multi-tank is a method of extending the usefulness of the basic metering element (shown in Figure 3-2). When each burst disc ruptures the metering element begins to operate at its initial condition again and the orifices open sequentially as the pressure drops. The burst discs are similar to the metering element in that they are pressure differential sensitive, but they operate in series and are positive seals.

For systems which have a consistent factor (view) for solar radiation an impulse booster heater can be utilized. The heater is merely a heat sink device, absorbing short wavelength heat and emitting long wavelength heat, which is positioned downstream of the shut-off valve, not affecting the reliability of that element. Steady state heater temperature is near 1000°F and typical heat input to the control gas is equivalent to 500 watts. Dynamic response is attenuated and typically may be increased by about 25 to 30 percent. Impulse improvement can be as high as 50 percent.

3.2 SYSTEM DESIGNS

This section presents improved system designs for two different and specific applications. The vehicles are the Biosatellite and the Pioneer sun probe. The Bios is a three axis stabilized system which normally operates in a rate control mode rather than position. Only at the termination of the mission does the Bios actually go to position control for retrofire, de-orbit and recovery.

The second design considered is for the Pioneer probe series. The vehicle is spin stabilized and only requires a jet thruster to precess the spin axis to the desired orientation. The initial spin is provided by a separate energy source and space environment does not cause any appreciable spin decay. Spin replenishment jets are therefore not required.

The designs presented are for specific applications. The Bios application requres the majority of correction for external torques and is only designed to have a life of thirty days. Hence this design does not have the constraints which would be applicable for a fully positioned stabilized vehicle which operates for periods longer than a year in a limit cycle mode with only occasional maneuvers and external torque corrections. The

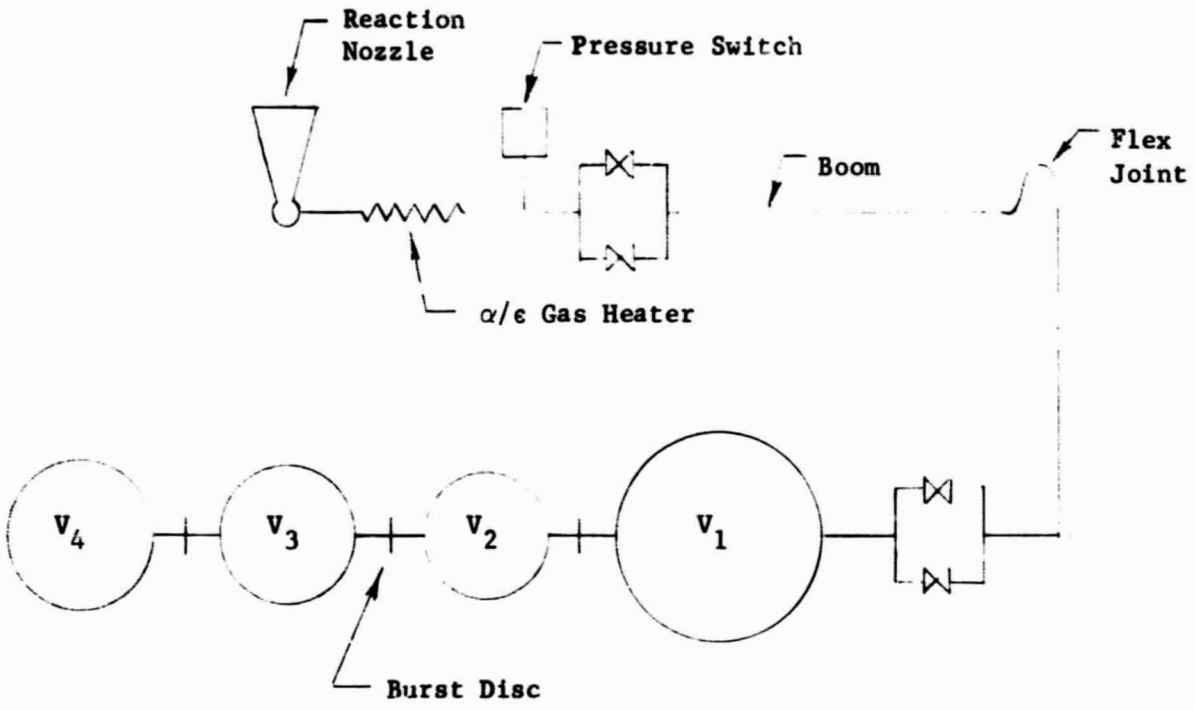

FIGURE 3-2 SCHEMATIC DIAGRAM

MULTI-TANK STORAGE AND SUPPLY SYSTEM - PIONEER SPACECRAFT

precess control system proposed for the Pioneer is not applicable to earth orbit satellites which normally have spin decay and also require spin control.

All of the elements of the proposed systems are considered within the existing state of the art. The proposed systems also consider the placement, command and function of the existing systems. More than one system is proposed for both the Bios and Pioneer vehicles. At least one of the proposed systems may have several component placement, guidance requirement or functional changes.

The preliminary design of each of the elements and subsystems is presented below. Appendix A provides the technical support only for the items incorporated in the proposed system selected for further investigation. Technical support for all systems proposed are contained in the Task IV Design Report. The proposed systems are considered equivalent to the existing systems and are based on information on performance, requirements, installation and control logic provided by NASA ARC.

3.2.1 PIONEER

The design and performance constraints of the existing Pioneer spacecraft were used as requirements for the proposed potential replacement systems. The proposed designs are considered capable of meeting all critical performance requirements while having an improved reliability and a higher probability of mission success.

Several comments concerning extended mission requirements are also discussed. The possibility of orbits having a minimum distance of the spacecraft from the sun of 0.25 AU were considered. Necessary design features in critical areas to maintain efficient system performance are described.

a. Proposed Systems. Two supply and distribution systems are proposed for the Pioneer spacecraft. Each of these proposed systems differs from the existing system in that a pressure regulator is not required. One system also eliminates completely the necessity of the relief valve. In addition, the delivered specific impulse (I_{sp}) at the reaction nozzle has been increased by utilizing solar energy to heat the gas prior to nozzle admission. Redundancy of all critical active elements is also provided so that any one failure will not cause a mission failure. The proposed systems are described below.

(1) Multi-tank. The multi-tank storage and supply system is shown in Figure 3-2. As shown, the storage and supply system consists of 4 tanks in series with a burst disc between each of the tanks. (As noted above, no pressure regulator is required with this system.) The working pressure level variation is shown in Figure 3-3. At time zero the supply pressure is equal to the pressure in the first tank (P_o). As gas in the first tank is depleted, the pressure decays to a level (P_B) such that the burst disc between V_1 and V_2 ruptures and the working pressure level in the two

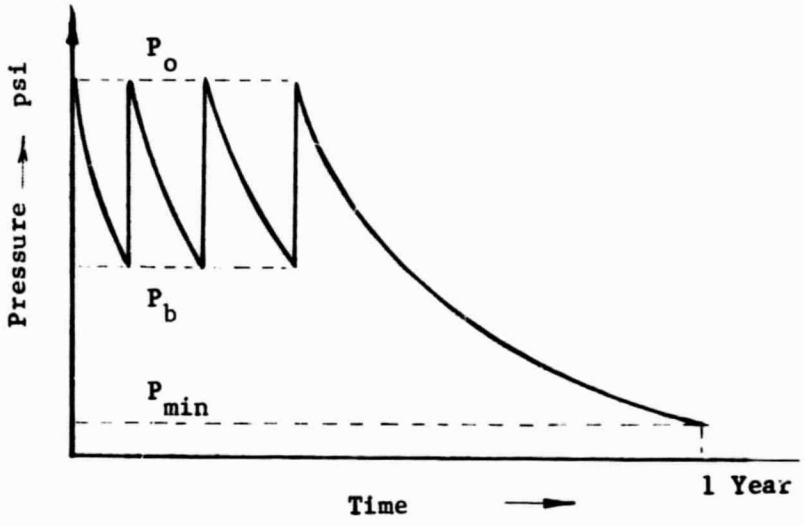

FIGURE 3 SUPPLY PRESSURE
MULTI-TANK STORAGE SYSTEM

tanks (V_1 and V_2) becomes equal to P_o. Again the pressure level decays with gas usage to the burst disc rupture level (P_B) and the disc between V_2 and V_3 ruptures. The pressure level in the three tanks becomes equal to P_o and the cycle is repeated. (This sequence of events may be repeated ad in finitium approaching a constant supply pressure level.) The proposed number of tanks, 4 and the pressure levels (in psia) P_o = 800, P_B = 200, and P_{min} = 50 are taken from the results of a parametric study presented in the Appendix. After all burst discs have been ruptured, the pressure level decays to its minimum usable value (P_{min}). The total mass in the system to this pressure level is considered usable.

The distribution system is also shown in Figure 3-2. This system consists of parallel valves between the multiple tank supply and the boom. The gas is heated in the boom to its normal temperature (a black paint with a solar absorbtivity to emissivity ratio (α/ϵ) = 1 has been selected as an appropriate boom surface coating). The gas passes through the boom and through a second parallel valve arrangement and is admitted to the gas heater. This heater employs a solar absorbtivity to emissivity ratio (α/ϵ) of approximately 10 to produce high heater metal temperatures. Said hot metal heats the gas to approximately 320°F at 1 AU prior to nozzle admission. This higher gas temperature results in a delivered I_{sp} of 91 seconds as compared to an I_{sp} of about 75 seconds at 70°F resulting in a lower mass depletion rate for a given thrust level.

In the proposed multi-tank system there are only four solenoid valve (active) elements, 3 (single action) burst discs, 4 high pressure GN_2 containers, 4 (inactive) fill connections, one (static) filter and a (passive) heating element. Failure protection of the lowest reliability element, the solenoid valve, is provided by functional redundancy so that any single failure will not cause a mission failure. The burst discs are also used in parallel to protect against failure to burst and extreme ΔP burst variation. (Leakage is not a problem and parallel paths are acceptable.) All the remaining elements are essentially inactive and once checked should not experience any failures.

If the thrust variation caused by the variable supply pressure is not tolerable a simple digital metering element can be used to reduce the thrust variation. The metering element would be placed between the final parallel shut-off valve and the booster heater. The metering device is pressure difference sensitive so that as the pressure level increases the flow area decreases. By using discreet steps the open-close set point can be accurately set. Using a greater number of elements will provide a more uniform thrust. If any single element of the metering device fails (open or closed) only an additional slight thrust variation is noted.

(2) Liquid N_2 Stroage. The nitrogen propellant gas can be stored as a cryogenic liquid, as a super-critical fluid, or as a gas in thermal equilibrium with the surroundings. Liquid storage in this case should more realistically be called saturated liquid storage because the nitrogen is in thermal equilibrium in two phases within the tank. This form of storage has been shown to have the least tank and system weight and volume of the three systems because the nitrogen is denser and it is stored at low pressure. The weight of the storage and transfer equipment is reduced

to such an extent that is far more than offsets the additional weight required for thermal insulation.

The disadvantages of cryogenic saturated liquid storage are the need for thermal insulation and/or availability of a radiation heat sink to maintain the cold temperatures, and the problems associated with launch preparations and two-phase fluid transfer in reduced or near zero gravity fields. Calculations show that it is possible to store liquid nitrogen for an indefinite period in space provided a "window" is provided for exposure of a portion of the tank to thermal radiation losses to space. The vacuum environment makes the super insulation type of material attractive for reduction of heat leakage from surrounding satellite structure into the tank to a very minimum. The low gravity fields in slowly rotating bodies can introduce fluid metering and withdrawal problems from storage tanks, and heating by pool nucleate boiling if required, can become increasingly difficult because liquid and vapor phases are stored in equilibrium saturated conditions, and buoyancy must be relied upon for separation.

The super-critical fluid storage concept has no problems relating to the effects of zero or reduced gravity fields. However, super-critical nitrogen must be stored at a pressure greater than 492 psia in order to exist in equilibrium in a single phase at all levels of temperature. This pressure is an order of magnitude greater than proposed for a saturated liquid storage system. Tankage weights must be proportionately higher in order to provide the necessary structural strength. Additionally, the volume requirements are high because the density is decreased from 47 Lb/Ft^3 at saturated liquid (and typical cryogenic storage temperature of -300°F) to 19.2 Lb/Ft^3 at the critical point. Because the system weight is the most important single criterion in selecting methods of nitrogen propellant storage, the cryogenic saturated liquid method has been chosen.

The cryogenic nitrogen system for the Pioneer consists of a central spherical storage tank and a flow system designed to maintain constant storage pressure by transferring a regulated amount of heat into the tank when nitrogen is withdrawn. This system functions as illustrated on Figure 3-4. Upon demand for gas by the thruster, nitrogen vapor is withdrawn from the center portion of the tank. This portion being filled with vapor because tank rotation causes the liquid to transfer to the periphery. The vapor withdrawn passes through an external heat exchanger where it is heated by conduction and radiation from surrounding materials inside the satellite. Because the nitrogen flow is very low and the temperature differential between the internal satellite environment and the nitrogen is initially 370°F, a small heating surface area, only 1.0 ft^2 is required. As shown, the nitrogen is thereby heated from -300°F to approximately 40°F and passes through a tube coil mounted inside the tank, where heat is rejected to evaporate sufficient nitrogen to maintain constant storage pressure. Again the low flow rates and relatively high mean temperature differences yield a small surface area requirement. It has been estimated that 2 feet of 0.25 inch O.D. tubing will suffice. This can be readily incorporated into the tank as a coil around the inside periphery. The nitrogen emerges from this coil at a temperature of -280°F and is ultimately passed through the boom to the thrust nozzle. While flowing through the boom it is heated first to the boom temperature and then further at the nozzle exhaust location by solar radiation.

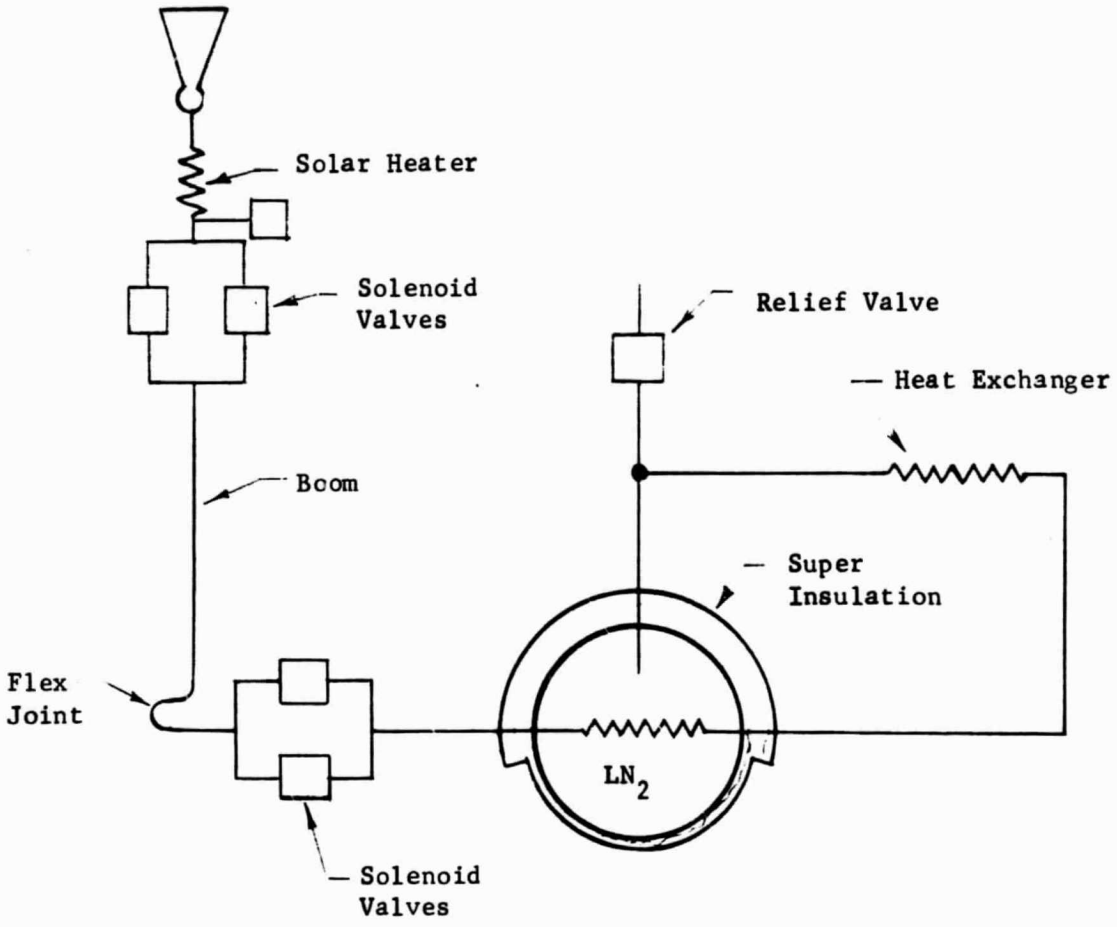

FIGURE 3-4 SCHEMATIC DIAGRAM
LIQUID N_2 STORAGE SYSTEM

The system shown in Figure 3-4 is comprised of four active solenoid valves, an inactive relief valve and backup burst disc, an insulated liquid N_2 storage tank and three heat exchanger elements. Specific components to be designed in this system include the tank and appropriate insulation, the external heat exchanger, the heat exchanger inside the tank, and the final gas heating system at the reaction nozzle.

The four solenoid valves provide functional redundancy to protect against a single leakage, failed closed or failed open element. The relief valve is backed up by a burst disc, since these will only operate if there has been a system failure or the system operating with non-design environment or duty cycle. The relief valve and burst disc are set to relieve at a pressure of about two times the design operating pressure. The remaining elements are inactive and should not contribute to system failures once checked out.

b. Existing Design Summary. The existing Pioneer spacecraft gas supply and distribution system is shown in Figure 3-5. As shown, the system consists of a storage tank, pressure regulator, feed line, solenoid valve, thrust nozzle, and pressure switch. The system just described has no redundant features and a singular failure of any component part of the system results in total system failure.

c. System Comparison. The proposed systems are compared with the existing system in summary in Tables 3.1, 3.2 and 3.3. Table 3.1 compares the three systems on the basis of performance criteria established in the program work statement. Tables 3.2 and 3.3 provide backup information for the first table. Each of the parameters noted in Table 3.1 are discussed below:

(1) Performance. The thrust variation of the proposed multi-tank system is greater than the existing system by virtue of the blowdown of four tanks in sequence. The thrust level will vary by the ratio P_o/P_B (4:1 thrust variation) over the programmed mission and by the ratio P_o/P_{min} over the latter part of the mission if excess gas was consumed or larger than planned slow maneuvers required. Thrust response on the proposed system will be comparable to the existing system, i.e., the volume downstream of the last shut-off valve is larger but the valve response is faster. The total duct manifold volume is less in the proposed system due to use of smaller diameter lines and the working pressure levels are higher. Command and environmental requirements for the proposed system are no different than for the existing system.

The thrust variation of the proposed LN_2 storage system will be somewhat greater than the existing system. The variation will not be as great however as the variation anticipated with the multi-tank system. Thrust variation will be experienced on a transient basis i.e., fluid (or energy) is withdrawing from the tank and the pressure will decay. Said decay will be compensated for by flash evaporation and the addition

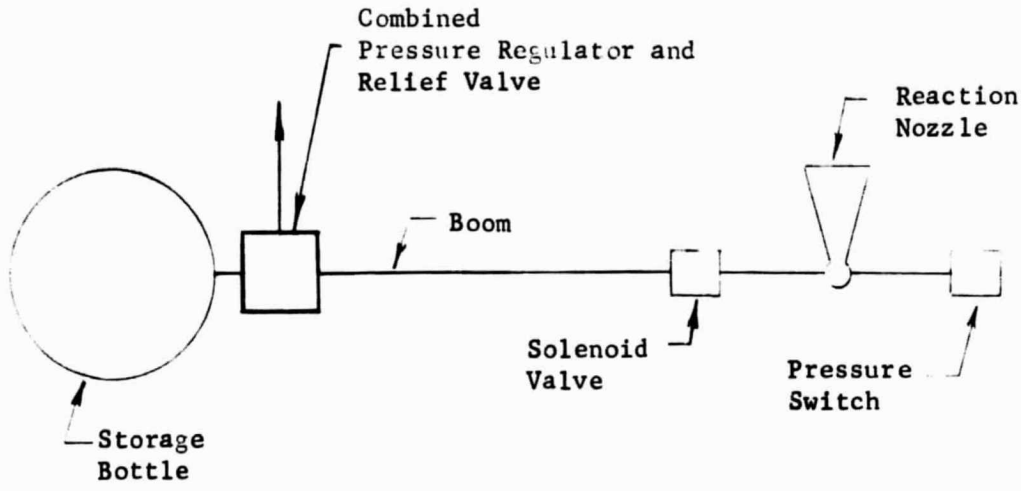

FIGURE 3-5 SCHEMATIC DIAGRAM

EXISTING GAS AND SUPPLY SYSTEM - PIONEER SPACECRAFT

TABLE 3.1

SYSTEM COMPARISON

	Existing Pioneer System	Proposed Multi-Tank System	Proposed LN_2 System
1. Performance			
Thrust Variation		Greater than existing	Some (5-10%) variation
Thrust Response		Comparable to existing	Comparable to existing
Command Requirements		Same	Same
Environment Requirements		Tanks pressurized to two levels	Pre-launch limitations
2. Total Impulse	65.3	65.3	65.3
3. Specific Weight = $\frac{\text{Total Impulse}}{\text{Total Weight}}$, $\frac{\text{lb-sec}}{\text{lb}}$	14.1	14.8	21.2
4. Specific Volume $\frac{\text{Total Impulse}}{\text{Total Volume}}$, $\frac{\text{lb-sec}}{\text{in}^3}$	0.50	0.41	0.35
5. Specific Power $\frac{\text{Total Impulse}}{\text{Total Power}}$, $\frac{\text{lb-sec}}{\text{watt}}$	3.1	2.3	4.1
6. Redundancy & Reliability	See Table 3.3 for comparison of active elements.		

TABLE 3.2

COMPONENT PARTS OF EXISTING AND PROPOSED SYSTEMS

Existing System	No.	Wt.	Vol.	Pwr.
Bottle	1	1.54 lb	104 $in.^3$	
Gas		0.87	-	
Valve	1	0.44	2	21 watts
Regulator	1	0.99	7	
Nozzle	1	0.01	-	
Transducer	1	0.21	2	
Pressure Switch	1	0.12	2	
Plumbing & Misc.	—	0.46	13	
TOTAL	6	4.64 lb	130 $in.^3$	21 watts
Multitank System				
Bottles	4	2.3 lb	140 $in.^3$	
Gas		0.73	-	
Valve	4	0.35	6	7 watts each
Transducer	1	0.21	3	
Pressure Switch	1	0.12	2	
Solar Heater	1	0.1	1	
Plumbing & Misc.	—	0.6	7	
TOTAL	11	4.41 lb	159 $in.^3$	28 watts
Liquid Nitrogen System				
Bottle	1	0.55 lb	47 $in.^3$	
Gas		0.73		
Valve	4	0.30	6	4 watts each
Transducer	1	0.21	3	
Pressure Switch	1	0.12	2	
Solar Heater	1	0.1	1	
Gas Heater	2	0.1	inside tank	
Plumbing & Misc.		0.5	6	
Insulation	—	0.46	124	
TOTAL	10	3.07 lb	189 $in.^3$	16 watts

TABLE 3.3

COMPARISON OF ACTIVE ELEMENTS

PIONEER SPACECRAFT

	Existing	Multitank	LN_2
Elements	1 valve	1 redundant valve (4 elements)	1 redundant valve (4 elements)
	1 regulator	3 burst discs	none
	1 relief valve	none	1 inactive 1 burst disc
	1 filter	1 filter	1 filter
Reliability	Low	High	High
	Any single failure fails mission	redundant elements on low reliability element. Any single failure of low rel. elements acceptable	redundant elements on low reliability element. Any single failure of low rel. elements acceptable. Relief valve only operates if a failure has already occurred.

of heat from the return line (on a steady state basis such thrust variation would not be realized. Some variation in practice is anticipated, however, due to the transient nature of the heat addition). The pneumatic response of the proposed system will be comparable to that of the existing system. The line length downstream of the last valve pair is slightly larger but valve response faster. In any case a delay can be compensated for in the guidance circuit. Command requirements for the proposed system are the same as those on the existing system. Environmental requirements are however more demanding. The cryogenic nitrogen must be protected on the launch pad to prevent excessive boil-off. One method of achieving this would be a helium gas purge.

(2) Total Impulse. The total impulse of the existing system is equal to the specific impulse ($I_{sp} \approx 75$ sec) times the mass of the nitrogen gas (W = 0.87 lb) which is: I_T = 65.3 lb-sec. The total impulse of the proposed system would be higher for the same amount of mass by virtue of the utilization of solar energy to heat the nitrogen gas in a small heat exchanger between the last valve pair and the reaction nozzle (see Figure 3-1). A gas temperature of 320°F is predicted at 1 AU. This will increase the I_{sp} from 75 seconds to 91 seconds. The total impulse of the LN_2 system will be comparable to that of the multi-tank system, i.e., the solar heat exchanger will raise the I_{sp} to a value comparable to that discussed in the multi-tank system.

(3) Specific Weight. The total weight of the proposed multi-tank system is nearly the same as the total weight of the existing system, i.e., the pressure regulator and relief valve have been eliminated but two paralleled valves have been used to attain redundancy and the nitrogen is stored in four tanks rather than one. Theoretically, the weight of the multiple tanks is the same as the weight of a single tank if each tank is optimized. This does not however account for such things as flanges, bosses, fittings, etc. Calculations indicate that the four tank weight is 2.3 pounds as opposed to 1.54 pounds for the existing bottle. Specific weights for the proposed and existing systems are shown in Table 3.1.

The weight of the LN_2 system is also comparable to the existing system, see Table 3.2. The storage bottle is lighter and the pressure regulator has been removed. Insulation and additional tubing have been added which offset the weight reduction.

(4) Specific Volume. The volume of the proposed multitank system will be greater than the volume of the existing system. Parametric studies have been completed which show the relative tank volumes for a multi-tank storage system. The storage volume for the proposed four tank system is 140 in^3, compared with an existing tank volume of 104 in^3.

The specific volume of the proposed LN_2 system will also be greater than that of the existing system. This is due primarily to the addition of the super insulation (0.46 pounds @ 266 in^3/lb).

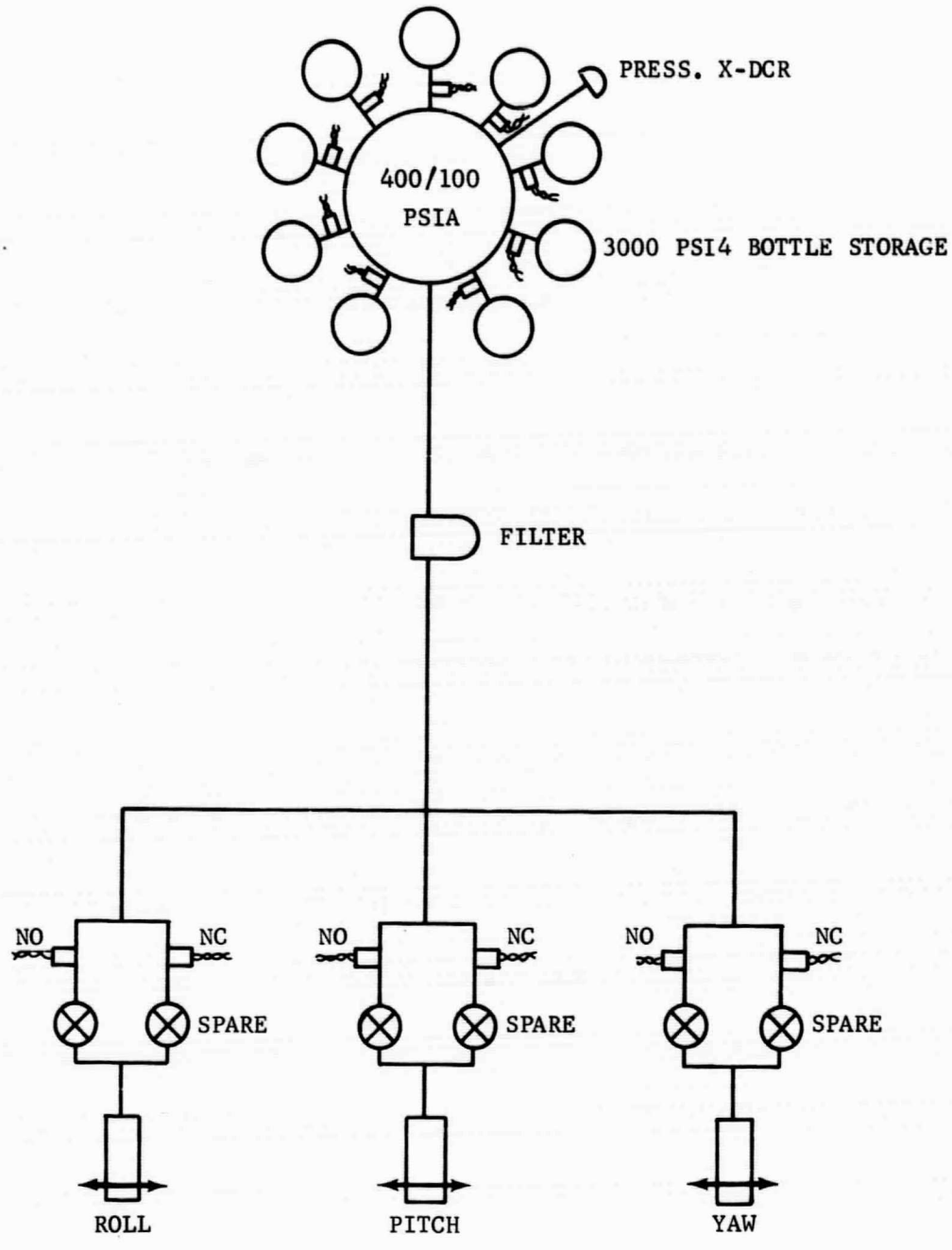

FIGURE 3-6. BIOSATELLITE COMMAND REDUNDANT SYSTEM

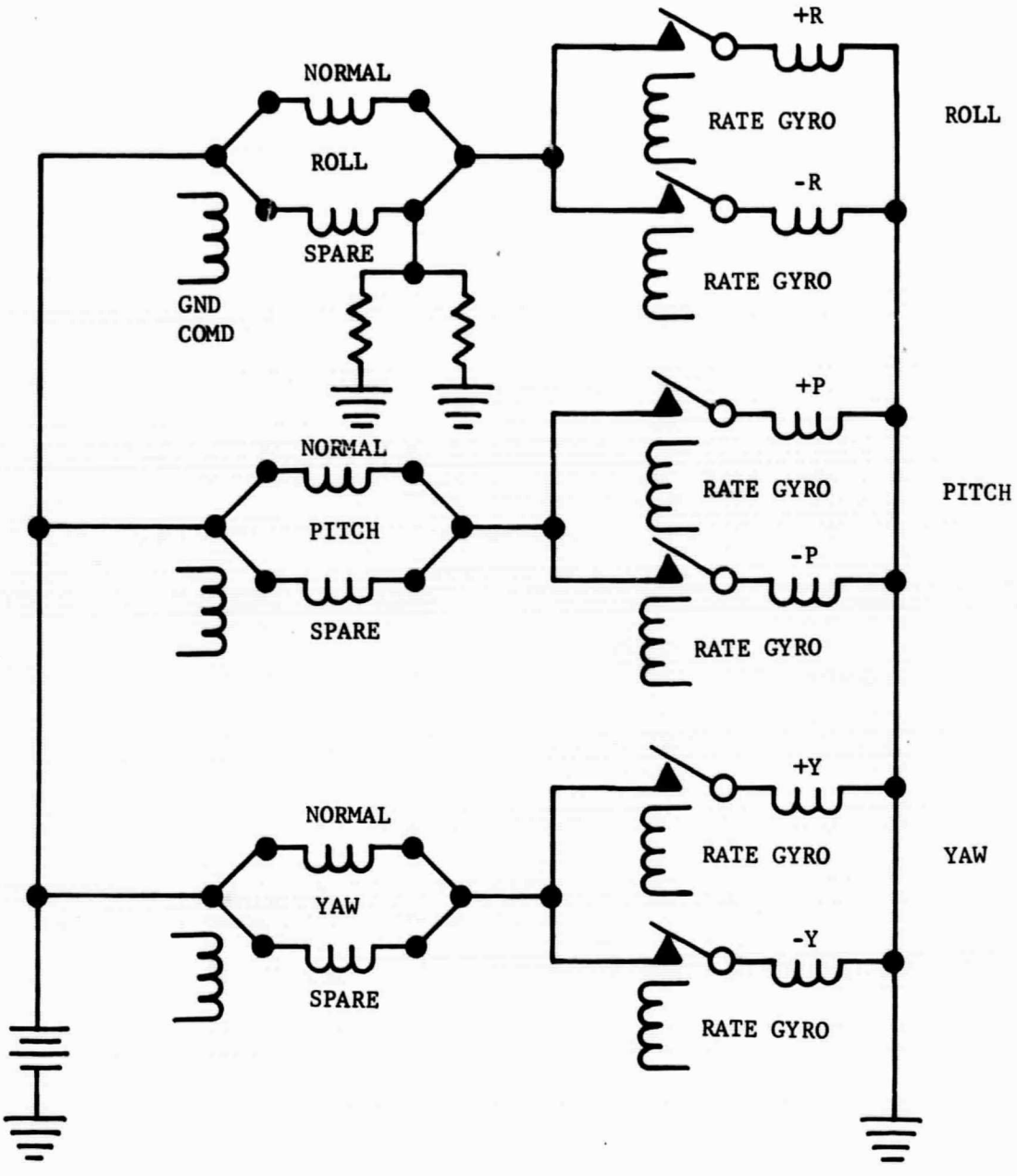

FIGURE 3-7. COMMAND REDUNDANT THRUSTER CONTROL CIRCUIT DIAGRAM

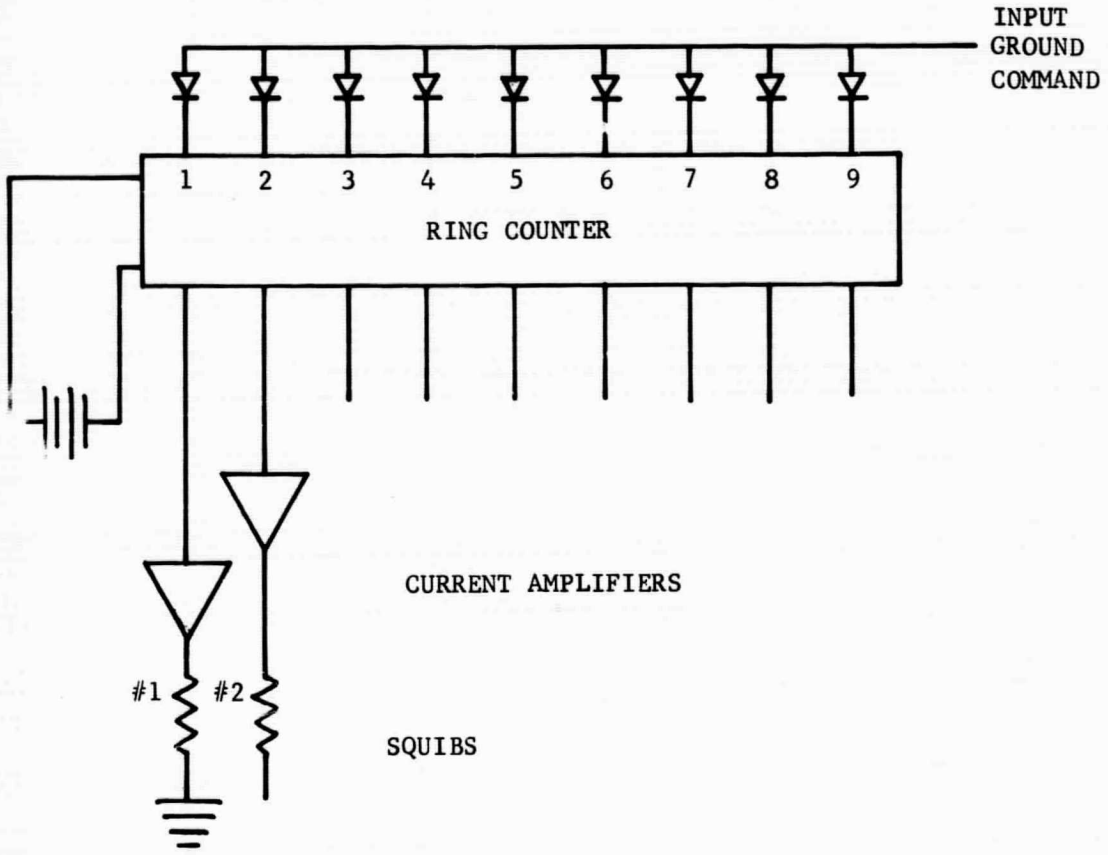

FIGURE 3-8. COMMAND REDUNDANT SQUIB CIRCUIT DIAGRAM

a supply line for each of the three control axes with an on-off valve and a diversion valve in each supply line. Each on-off valve that is normally operational is in series with a normally open squib valve and in parallel with a spare on-off valve and normally closed squib valve. The multitank gas supply consists of nine small tanks, each pressurized to 3000 psi and connected through a ground commanded squib valve (or similar device) to the "regulated" tank whose pressure is initially set at 400 psi. The pressure in the regulated tank is allowed to cycle from 400 to 100 and back to 400 by appropriate ground commanded firing of the squib valves. The regulated tank pressure is telemetered and allows ground command control of the tank pressure by employing the circuit shown in Figure 3-8.

The ring counter shown in Figure 3-8 is a circuit that sequentially transfers voltage from one load to the next when a number of loads are connected in parallel. When power is applied to the ring counter, all stages are initially off. A pulse input to the common input will sequentially energize each load. If the count is stopped at any stage, say the third, and the power to the ring counter interrupted, the ring counter will automatically reset to zero when the power is again applied. Four pulses must then be fed to the input to energize the fourth stage. The ring counter does not have a memory when the power is turned off. The output off each stage of the ring counter will go to a current amplifier which will fire a squib when that stage is energized. Flip-flops and other logic circuits can perform this function. However, the ring counter requires fewer components. Figure 3-8 is a block diagram of a nine stage ring counter with input and output stages.

Normal operation of the entire system is as follows. Subsequent to separation of the spacecraft, the system is activated. Acceleration about any of the three control axes is then accomplished by an onboard signal from the rate gyro actuating the appropriate on-off and diversion valves as indicated in the schematic diagram. Simultaneous control about any two or all three axes is similarly obtained.

Redundancy is provided in this system in several ways. Internal leakage of the thruster on-off valves is considered to be the most probable source of system failure. Provision for leakage protection is achieved by use of the spare on-off valve provided in parallel with each of the normally operated on-off valves. (The seriousness of a leak is diminished by use of the diversion valve since no net system torque can be produced by the leak.) Use of the spare on-off valve is accomplished by ground command switching the electrical circuitry to this valve and simultaneously firing the normally open and normally closed squib valves as indicated in the schematic diagrams. The possibility of a leaking regulator and subsequent gas loss through the relief valve or a leaking relief valve is, of course, eliminated by the multitank design. Parallel connecting of the pressure tanks to the regulated tanks (rather than series connecting) provides redundancy against a squib valve failure. Mechanical failure of the diversion valve is considered to be too improbable to be of consequence, since in the operating condition leakage of a small percentage through the closed port can be tolerated and in the nonoperating condition spring forces are so great as to make a stuck-closed valve almost inconceivable. Current data show that the diversion valve is more than an order of magnitude more reliable than normal on-off solenoid valves.

(2) Self-Contained Redundant Systems. A functional component schematic of the proposed self contained redundant system (SCRS) is presented in Figure 3-9. Figures 3-10 and 3-11 show an electrical circuit schematic and diversion valve "A" command circuit. Complete redundancy of all critical elements is attained by on-board components and no ground commands are required to protect against a single failure.

The basic components of this sytem, shown in Figure 3-9, consist of the LN_2 tank with relief valve, a heat exchanger (flash boiler), 3 parallel valves, and four diversion valves arranged as indicated in the schematic. Use of the LN_2 eliminates the regulator and reduces the volume compared with the original arrangement.

Normal operation of the system is as follows: The relief valve is located at the top of the tank so as to insure vapor venting prior to and during liftoff. During zero "g" conditions the vapor will position itself around the liquid. Separation of vapor and liquid is accomplished by use of radial fins[8] which by capillary action locate the liquid at the center of the sphere. The system will be maintained at approximately 50 psia by the relief valve. Acceleration for control is then accomplished by a command signal which operates the proper solenoid valves and diversion valves for the correction required. Simultaneous roll and pitch correction requires that diversion valve "A" be nulled. This is done by the electrical circuit shown in Figure 3-11 so that with both pitch and roll commands no current is supplied to valve "A". The greatest electrical power requirement occurs when simultaneous torques about all three axes are demanded. In that case, current must be supplied to six on-off valves and three diversion valves.

In Figure 3-11, current flow through R_R generates a signal to amp A_R. The output of amp A_R turns Q_R on. The same is true for R_P, A_P and Q_P. Amp A_{RP} turns Q_{RP} on when Q_R or Q_P is on. Input to amp Q_{RP} is unbalanced. When Q_R and Q_P are both on or both off, input to Amp A_{RP} is balanced and the output is zero and the diversion valve nulled and Q_{RP} is off.

System redundancy is provided by the parallel valves in series for the on-off valves and a "quad" relief valve arrangement (since the relief valve is about 1 $in.^3$ the weight and volume penalty is not great). Again, the diversion valve essentially has no leakage type failure mode. In the control valve arrangement shown in Figure 3-9 if the common parallel on-off valve leaks there is no system gas loss. If one or both of the downstream parallel on-off valves leak, one manifold full of gas is lost each orbit (system is assumed to be active only 5 minutes per orbit as is existing system). The manifold volume is only 1/2 $in.^3$ and the pressure is about 50 psia so only .00007 pound of gas is lost each orbit. This gas weight loss is negligible when compared with the control gas requirement for each orbit.

The proposed nitrogen storage system must provide gas for life support in the experiment section of the vehicle. The gas to that system primarily would be drawn from the liquid cluster and vaporized in a flash heater. However a parallel circuit is provided so that some vapor from a capacitance volume is used on each cycle for life support flows. Approximately 6 pounds

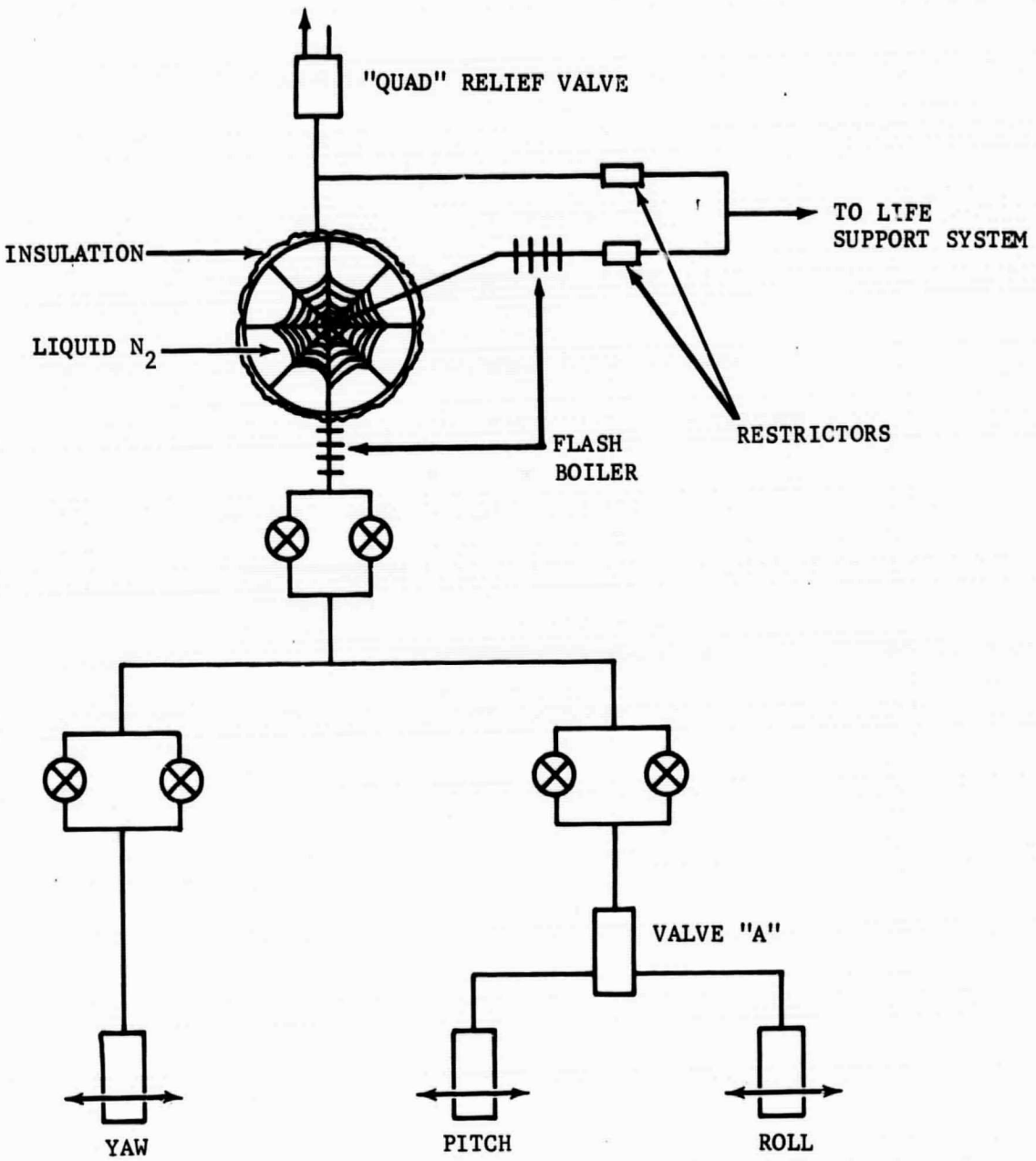

FIGURE 3-9. BIOSATELLITE SELF REDUNDANT SYSTEM

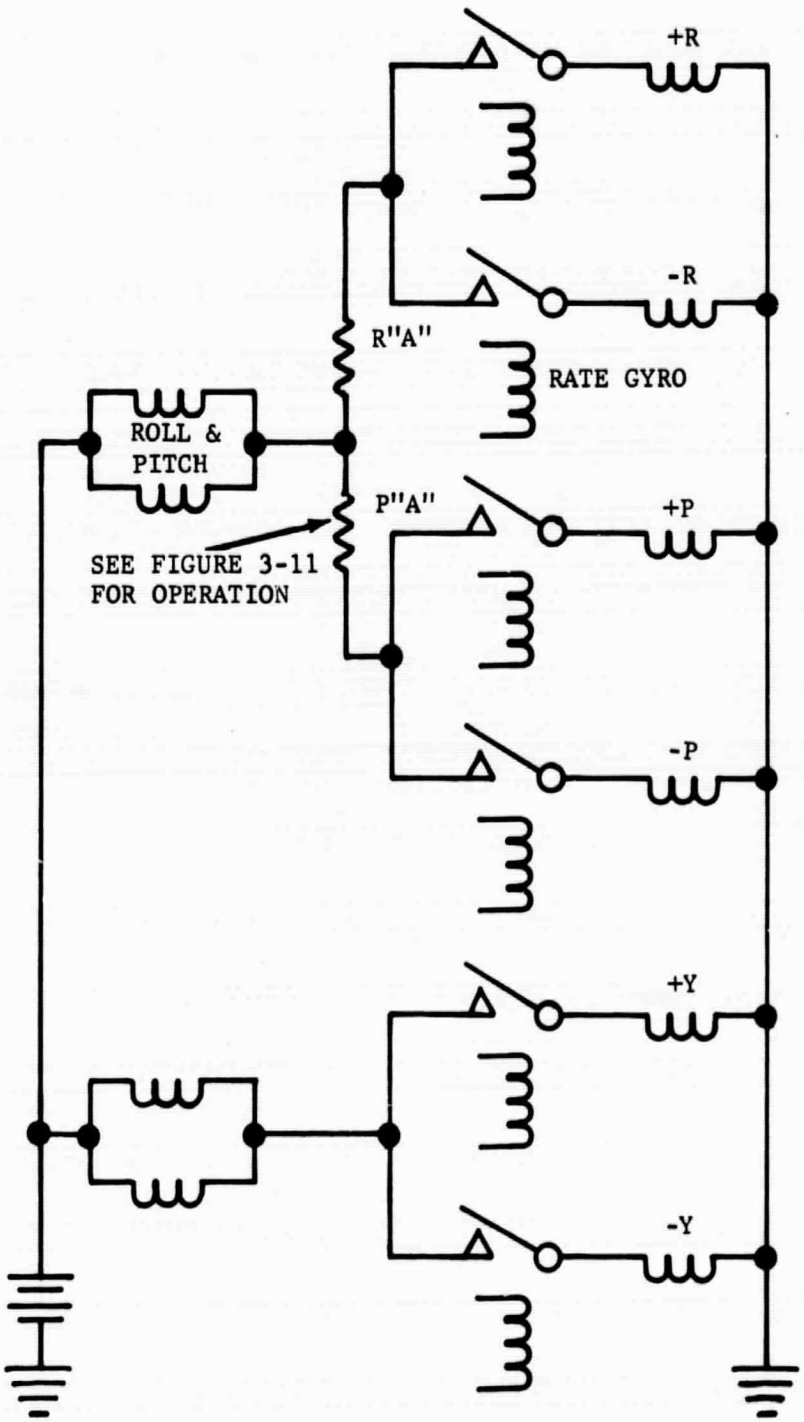

FIGURE 3-10. SELF REDUNDANT SYSTEM CONTROL CIRCUIT DIAGRAM

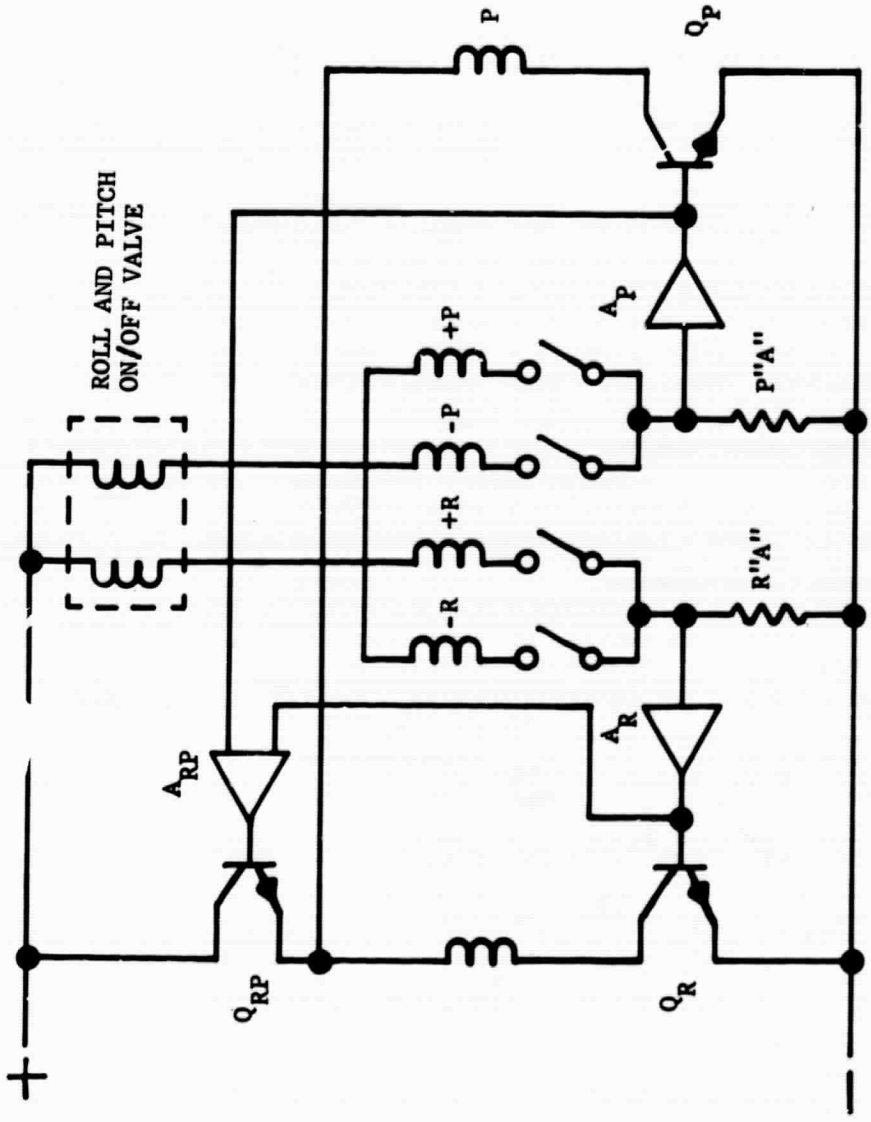

FIGURE 3-11. DIVERSION VALVE "A" COMMAND CIRCUIT DIAGRAM

of boiloff has to be vented in a 30-day period for the tank design selected. The Bios experiment section uses about 12 pounds of N_2. The life support flow circuit, illustrated in Figure 3-9, will have the volume and restrictors sized so that about 3 pounds of vapor will then be injected into the experiment flow for a nominal (12-pound usage) mission. In this way only about 3 pounds of N_2 will have to be vented (and lost) by the relief valve to maintain system pressure.

b. Existing Bios System. The existing Biosatellite is shown schematically in Figure 3-12. Performance factors, installation information and system requirements for the Biosatellite were provided by NASA-ARC.

c. System Comparison. The two proposed systems are compared to the existing system on the basis defined in the work statement. The factors for comparison are: (1) performance (thrust variation, thrust response, command requirements, environmental requirements, and minimum impulse bit size), (2) total impulse, (3) specific weight, (4) specific volume, (5) specific power and (6) functional redundancy.

Table 3.4 presents a tabulated comparison of the proposed systems with the existing based on the criteria called out in the program work statement. Comments on each of the comparative parameters are contained in the table to summarize system characteristics previously covered. The detailed weight and volume breakdown of the systems to calculate the specific weight and specific volume are presented in Tables 3.5 and 3.6, respectively.

The multitank GCRS is a little heavier and bulkier than the existing system. Since the stored total impulse is identical the specific weight and volume figures are poorer. However, the GCRS has the same specific power as the existing system. The LN_2 SCRS system is lighter and smaller than the existing system, hence the specific weight and volume figures are better. More solenoid operated valves are used on the SCRS arrangement and therefore the specific power factor is a little worse than that of the existing system.

As reflected in the summary table the greatest improvement of both the proposed systems as compared to the existing systems is in functional redundancy. The work statement says (quote) - "and most important of all functional redundancy." The proposed systems both provide sufficiently redundant systems so that any single failure)(of active or most likely failure modes) can be tolerated without mission failure. The functional redundancy is provided without significant sacrifice of other comparative parameters, in fact some improvements are provided, and it is concluded that the proposed systems are superior.

3.3 SYSTEM SELECTION

On October 24, 1967, the improved conceptual system designs for the Pioneer and Biosatellite were presented in a joint meeting between NASA Ames Research

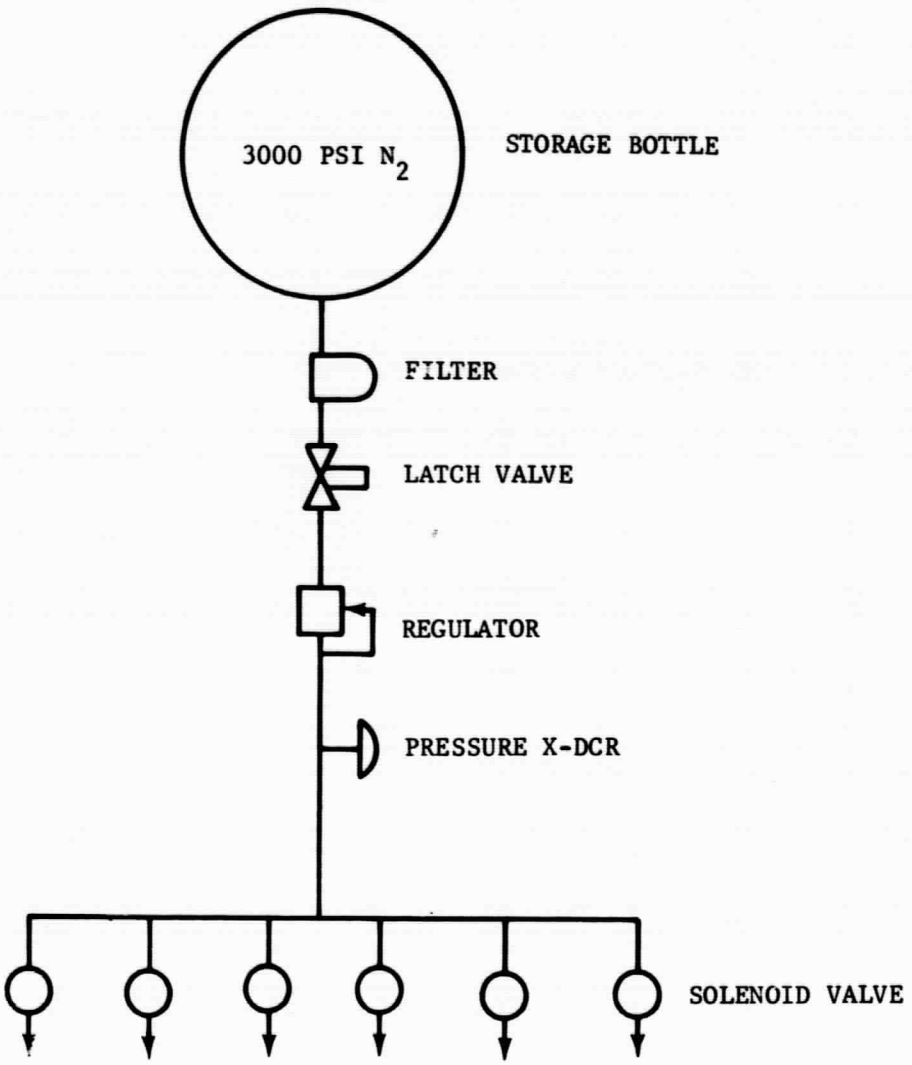

FIGURE 3-12. EXISTING BIOSATELLITE SYSTEM

TABLE 3.4

COMPARISON OF EXISTING AND PROPOSED BIOS SYSTEMS

	EXISTING SYSTEM	PROPOSED GROUND COMMAND REDUNDANT SYSTEM	PROPOSED SELF-CONTAINED REDUNDANT SYSTEM
1. **PERFORMANCE**			
a) thrust variation	thrust variation is small because of regulator & close coupling of on/off valve to thrustor	thrust variation is larger because of pressure variation in multitank arrangement	about the same as existing system
b) thrust response	good because of close coupling of valve to thrustor	essentially the same but slightly slower because of larger volumes	essentially the same as existing system
c) command requirements	latching and unlatching of tank valve and rate gyro signals are only command required	one additional ground command required. Latch valve circuit used to open multitanks and additional circuit for switch to spare valves	no commands other than signals from rate gyros. (Decrease of one ground command)
d) environmental requirements	no special requirements	essentially the same	cannot be held in ready condition for long periods without replenishing liquid nitrogen
e) min impulse bit size	small	smaller because of faster valve response and nulling of the diversion valve terminates thrust even though gas is still flowing	same comment as for previous system
2. **TOTAL IMPULSE**	1125 lb-sec	1125 lb-sec	1125 lb-sec
3. **SPECIFIC WEIGHT**	gas + components + plumbing, wiring and mounting brackets estimated at 40 lb total, corresponds to 28.2 lbsec/lb	slightly higher system weight estimated to be about 43.6 lb corresponds to 25.3 lbsec/lb	estimated system at 29.3 lb, corresponds to 38.5 lbsec/lb
4. **SPECIFIC VOLUME**	system volume estimated at 1900 in^3 corresponds to .59 $lbsec/in^3$	estimated volume = 2900 in^3 corresponds to .39 $lbsec/in^3$ approx. 25% less because of multiple tankage	estimated system volume = 1500 in^3 corresponds to .75 $lbsec/in^3$

TABLE 3.4 (continued)

	EXISTING SYSTEM	PROPOSED GROUND COMMAND REDUNDANT SYSTEM	PROPOSED SELF-CONTAINED REDUNDANT SYSTEM
5. SPECIFIC POWER	15 watts/valve assumed, worst case = 3 valves in operation at 15 watts/each hence 25 lbsec/watt	worst case requires 3 on/off valves (7 watt/each) plus 3 div. valves @ 2 watt/each) hence 41.6 lbsec/watt	worst case uses 6 on/off valves & 3 diversion valves. Valve design would be 4 watts/ on-off and 2 watts/ diversion, hence 37.5 lbsec/watt
6. FUNCTIONAL REDUNDANCY	no redundancy provided. Mission can be lost by a single failure in regulator, relief valve, or any of six thrustor valves, or latch valve failure to open	regulator, relief valve, and latch valve have been eliminated leak paths from tank are reduced from seven to three, paralleling pressure tanks provide redundancy against squib valve failure, spare on/off values and diversion valves provide redundancy against thrustor valve failure. Valve leaks do not produce disturbing torques which effectively cuts effect of leak in half because no gas needed to provide a counter torque	attitude control system has only 2 leak paths in place of seven. leak path protected by paralleled valves in series for on/off valves and "quad" relief valve configuration. valve leaks do not produce torques. Regulators and latch valve are eliminated from system.

TABLE 3.5

SYSTEM WEIGHT ESTIMATE

Item	Existing System	Multitank System	LN_2 System
gas	15.1#	15.3#	18.0#
tank	16.1#	14.9#	3.0#
insulation	none	none	0.2#
tank bosses & mtg. brackets	incl. above	2.0#	0.8#
tank connecting lines & squib valves	none	4.0	none
filter	.4#	.4#	none
latch valve	1.9#	none	none
regulator & relief valve	1.4#	none	0.2
press. x-dcr	.2#	.2#	.2#
heat exchanger	none	none	0.5
plumbing lines, ftgs & mtg. straps.	1.5#	2.0#	2.0#
on/off valves	2.4#	3.0#	2.4#
diversion valves		.8#	1.0#
thrusters	nil	nil	nil
wiring harness & mtg	.5#	1.0#	.8#
TOTAL	ϵ = 39.5#	43.6#	29.1#

TABLE 3.6

SYSTEM VOLUME ESTIMATES

Item	Existing System	Multitank System	LN_2 System
tank	1766 in^3 + 96.6 in^3 = 1863 in^3	52% larger = 2832 in^3	905 in^3
insulation (1" thick)	-----	-----	528 in^3
tank losses & mtg brackets	-----	8	2
squib valves & lines	-----	16	-----
filter	4 in^3	4	-----
latch valve	7 in^3	-----	-----
reg. & relief valve	6	-----	1
press. x-dcr	1	1	1
heat exchanger	-----	-----	12
plumbing lines, ftgs. & mtg. straps	20	20	20
on/off valves	12	14	8
diversion valves	-----	3	4
thrusters	-----	-----	-----
wiring harness & mtg.	3	4	4
ϵ =	1916 in^3	2902	1485

Center and Aeronutronic personnel. The purpose of the meeting was to select the most suitable system, or critical portions thereof, which would be evaluated in Task V of the program. After presentation, the concepts were discussed as to their relative performance, specific weights, specific volumes, specific power, functional redundancy, actual vehicle installation and envelope available, prelaunch and launch environment, and guidance and control command requirements. Based upon these considerations the multitank Pioneer system was selected as the system capable of meeting all system integration problems while providing a potential reliability improvement.

In order to meet envelope limitations a tank design which incorporated a single large plenum tank with the three smaller high pressure storage bottles contained within it was considered feasible. The tank weight would increase slightly above that shown in Table 3.2, however the multitank system is lighter than the existing system so some weight increases could be tolerated. The impulse booster heater was considered a unique component which has the potential of marked delivered impulse improvement and associated system weight saving with no sacrifice of reliability. Variation of thrust was acceptable since an electronic impulse integration ($K \int Pdt$) circuit was being considered to improve antenna pointing accuracy. However it was considered desirable to use a metering element to reduce the thrust variation from the 4:1 pressure variation to about 1.4:1 (using a three-element metering device).

As a result of this meeting, Aeronutronic was directed to build and test critical parts of the Pioneer thruster system. The elements deemed critical were the metering device and the booster heater. Besides actual steady-state thrust and impulse performance, the transient response was also considered important. The storage tank and burst disc arrangement was considered state-of-the-art which would require only development efforts. The metering element and impulse booster heater were to be sized for the approximate thrust level of the Pioneer spacecraft and the variable plenum pressure (800 psi to 200 psi) was to be simulated.

SECTION 4

SIMULATED PIONEER THRUSTER SYSTEM TESTS

Performance and response of the simulated Pioneer thruster system and concept feasibility were determined in Task V of the inert gas thruster system study program. The basic objectives of this phase were:

(1) Demonstrate the performance and dynamic response of the metering element as a function inlet pressure (800 psi to 200 psi).

(2) Demonstrate adequate heat transfer between heater and the flowing gas for the element size proposed and convert to equivalent specific impulse improvement.

(3) Demonstrate response of system downstream of shut-off valve for comparison with existing system specifications.

The simulated Pioneer thruster system is composed of a shut-off valve, metering element, booster heater and a reaction nozzle. The inlet pressure to the shut-off valve was varied from 800 psi to 200 psi to simulate the plenum pressure to be supplied by the multiple-tank burst-disc arrangement. The multiple storage tanks for the inert gas supply along with a flow metering element is essentially a "digital" pressure regulator. As the pressure of the supply tank falls, the metering element opens up additional flow orifices thereby reducing the degree of variation in flow rate. The burst discs which operate only once have a very high reliability. The metering device is reliable since a failure of one orifice element, or the complete device, will only effect the performance slightly so that a catastrophic failure will not occur and the mission possibly still completed.

The impulse booster heater has the effect of increasing the total impulse of the system and/or decreasing the specific weight. Operation of heater is based upon the use of an external surface condition, such as polished gold plate, which has a higher absorptivity coefficient for the short wave length solar radiation than an emissivity coefficient for its own lower temperature longer wave length radiation. As a result of this high "α/ϵ" ratio, equilibrium temperatures of 1000°F and 400°F at solar distances of .25 AU and 1.0 AU respectively, are predicted. Corresponding specific impulse improvements of approximately 50% and 20% are to be expected. Figure 4-1 shows the relative location and sizes of the various components in the complete Pioneer system.

The design, fabrication and tests of the metering element, booster heater and complete subsystem (valve-meter-heater-reaction nozzle) are presented in the paragraphs below.

4.1 FLOW METERING ELEMENT

4.1.1 PRINCIPLE OF OPERATION

The metering element is a "stepped" pressure regulator, in that, as the upstream pressure falls, it provides a saw tooth variation to the downstream pressure. Individual orifices are opened in the metering element in a series of steps as the pressure differential across the element falls. The use of this device in conjunction with the multi-tank gas storage, as proposed in the Task IV design report, eliminates the unreliability of the conventional regulator and relief valve. A conventional regulator, sized for the flow of the Pioneer thruster, must have a very small effective port size in order to regulate at the initial tank pressure of 3200 psi. Hence the possibility of leakage due to wear particles or system particle contamination is very real and must be provided for by the addition of a relief valve. This addition makes it possible that the gas supply may be lost overboard without being used. Such a possibility does not exist with the multi-tank and metering element system. With 4 storage tanks, the highest pressure the metering element ever "sees" is only $\frac{1}{4}$ that of the conventional regulator, hence its port size is four times as large. Also there is no requirement that the metering element ever be completely shut off, in fact, one orifice is always open. Therefore leakage in this sense does not exist and there is no requirement for a relief valve.

The acceptable degree of pressure (thrust) variation at the thruster nozzle determines the number of individual orifices required in the metering element. If the multi-tank arrangement allows a 4:1 pressure variation, then "n" orifices in the metering element will provide a downstream pressure variation of $(4)^{1/n}$. Hence two orifices give a 2:1 thrust variation; 3, a 1.59:1 variation; 4, a 1.415:1 variation, and

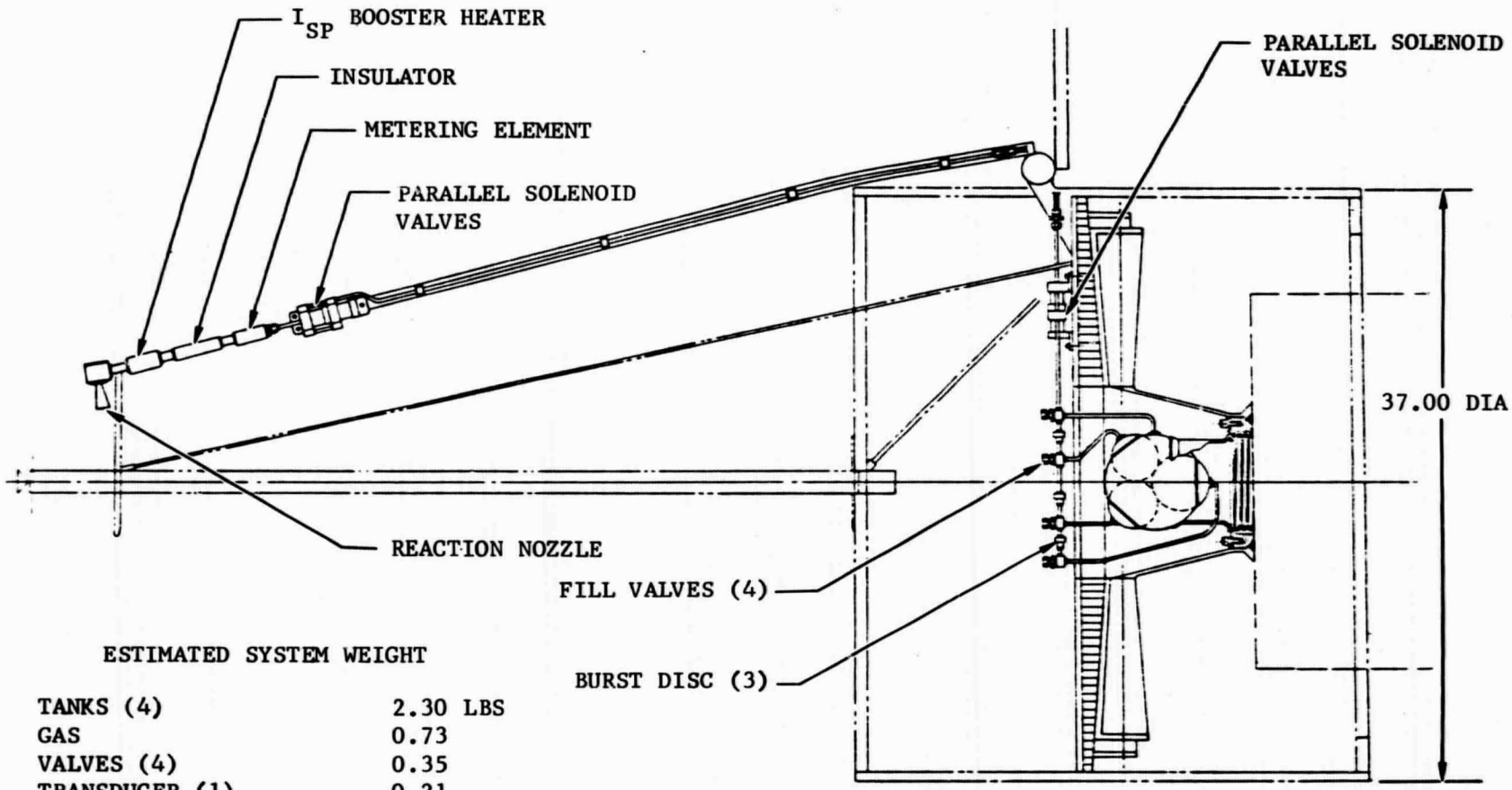

ESTIMATED SYSTEM WEIGHT

TANKS (4)	2.30 LBS
GAS	0.73
VALVES (4)	0.35
TRANSDUCER (1)	0.21
PRESSURE SWITCH (1)	0.12
SOLAR HEATER (1)	0.10
PLUMBING & MISC	0.60
TOTAL	4.41 LBS

FIGURE 4-1. PIONEER INERT GAS MULTI-TANK SYSTEM

so forth. Four orifices for this design seemed a reasonable compromise between pressure variation and component complexity. The number of orifices dictates their size. Unfortunately, they must all be sized differently if the pressure ratio (thrust ratio) from one step to the next is to be constant. Hence, if the pressure ratio is 1.415 (as above), the area of the second orifice is such that $1.415\ A_1 = A_1 + A_2$. The area of the third orifice is such that $1.415\ (A_1 + A_2) = A_1 + A_2 + A_3$ and similarly for the fourth orifice. For the design chosen here the pressures and orifice sizes come out to be the following:

Pressure at thruster = 50 psia minimum, 71 psia maximum (1.415 ratio)

Orifices Sizes	Opening Pressure
A_1 = .015 inches diameter	Always open
A_2 = .0096 inches diameter	Opens @ 566 psi
A_3 = .0115 inches diameter	Opens @ 400 psi
A_4 = .0136 inches diameter	Opens @ 283 psi

These areas are calculated on the basis of .17 lbs thrust with a specific impulse of 75 seconds and a .75 discharge coefficient. The chosen thruster pressures are arbitrary. They could be any values having the same 1.415 ratio. 50 and 71 were chosen as being reasonably near that of the present Pioneer system.

4.1.2 METERING ELEMENT GEOMETRY

Figure 4-2 shows a sketch of the assembled metering element. The lower part of Figure 4-2 is an enlarged view of one of the on/off orifices. In operation, when the upstream pressure is at 800 psi, all three on/off orifices are closed. Their caps are sealed tight against their flow tubes. The actual flow metering area is the annulus between the I.D. of the cap and the O.D. of the flow tube. When the upstream pressure falls from 800 psi to about 570 psi, the tension spring on one orifice is so adjusted to lift the cap off the tube and allow flow to occur re-establishing the downstream pressure to its initial value. The second on/off orifice is adjusted to open at 400 psi and the third one at 285 psi. In this way the downstream pressure varies in a saw tooth manner from approximately 70 psia to 50 psia, in four steps, as the upstream pressure falls from 800 to 200.

The design shown in Figure 4-2 was not the first design built. The first metering element was built using the concept as outlined in the Task IV design report wherein individually cantilevered reed elements uncovered

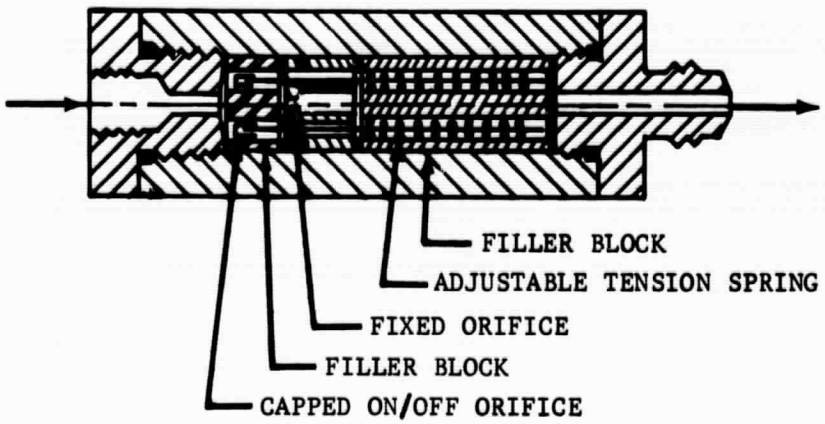

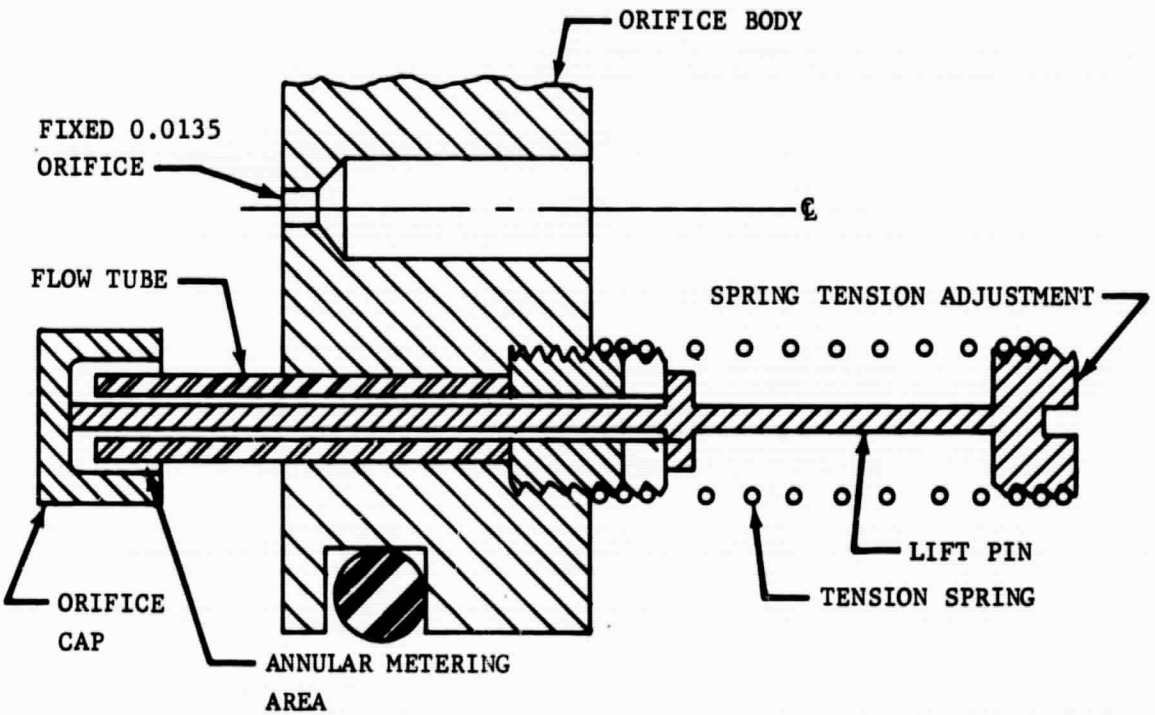

ON/OFF ORIFICE SHOWN IN ON CONDITION

FIGURE 4-2. ASSEMBLED METERING ELEMENT

additional flow ports as required by the falling upstream pressure. The concept was sound, but the degree of adjustment required to locate the spring loaded reeds exactly the right distance from the port entrance so that the opening differential pressure could be set as desired proved to be very difficult. If they were set to open properly they might never close and vice versa. The problem was the large change of pressure and flow forces with reed stroke. The design fabricated eliminates this problem because the actual movement of the cap can be quite an appreciable displacement without changing the differential pressure required to close the orifice.

4.1.3 METERING PERFORMANCE

The first tests of the metering element were made for the single purpose of adjusting the orifice sizes and spring tensions so as to provide the desired downstream pressure regulation. During these tests no attention was paid to the system response time. The filler blocks and other refinements shown in Figure 4-2 were not in the metering element. Figure 4-3 shows the results of these preliminary tests of the metering performance. The upstream pressure has been decreased in increments of 100 psi from 800 psi down to 200. As the curves show, the metering performance varies in the following manner:

Supply Pressure	Metered Pressure - Psig
800	44
700	33
600	58
500	65
400	48
300	49
200	28

These results are not as good as desired and reflect the fact that the orifice sizes and spring tensions were not adjusted to the proper values at the time these records were made. They do show, however, the regulating character of the metering element, as for example, the metered pressures at 800 and 300 are practically the same. It is clear that the first orifice opened somewhere between 600 and 700 psi, hence the spring tension was too great; the second orifice opened between 500 and 600 (instead of 400) again too much spring tension; and the third orifice opened between 300 and 400. Subsequent adjustments of the spring tension and orifices gave results very close to the design values.

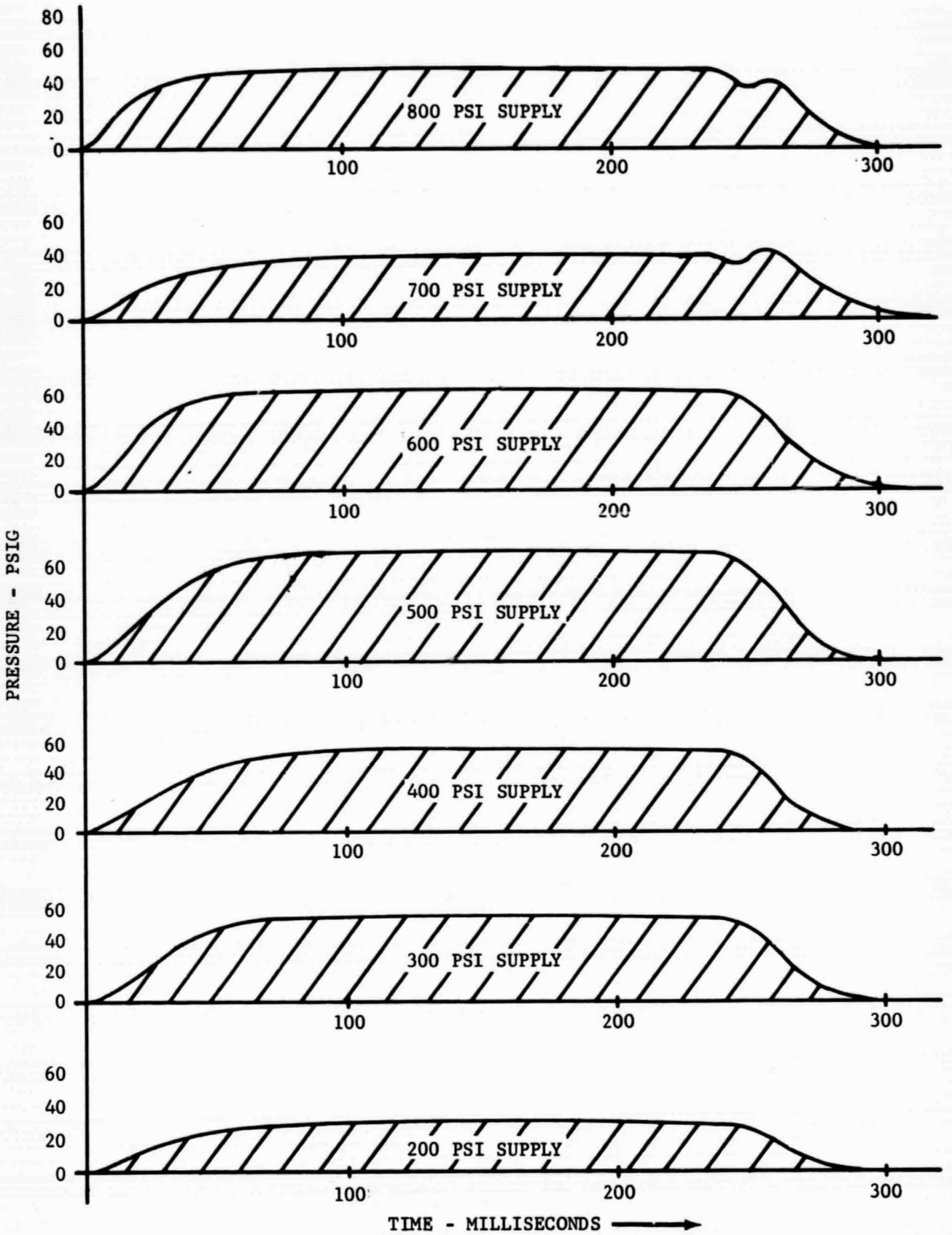

FIGURE 4-3. METERED PRESSURE VS SUPPLY PPESSURE

4.1.4 PRESSURE RESPONSE TIME

When the supply line to the metering element is opened the pressure on the upstream side of the metering orifices rises very rapidly to the value of the supply pressure. The pressure on the downstream side of the orifices takes a relatively much longer time to reach equilibrium since the downstream volume is being filled through the small metering orifices while at the same time it is being exhausted through the thruster. Similarly, when the supply line is closed the pressure at the thruster nozzle has an appreciable decay time because not only must the low pressure gas bleed out, but it is being replenished by that from the high pressure side.

A simplified analysis of this system was made by assuming two plenum chambers connected in series with a sonic orifice between them. As a further simplification, the gas temperature in the plenums was considered to remain constant as the filling or bleed down process occurred. The assumed system model is shown below:

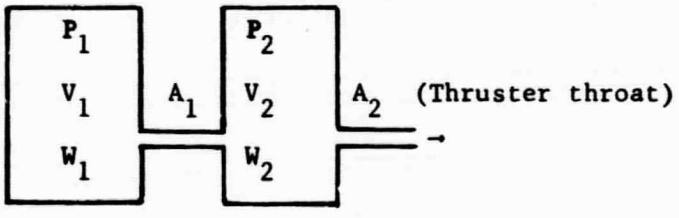

The results of the analysis for the system decay time are:

$$\frac{P_2}{Po_2} = \frac{L_2^*}{L_2^* - L_1^*} e^{-t/\tau_2}, \quad L_1^* \neq L_2^*$$

when $L_1^* = L_2^*$ the solution is:

$$\frac{P_2}{Po_2} = (1 + \frac{t}{\tau}) e^{-t/\tau}, \quad L_1^* = L_2^*$$

where: P_2 = pressure at thruster at time, t

$$L_2^* = \frac{V_2}{A_2} \quad , \quad L_1^* = \frac{V_1}{A_1}$$

V_1 = volume upstream of metering element orifices

V_2 = volume downstream of metering element orifices

A_1 = area of metering element orifice

A_2 = area of thruster nozzle throat

e = base of natural logarithms

t = time after supply has been closed

$$\tau_1 = \text{time constant} = \frac{C^* L_1^*}{gRT} \quad , \quad \tau_2 = \frac{C^* L_2^*}{gRT}$$

C^* = characteristic velocity of fluid at temperature T

g = acceleration of gravity

R = gas constant

T = temperature

These equations are plotted in Figure 4-4. The time constant τ_2, is the time it would take for the pressure in volume 2 to fall to $1/e^2$ (.368), of its original value if it were not being replenished from volume 1. (The curve for $L_1^* = 0$ shows this limiting condition.) The curves show that as L_1^* increases the decay time increases markedly. But they also show that even when L_1^* is reduced to zero (that is, V_1 is reduced to zero) the decay time can still be appreciable if τ_2 is large. Hence it is just as necessary to reduce V_2 as it is to reduce V_1 to achieve minimum decay time. For example, if $L_1^* = L_2^*$, it takes approximately 4 time constants to drop to 10% pressure (thrust). If V_1 is halved it takes only 3 time constants or 75% as much time, however if V_2 is halved it still takes 4 time constants but this is only 50% as much time since the time constant is now half as large. Even though the system model used for this analysis is greatly simplified, in that the actual four orifices of the metering element have been ignored and only the high pressure fixed orifice has been considered, the results are probably conservative. During the fill process, the opening of all four orifices will increase the rate of filling; during the decay process, the opening will at first delay the fall rate but later assist it so the net result expected is an increased rate of fall. Also the assumption of constant temperature is a conservative one, since on filling, the temperature will actually rise and on discharge will fall. This effect will cause more rapid rise and fall times than those calculated.

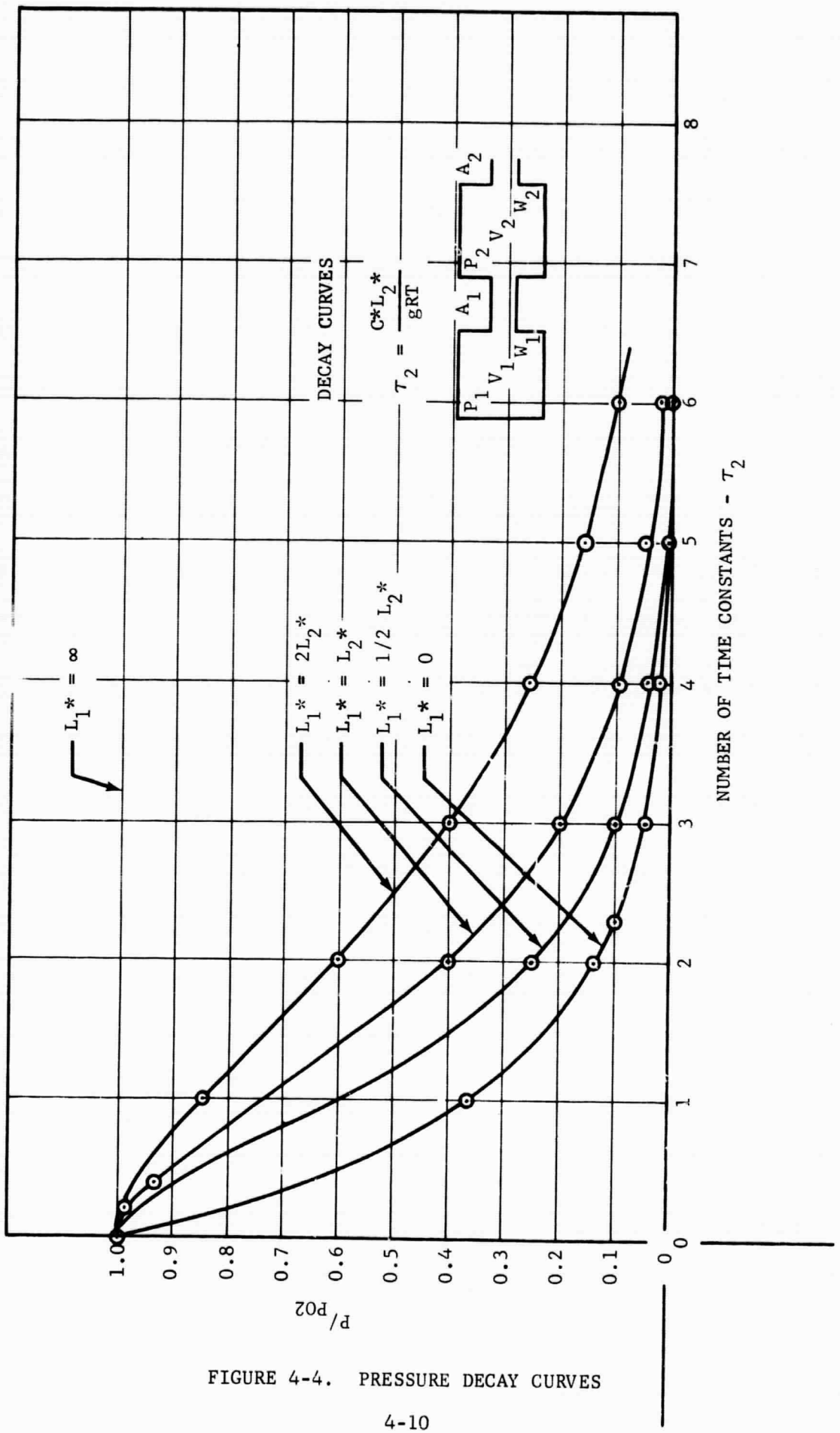

FIGURE 4-4. PRESSURE DECAY CURVES

4.1.5 MODIFICATIONS

The metering element was fabricated for the purpose of demonstrating its effectiveness in maintaining the downstream pressure. It was not made with the express purpose of minimizing internal volume. Therefore when the system dynamic response was measured, as reported in the next section, and it was found that the rise and fall times were longer than desired, it became necessary to modify the design so as to decrease the internal volume. The modifications consisted of the two filler blocks shown in Figure 4-2, remachining the inlet so as to screw directly onto the valve, the insertion of gaskets between the various component parts so that gas could not be trapped around threads, and rework of the exit end so that the pressure transducer might be close coupled directly to the metering element without requiring the additional volume of fittings previously used. If a new unit were to be designed and fabricated, it is evident from Figure 4-2 that there are other areas where volume reduction could be made. Figure 4-5 is a photograph of the assembled unit showing the close coupled pressure tap.

4.2 IMPULSE BOOSTER HEATER

4.2.1 PRINCIPLE OF OPERATION

Operation of the impulse booster heater is based on the use of a polished metal surface which has a relatively large absorptivity for the predominantly short wavelength radiation of the sun and a relatively poor emissivity for its own longer wavelength radiation. Since the sun approximates a black body at 6000°K its maximum radiation, by Wien's displacement law, is at .3/6000 cm or ½ micron; while the heater, if it is assumed a black body at 600°K, is in the infrared at 5 microns. Figure 4-6 shows the type of variation of emissivity and absorptivity to be expected with these different wavelengths. As the curves indicate, for a polished metal, the absorptivity for 6000° radiation is approximately 10 times as high as the emissivity at 300°K. With this ratio of absorptivity to emissivity plus the ratio of absorbing area to emitting area and a value for the solar heat flux, the equilibrium temperature of the booster heater can be directly calculated. For example:

$$\text{Using } \frac{\text{absorptivity}}{\text{emissivity}} = 7$$

$$\frac{\text{projected area}}{\text{radiating area}} = .30$$

$$\text{Solar constant} = 442 \text{ Btu/hrft}^2$$
$$\text{(at Earth)}$$

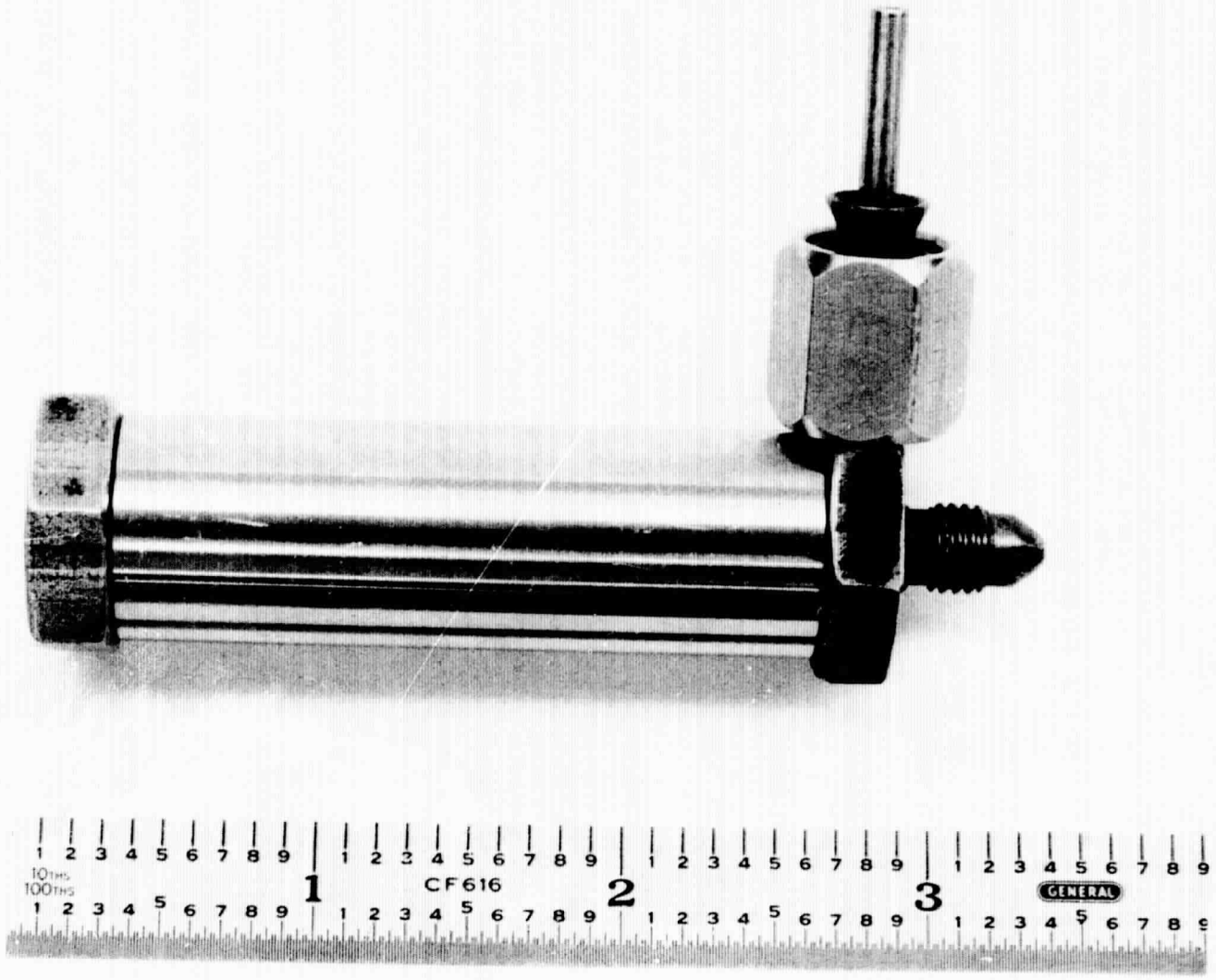

FIGURE 4-5. PHOTOGRAPH OF METERING ELEMENT

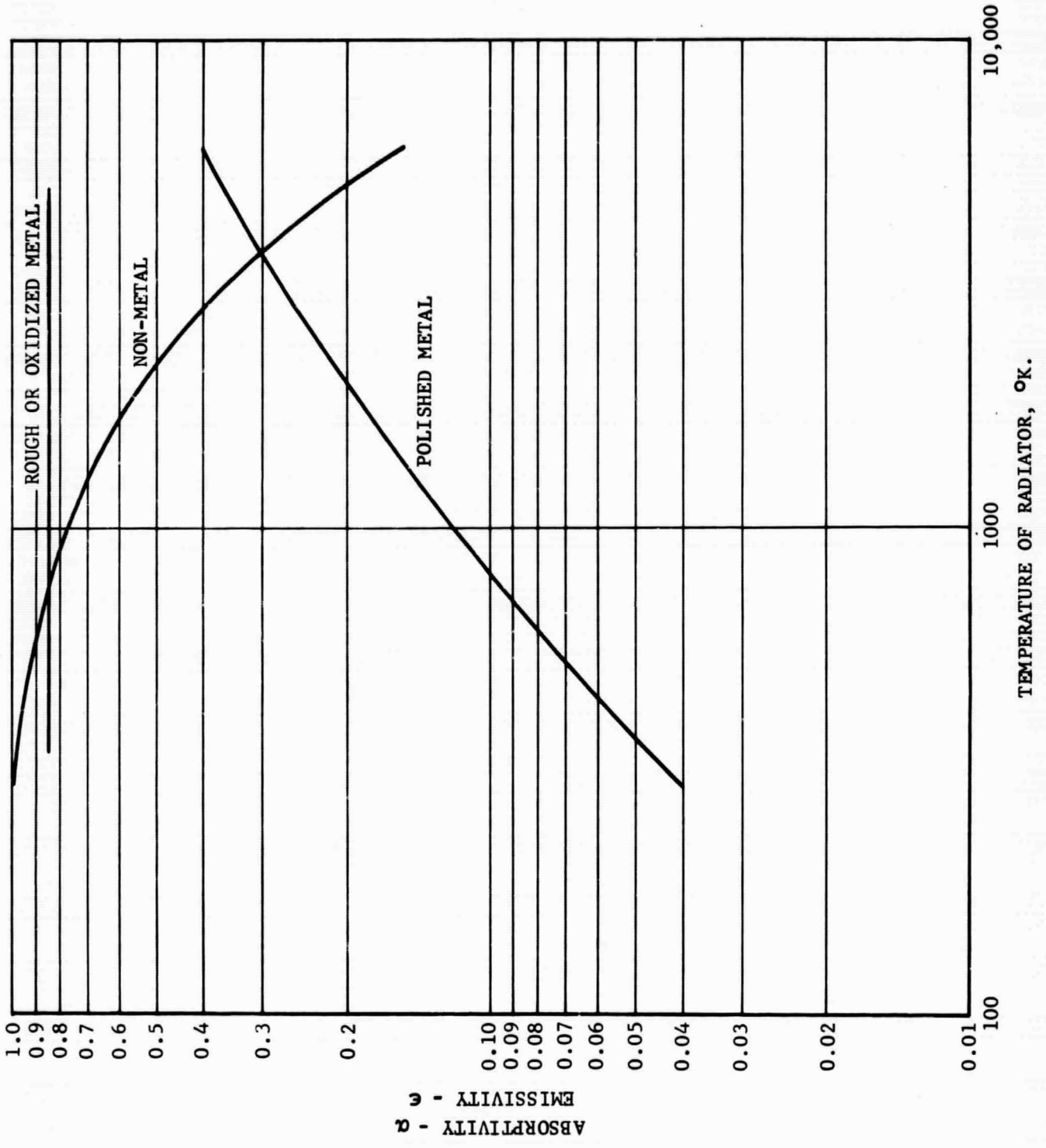

FIGURE 4-6. TYPICAL VARIATION OF ABSORPTIVITY AND EMISSIVITY WITH RADIATOR TEMPERATURE

The equilibrium temperature is calculated as:

$$\text{energy in} = \text{energy out}$$

$$7 \times .30 \times 442 = .1714 \times 10^{-8} \times T^4$$

$$\text{or } T = \sqrt[4]{\frac{928}{.1714}} \times 10^2$$

$$= 858^\circ R$$

$$\boxed{\text{or} \sim 400^\circ F}$$

At a distance of ½ astronomical units the solar flux would be 16 times greater hence the temperature would be double, but the emissivity increases so that $\alpha/\epsilon = \sim 4$

$$\text{hence } T = 858^\circ R \times 2 \times \sqrt[4]{4/7}$$

$$= 1490^\circ R$$

$$\boxed{= \sim 1000^\circ F}$$

The computed equilibrium temperature of the booster heater versus distance from the sun is given in Figure 4-7.

4.2.2 BOOSTER HEATER GEOMETRY

As described in the previous section, the impulse booster's equilibrium temperature is calculated by equating the heat emitted from its surface to the heat absorbed from solar radiation. All of the surface of the heater is effective in radiating heat, but only a portion of the surface intercepts the solar radiation. Also, since the heater is rotating with the satellite, the surface area intercepting solar radiation varies from a maximum broadside condition to a minimum end view condition. If the heater were a thin plate oriented edgewise to the sun it would intercept no solar radiation and its temperature would tend to zero. If it were oriented broadside, it would intercept a maximum. For the thin plate, oriented broadside, the maximum absorbing area is 50% of the total emitting area. Due to the rotation, the absorbing area varies sinusoidally from a maximum of 50% to zero. The time average of this sinusoidal variation is $2/\pi$. Hence, the ratio of the effective absorbing area to the emitting area is: $2/\pi \times .50 = 32\%$. In the Task IV design report a cylindrical heater was proposed. For this geometry, the maximum broadside area is length x diameter, while the emitting area (neglecting ends) is π x length x diameter. The ratio of absorbing to emitting area is therefore: $2/\pi \times 1/\pi$ = approximately 20%. Increasing this ratio 60% (i.e., 20% to 32%) means the heater receives 60% more solar energy. Since its radiation is

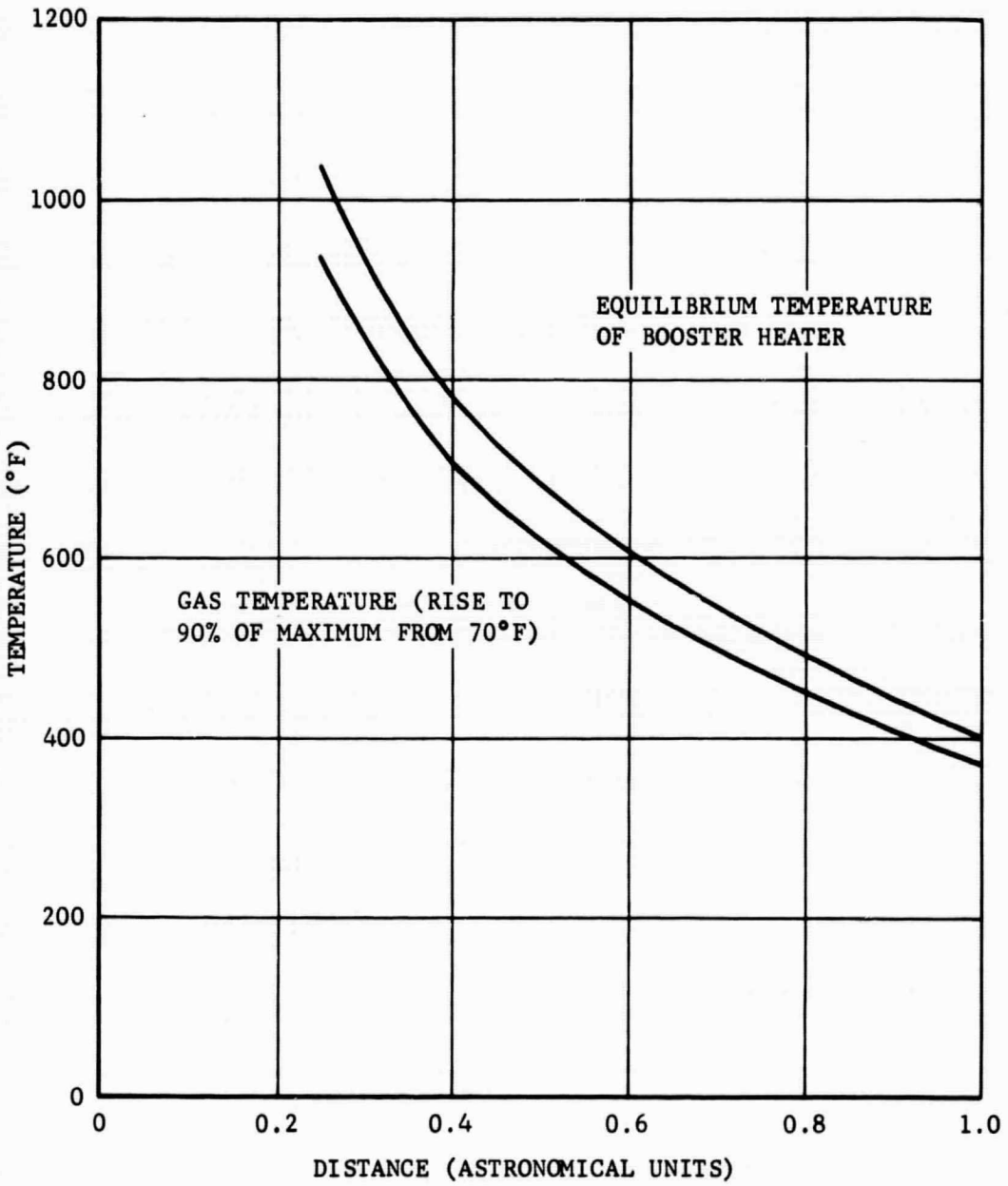

FIGURE 4-7. EQUILIBRIUM TEMPERATURE OF BOOSTER HEATER

proportional to the fourth power of the temperature (and neglecting the small increase in emissivity with temperature), the resulting equilibrium temperature for the flat plate heater is $(1.6)^{\frac{1}{4}}$ or approximately twelve percent greater than for the cylindrical geometry. The specific impulse improvement is correspondingly about 6 percent. Hence, from a specific impulse viewpoint, the flat plate heater configuration is preferable and was the type chosen for this evaluation.

4.2.3 MATERIALS FOR CONSTRUCTION

Since both volume and weight are important considerations, a desirable material for heater construction must have high volume heat capacity as well as high weight heat capacity. Figures 4-8 and 4-9 show bar graphs of some materials rated with respect to these two parameters. Beryllium is the best candidate from the standpoint of heat capacity. However, because of its toxic effect and for the problems of procurement, machining, joining, and plating it was decided to use one of the more conventional materials. Copper was selected because of its availability, its high volume heat capacity, its ease of joining, ease of machining, platability and exceptional thermal conductivity. Nickel also appears to be a desirable candidate.

4.2.4 HEAT TRANSFER AREA REQUIREMENTS

The internal area of the booster heater exposed to the gas stream determines the temperature rise of the gas for a given flow velocity and density. The pressure loss through the heater must be balanced against this flow velocity and area. Also the rise and decay times of the system thrust must be balanced against the gas volume contained in the heater. Hence it is desirable that the heater have large area, small volume, and a gas velocity large enough to get adequate heat transfer, but small enough to minimize pressure losses.

Assuming a constant wall temperature and heat transfer coefficient, the heat flow equation expressing the flow of heat from the wall to the gas is integrated to:

$$\frac{T_{gas\ out} - T_{gas\ in}}{T_{wall} - T_{gas\ in}} = 1 - e^{-\frac{hA}{WC_p}}$$

where:

h = heat transfer coefficient - $Btu/ft^{2o}F$

A = wall area - ft^2

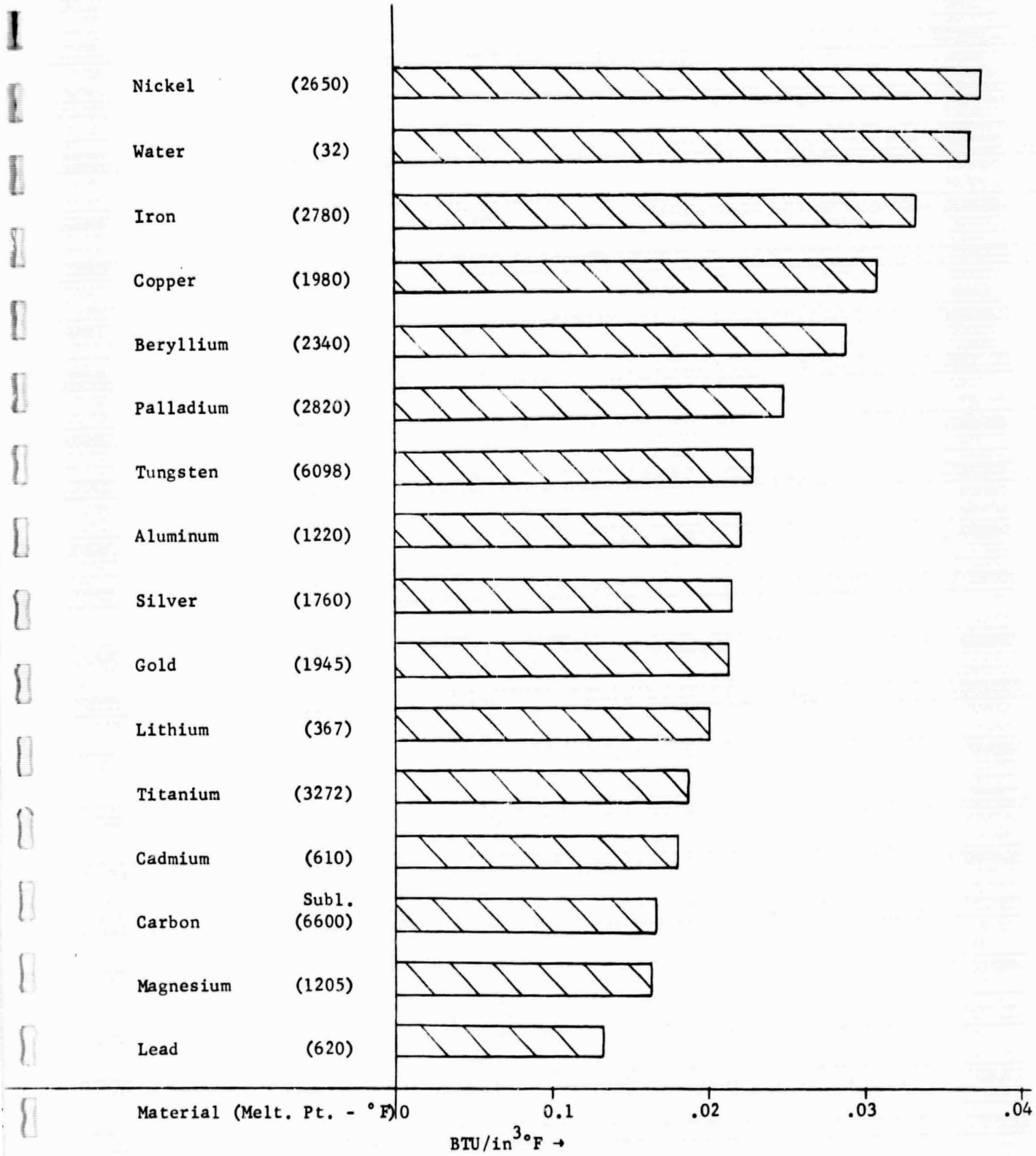

FIGURE 4-8 HEAT CAPACITY OF MATERIALS PER UNIT VOLUME

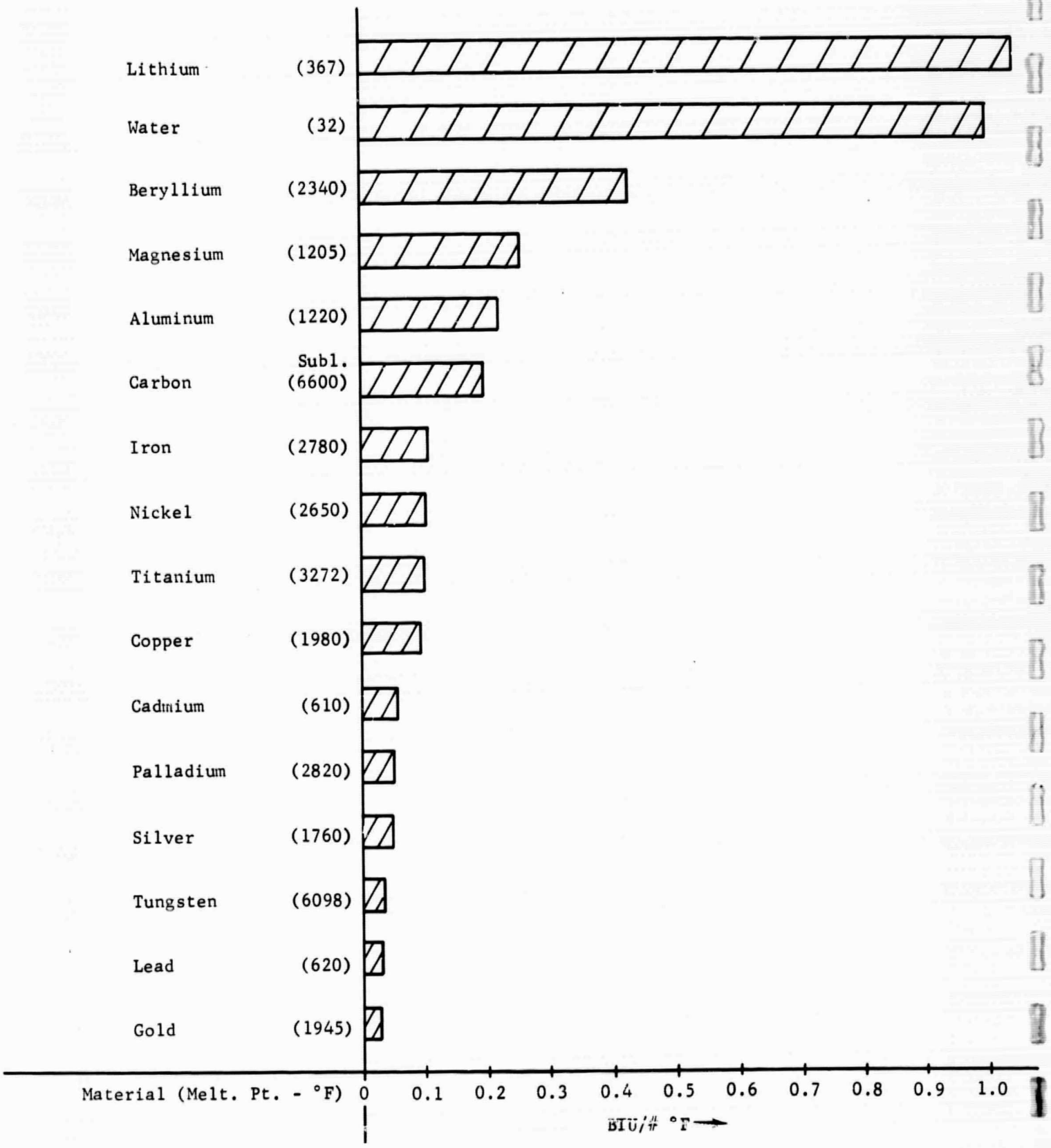

FIGURE 4-9. HEAT CAPACITY OF MATERIALS PER UNIT WEIGHT

W = flow rate - lbs/sec

C_p = specific heat of gas - Btu/lb^{o}F

For a temperature rise to 90% of the theoretical maximum, $hA/WC_p = 2.3$.

Letting, $h = .002\ \rho\ V\ C_p$

W = .002 lbm/sec

C_p = .25 Btu/lbm^{o}F

where, V = velocity - ft/sec

ρ = density = .3 lbm/ft^3

gives: $.002 \times .3 \times V \times .25A = 2.3 \times .002 \times .25$

so $A \times V = 7.7$ ft^3/sec

An average velocity of 300 feet/sec would not be expected to give an unreasonably large pressure drop; hence the required area of the heater is: $\frac{7.7}{300} \times 144 = \sim 4$ in^2

The configuration proposed in the Task IV design report was 4, 1/8 inch diameter holes x 6½ inches long giving a total area of approximately 10 square inches. Velocity for this configuration was approximately 20 ft/sec and total volume was .32 cubic inches. The above design would, therefore, be expected to give a greater temperature rise. Initial temperature rise to 90% maximum is shown in Figure 4-7.

4.2.5 BOOSTER HEATER FABRICATION

Two heater configurations were constructed. The first one was based on the proposal as presented in the Task IV design report with the minor modifications that copper was used in place of beryllium, the shape was changed to flat instead of cylindrical and the flow passages were connected in series instead of parallel. These modifications were made for the reasons discussed in the previous sections. This heater was operated several times, the heat transfer was as expected and the pressure drop was small. As a heat exchanger it was quite satisfactory, but when the system response time was measured it became evident that the internal gas volume was too large. Figure 4-10 shows a sketch of this heater, and Figure 4-11 shows a sketch of a similar heater but with parallel passages.

The second heater configuration was constructed for the express purpose of decreasing the volume as much as possible. A sandwiched type construction was utilized as shown in Figure 4-12. The area exposed to the gas stream is approximately 4 square inches. The calculated volume

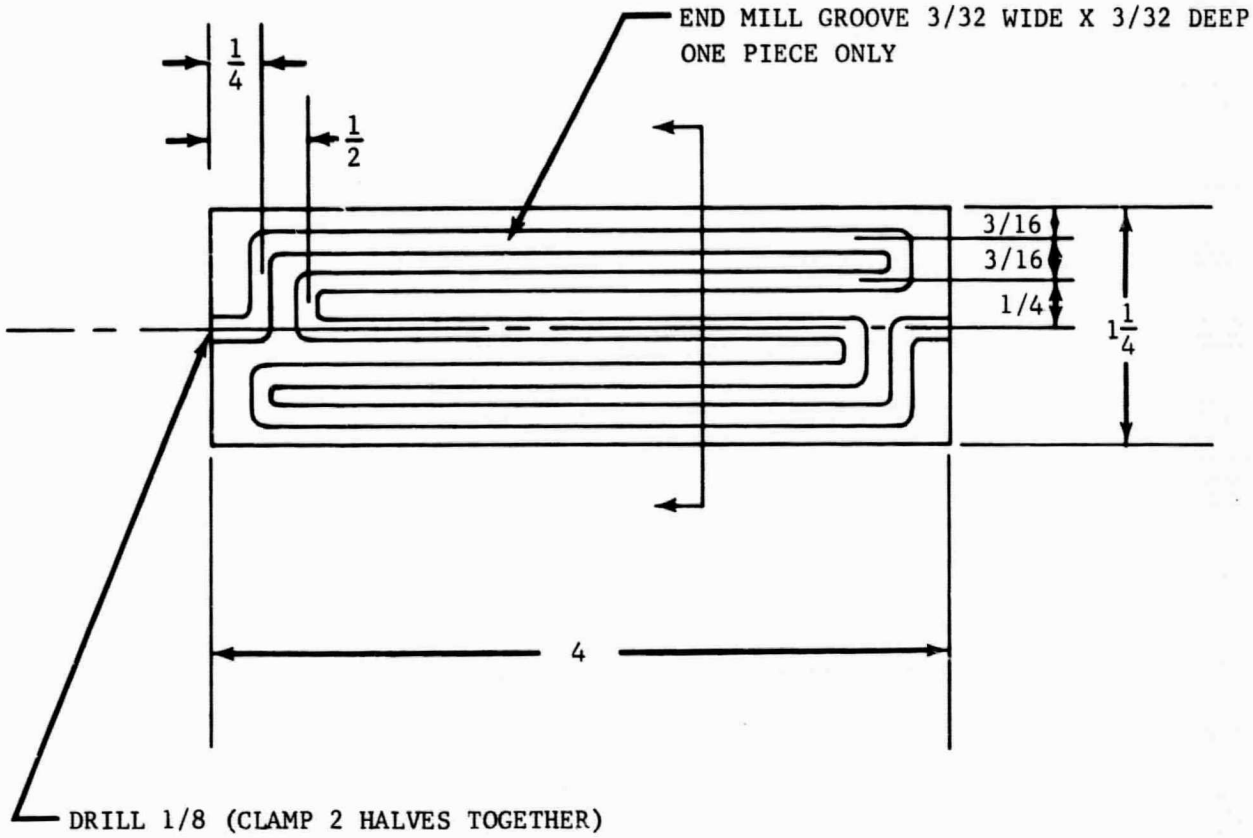

MATERIAL: COPPER

CROSS SECTION

FIGURE 4-10. IMPULSE BOOSTER HEATER

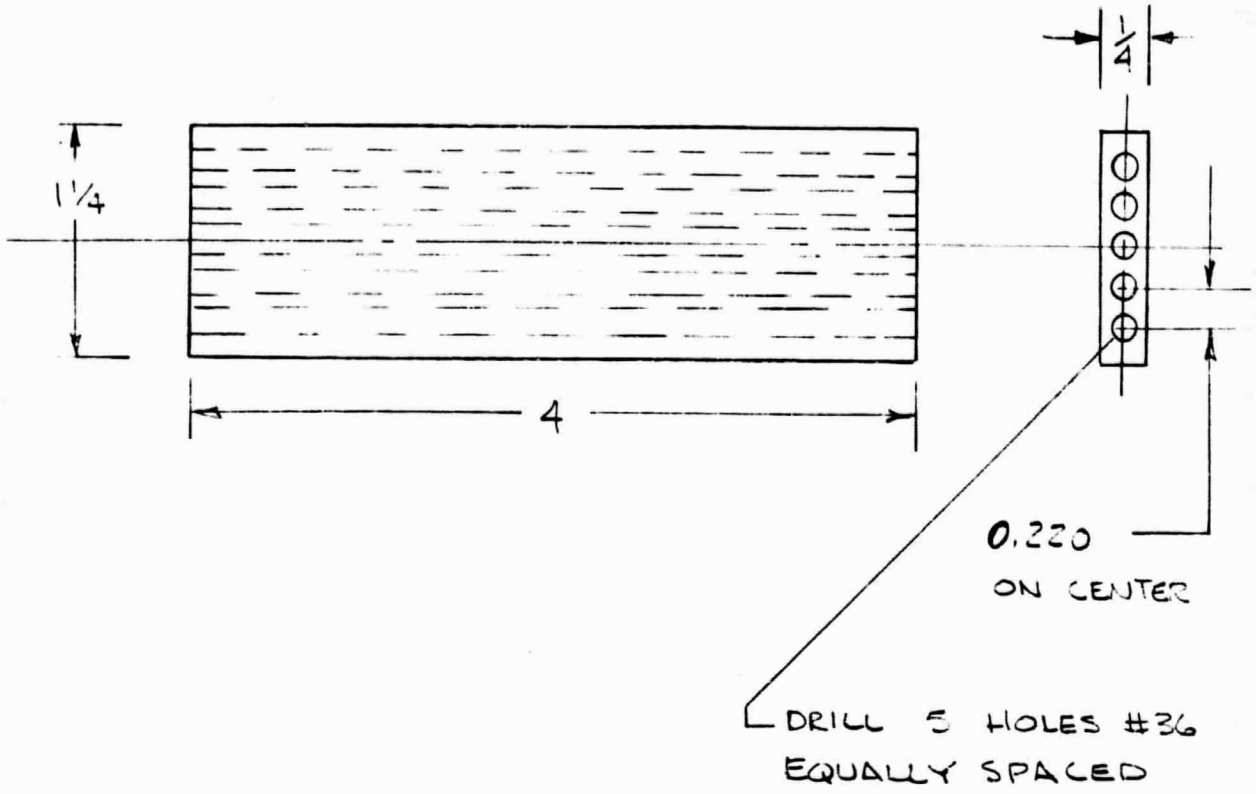

FIGURE 4-11. PARALLEL PASSAGE IMPULSE BOOSTER HEATER

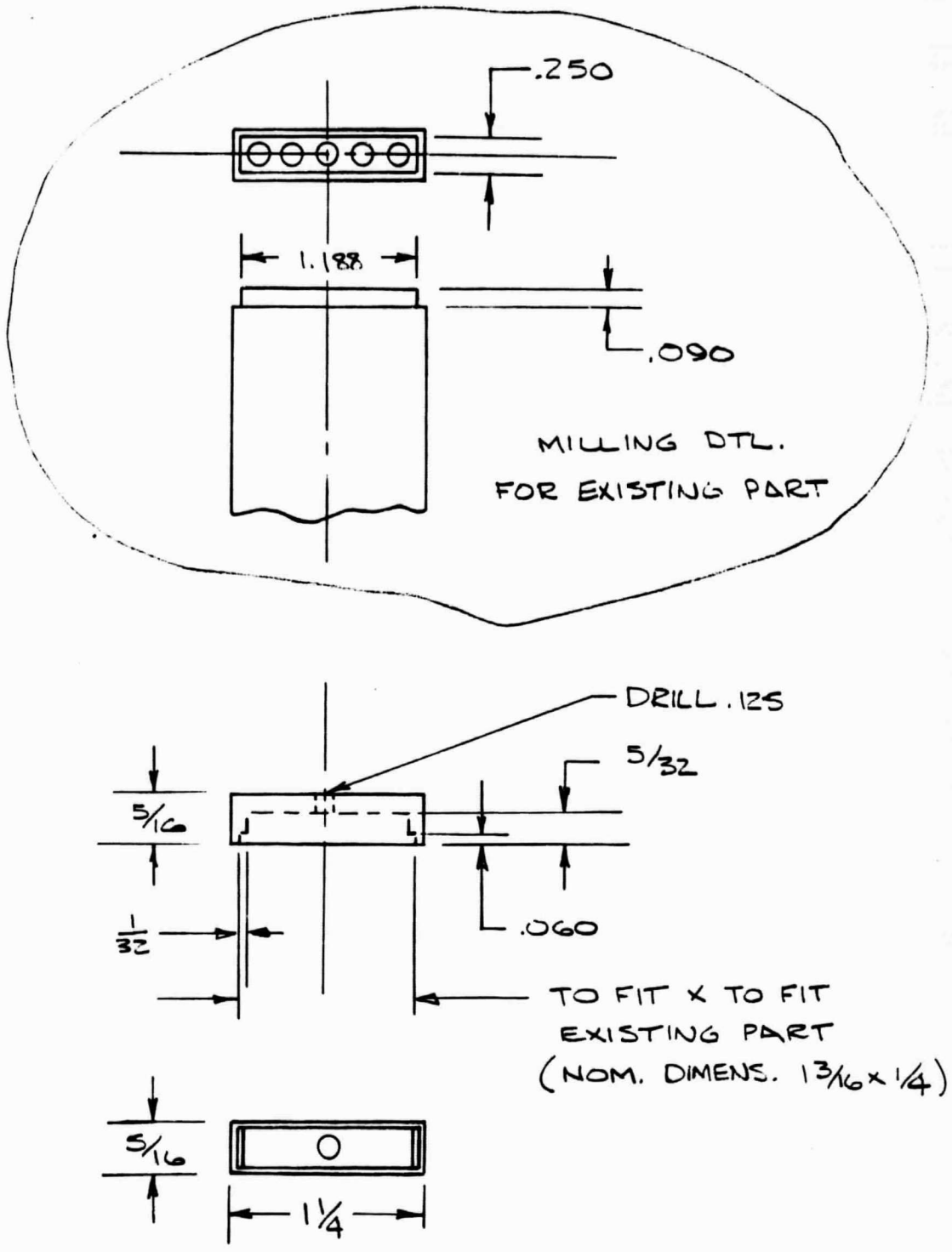

FIGURE 4-11. PARALLEL PASSAGE IMPULSE BOOSTER HEATER (continued)

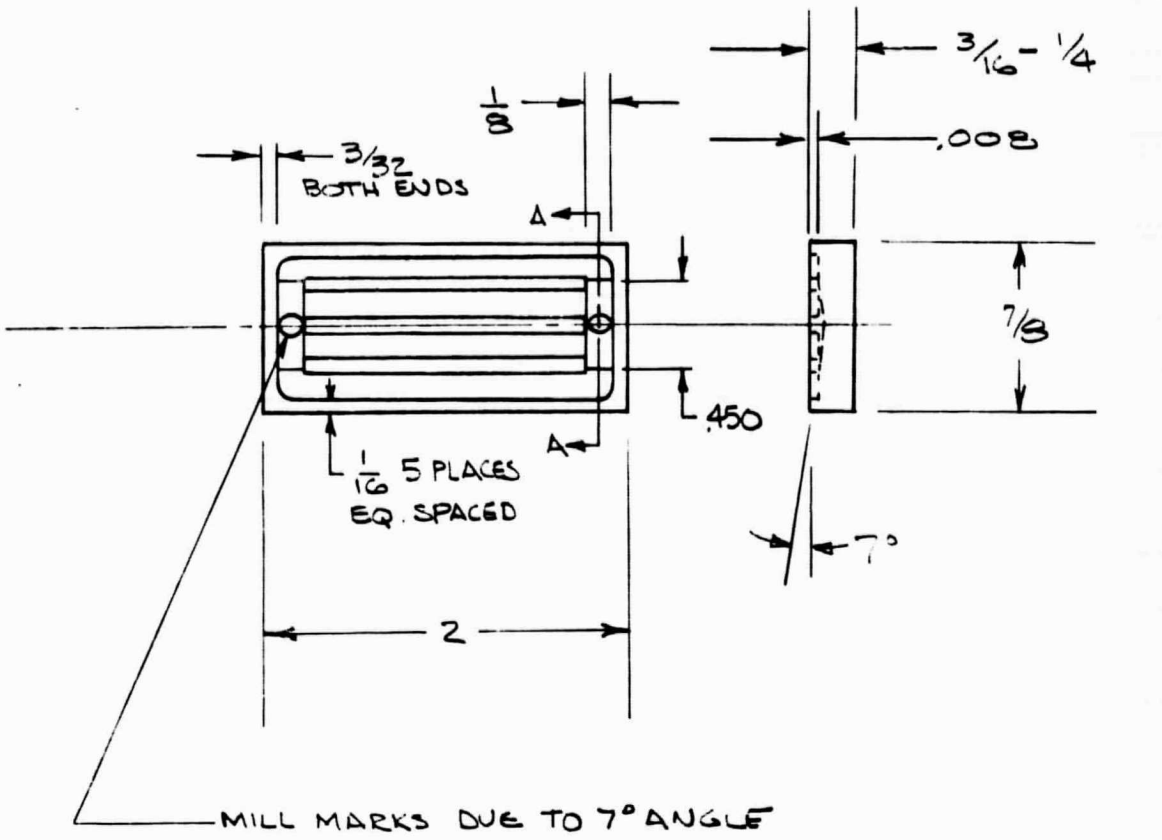

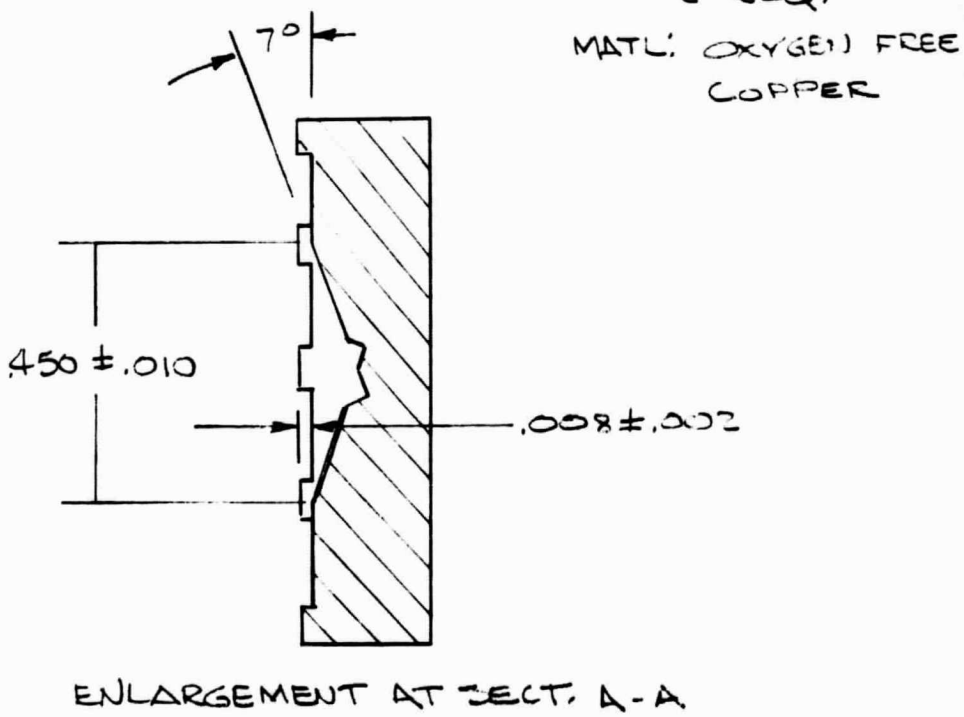

FIGURE 4-12 MINIMUM VOLUME IMPULSE BOOSTER HEATER

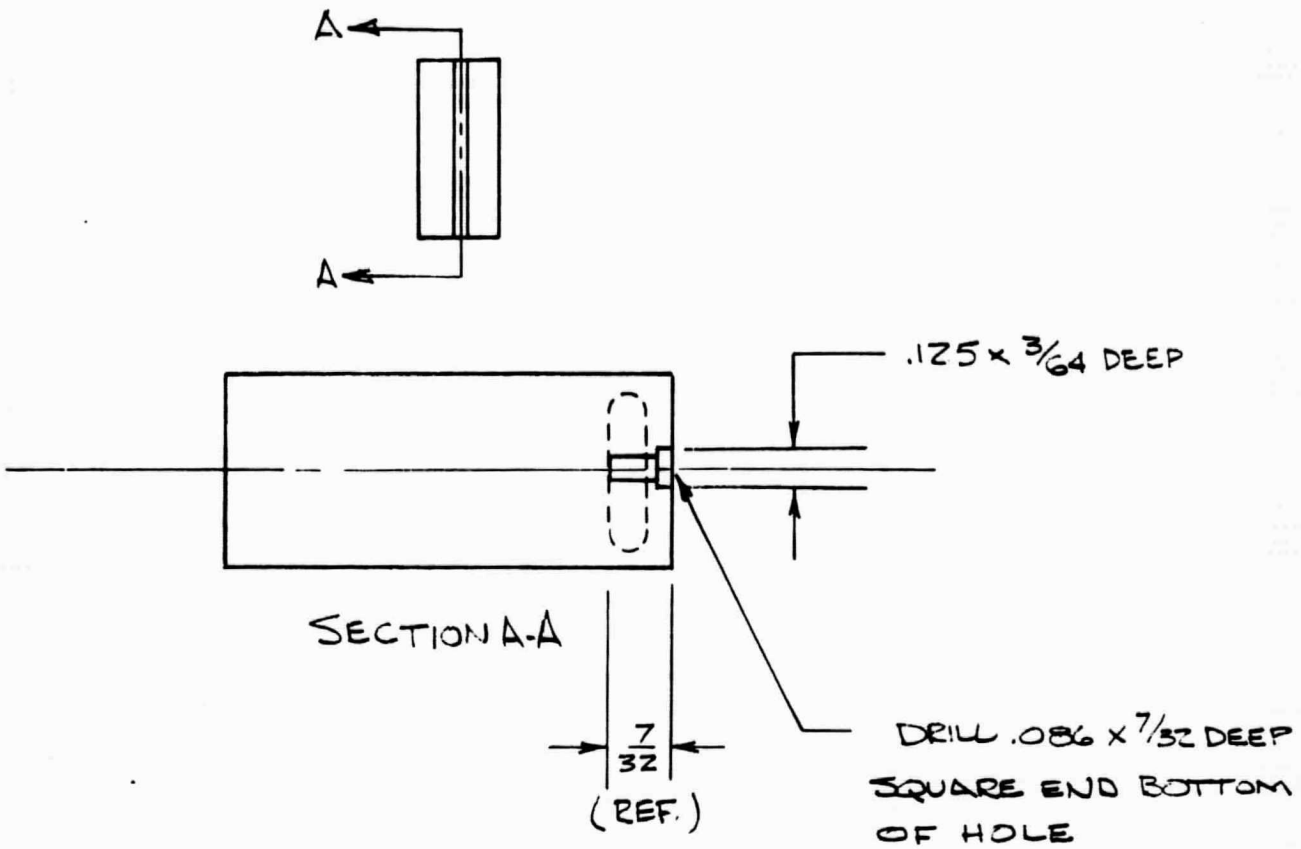

FIGURE 4-12. MINIMUM VOLUME IMPULSE BOOSTER HEATER (continued)

including the tube fittings, not shown in this figure, is .023 cubic inches, a reduction by a factor of fourteen from the initially proposed heater. Needless to say, the pressure drop was considerably higher but still gave a calculated value of only about 5 psi, certainly acceptable. Figure 4-13 is a photograph of the gold plated heater.

Fabrication of the heater was somewhat difficult due to the problem of joining the three pieces without getting silver solder into the flow passages. Since the flow passages are only .008 deep and the silver solder joint is nominally .001 to .003, a small amount of solder wetting the surface and running into the passage can cause considerable restriction or even total blockage. The most satisfactory result was obtained by pretinning the two outside pieces with a .003 sheet of silver solder, before milling the .008 grooves. A very thin wash of flux was then applied, to the lands only, of the two outside pieces. The .030 inner piece was then sandwiched between the two tinned pieces and the whole assembly including entrance and exit tubes heated to soldering temperature. This technique proved reasonably, but not entirely, satisfactory. Flow tests showed considerably more pressure loss than calculated. Subsequent sectioning and microscopic examination revealed that the solder had in fact flowed into some of the passages and caused partial blocking. Three more heat exchangers were then made using the same joining technique. The pressure drops varied from something like 25 psi to 80 psi. It was found that the passages could be somewhat cleared of silver solder by allowing a dilute nitric acid solution to flow through them. This method was used until the pressure drop was decreased to approximately 20-25 psi on each heat exchanger. Although this indicated there was still partial blocking of the passages, it did not seem desirable to attempt further refinement at this time, since for the tests intended, this much pressure drop would not greatly affect the results.

4.2.6 HEATER TEST RESULTS

Tests of the booster heater were made only to demonstrate satisfactory heat transfer from the heater to the flowing gas (nitrogen). No tests were made to demonstrate the effective absorptivity/emissivity ratio. Although this was considered, it was decided that the use of a solar simulator would be too difficult a requirement for the scope of the present task. All the tests were made using the breadboard assembly, shown schematically in Figure 4-14 and photographically in Figure 4-15. Since, for these tests, the N_2 supply tank, shown in Figures 4-14 and 4-15 did not have sufficient capacity to provide the desired length of run, it was necessary to leave the fill valve open and hooked up to the laboratory 800 psi regulated N_2 supply. The flow rate then remained constant being determined by the fixed 800 psi upstream pressure and the fixed orifice in the metering element (or a fixed orifice which was inserted in the system if the metering element was removed). The flow rate was approximately .002 lbs/sec. The tests consisted of bringing the booster heater up to a temperature of 1000°F, by radiation from an electrical heating coil enclosed in the cylindrical ceramic housing, shown in Figure 4-14, and allowing nitrogen

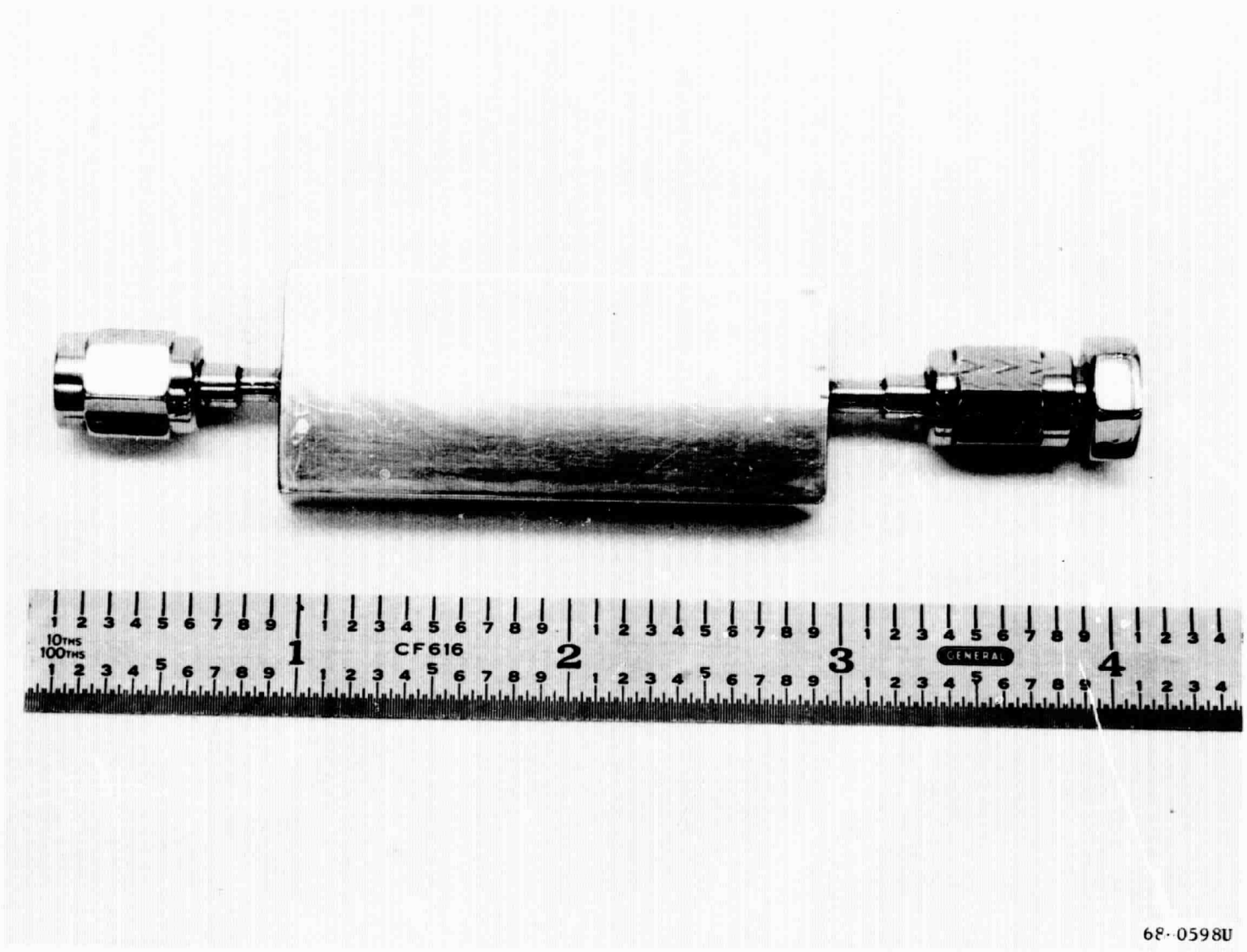

FIGURE 4-13 PHOTOGRAPH OF GOLD PLATED I_{sp} BOOSTER HEATER

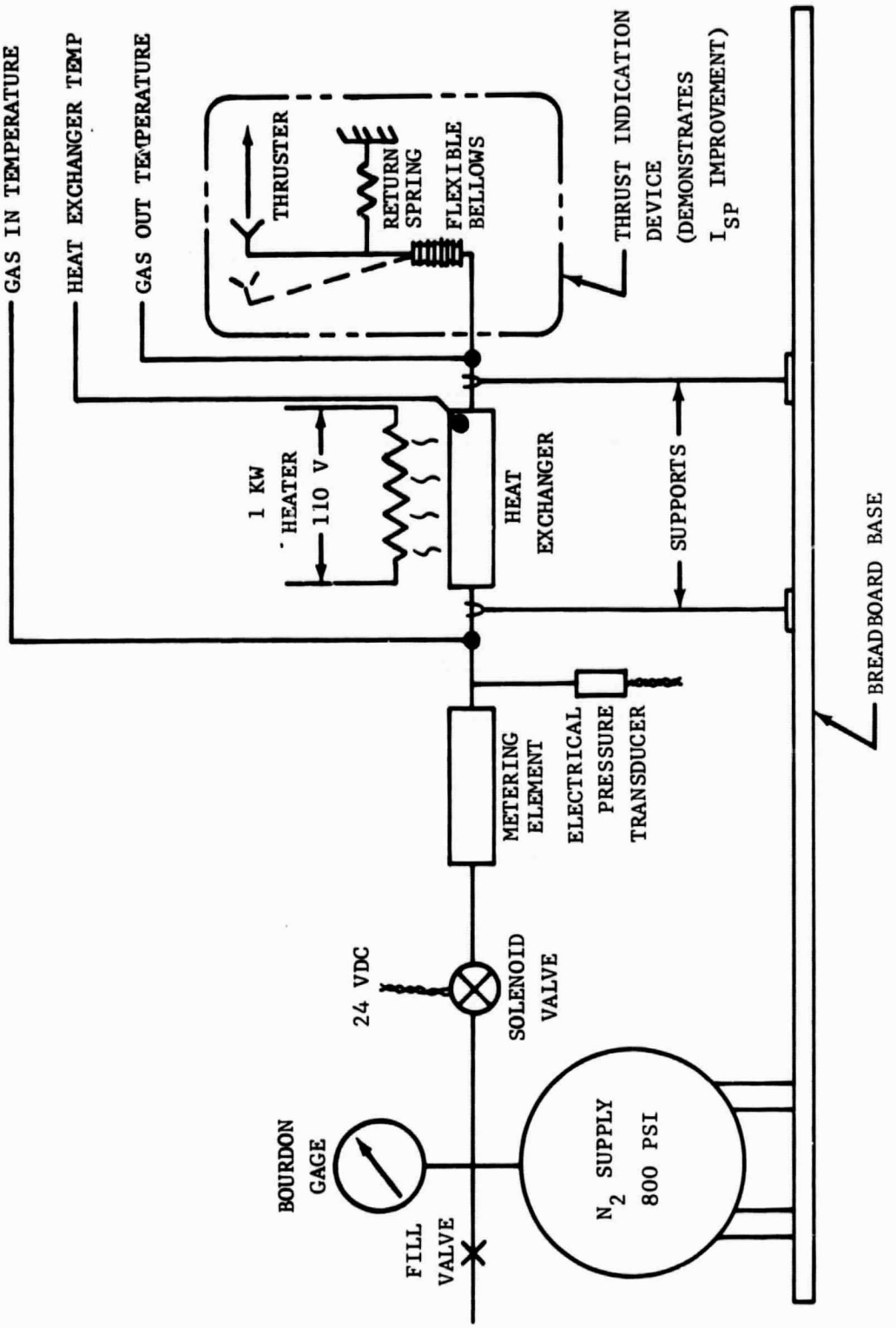

FIGURE 4-14. SIMULATED PIONEER THRUSTER SYSTEM

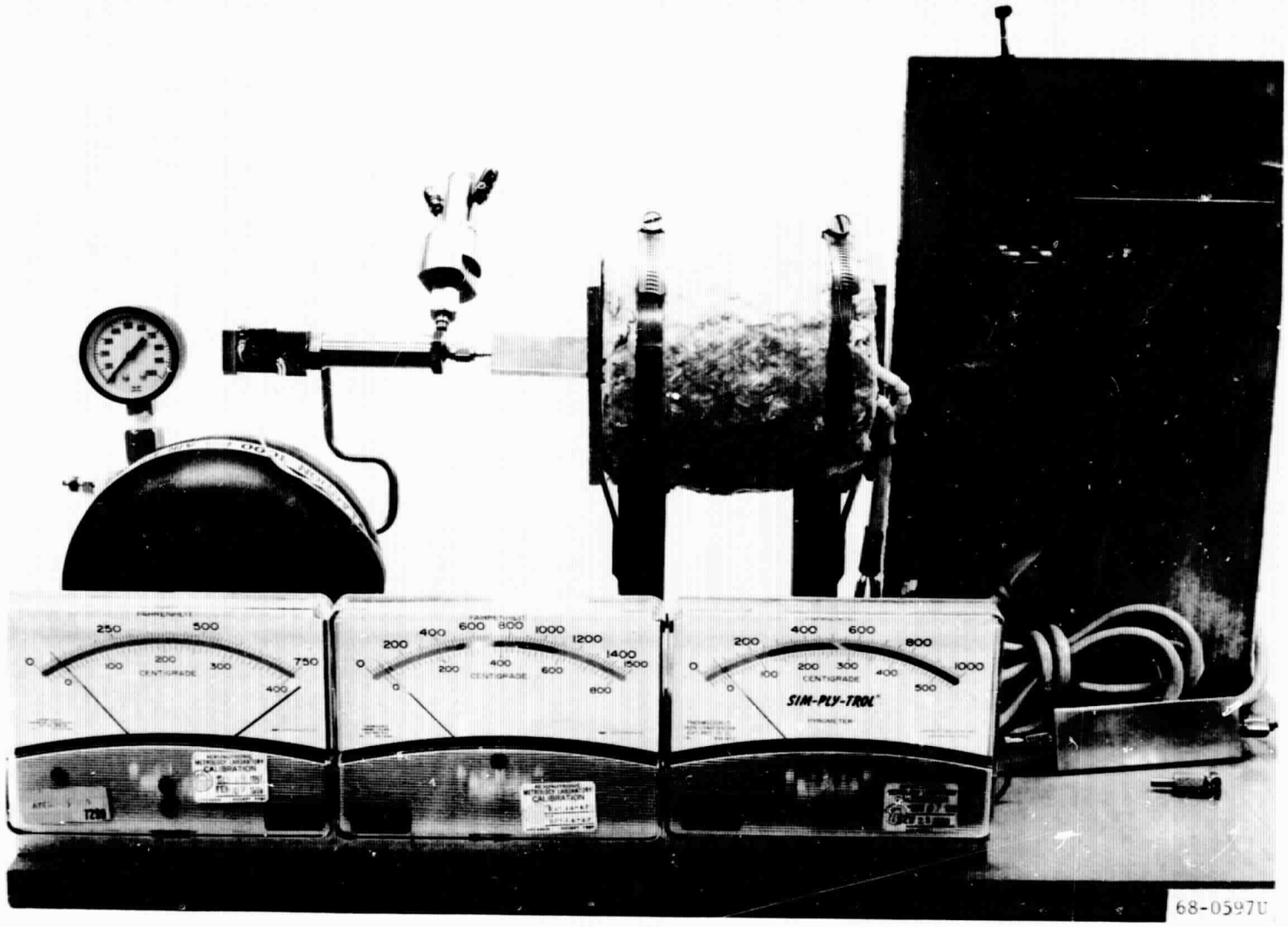

FIGURE 4-15 PHOTOGRAPH OF ASSEMBLED COMPONENTS FOR SIMULATED PIONEER THRUSTER SYSTEM

to flow through the heater. Temperatures of the in-flow gas, the booster heater and the exit gas were measured by visual indicating pyrometers using chromium-constantan, chromel-alumel, and iron-constantan thermocouples.

Tables 4.1 and 4.2 are tabulations of visually recorded data taken for the heat exchangers shown in Figures 4-10 and 4-11. The first column in the table is the time at which a reading was taken. The second column is the gas temperature leaving the heat exchanger (in all cases the inlet temperature was 70°F). The third column is the body temperature of the heat exchanger and the last column is the pressure measured at the heat exchanger entrance. Since the flow rate is constant at .002 lbs/sec this pressure reading is indicative of the specific impulse. Examination of Table 4.1 shows the maximum temperature reading of the exit gas to be 810°F. recorded 10 seconds after flow commenced. The fact that the maximum reading does not occur sooner is attributable to the response time of the pyrometer. If the temperature difference between heat exchanger and exit gas is plotted and extrapolated back to t = 0 it would appear that the initial temperature of the exit gas was around 860°F. Similarly, for Table 4.2, the initial gas temperature was about 720°F. As expected, the data show the series passage heat exchanger to be the better. The fact that the data show a relatively small difference between heater temperature and gas temperature, after the first 10 seconds, indicates that the heat transfer is very good.

The improvement in specific impulse produced by the heat exchanger can be calculated from the rise in temperature or the rise in pressure (since the flow rate was held constant). In the first instance the temperature increase is from 530°R to 1320°R the corresponding specific impulse improvement would be $(1320/530)^{\frac{1}{2}} = 1.58$ or 58 percent. On the basis of the pressure, from Table 4.1, the pressure increase is from 75 psia when cold to 125 psia when hot. The corresponding specific impulse improvement would be 125/75 = 1.67 or 67 percent improvement. The reason the latter calculation gives a greater value can be attributed to the fact that the pressure was not measured at the thruster nozzle, but upstream of the heat exchanger. The pressure reading therefore includes the pressure drop through the heat exchanger. To a first approximation, the pressure drop through the heat exchanger is directly proportional to the absolute temperature. If this pressure drop is included the two calculations compare very closely.

Data for the minimum volume heat exchanger of Figure 4-12 was confined to a single visual observation of the maximum pyrometer reading after flow was initiated. In this instance a maximum reading of about 700°F was obtained, not as good as the large series connected heat exchanger, but slightly better than the large parallel one. Although the temperature rise, to a rough approximation, is independent of the rate of flow as indicated by Section 4.2.4, in all the tests made here the rate of flow was kept constant by an upstream metering orifice. The flow rate was approximately .002 lb/sec.

The tests made here show the small heat exchanger to be satisfactory from the standpoint of heat transfer, other tests, as discussed in

TABLE 4.1

TEST OF SERIES PASSAGE HEAT EXCHANGER

Time-secs.	N_2 Temp.-^oF	HX Temp.-^oF	N_2 Press.-psig*
0-	70	70	60
0	230	1000	110
5	800	960	111
10	810	890	110
20	760	810	108
30	710	750	104
40	660	680	102
50	620	630	101
60	580	590	98
70	540	550	96
80	510	520	95
90	490	500	94
100	460	480	93
110	445	460	92
120	430	440	91
130	410	425	90
140	400	415	89
150	385	400	89
160	380	390	88
170	370	380	87
180	360	370	86.5
200	340	360	86
220	325	345	85
240	315	330	84.5
260	305	320	84
280	295	310	83.5
300			

*measured at heat exchanger entrance.

TABLE 4.2

TEST OF PARALLEL PASSAGE HEAT EXCHANGER

Time-secs.	N_2 Temp.-°F	HX Temp.-°F	N_2 Press.-psig*
0-	70	70	60
0	210	1000	89
5	670	980	89
10	680	940	89
20	640	870	87
30	620	810	86
40	570	760	85
50	540	710	84
60	540	670	83
70	490	640	82
80	475	610	81
90	460	590	80
100	490?	570	79
110	430	550	78
120	420	540	78
130	410	530	77.5
140	410	520	77
150	390	510	77
160	390	500	77
170	390	490	76.5
180	385	490	76.5
190	385	490	76
210	380	480	76
230	375	480	76
250	375	480	76
270	370	470	76
290	365	470	75.5
310	360	460	75

*measured at heat exchanger entrance.

Section 4.3, show it also satisfactory from the standpoint of system response. It is clear that more effort on the joining technique could reduce the pressure drop and improve both the heat transfer and response.

4.3 DYNAMIC PERFORMANCE OF SIMULATED PIONEER THRUSTER SYSTEM

4.3.1 BREADBOARD ASSEMBLY

A breadboard assembly of components simulating the Pioneer thruster system was put together as illustrated schematically in Figure 4-14. Figure 4-15 shows a photograph of the assembly with the close coupled solenoid valve, metering element, water cooled pressure transducer and small heat exchanger as used in the later experiments. The larger heat exchanger, used in the first tests, is shown in the lower right hand corner beside the electrical cord. Also visible, are the tank pressure gage, gas storage sphere, insulated cylindrical heater with end doors, thrust indicating device, and visual indicating pyrometers.

4.3.2 DEMONSTRATION OF I_{sp} IMPROVEMENT

Using the breadboard assembly, a qualitative demonstration of I_{sp} improvement was made by turning on the nitrogen when the heat exchanger was cold and adjusting the spring on the thrust indicator so that the indicator would just lift off the pin; when the heat exchanger was subsequently brought to temperature, and the gas turned on again, the thrust indicator would pin itself in the opposite direction.

A more quantitative measurement of the I_{sp} improvement was made by disconnecting the thrust indicating device, close coupling a pressure gage and thruster nozzle immediately downstream of the heat exchanger, and running the system both cold and hot. For short run times such that the pressure in the supply tank remains essentially constant the flow rate will be the same whether the system is cold or hot because of the fixed orifice in the metering element. (The metering element is the one previously described in 4.1)Therefore the pressure measured at the thruster nozzle is directly proportional to the specific impulse. In this way it was possible to quantitatively demonstrate an improvement of somewhat better than 50% when the heat exchanger was near 1000°F. The separate nozzle used for this demonstration is shown, located in front of the large heat exchanger, in the photograph of Figure 4-15.

4.3.3 FIRST MEASUREMENTS OF SYSTEM RESPONSE

The solenoid valve used for these experiments, shown in Figure 4-15, was a flexure mounted Aeronutronic design operating on 6 watts at 24 v.d.c. with 800 psi. Its response time, from signal to full open, was approximately 8 ms; from signal to full closed, approximately 6 ms. Figure 4-16 shows a typical blowdown curve for the assembled breadboard system. Notice that the figure is for <u>one</u> continuous blowdown curve cut in three

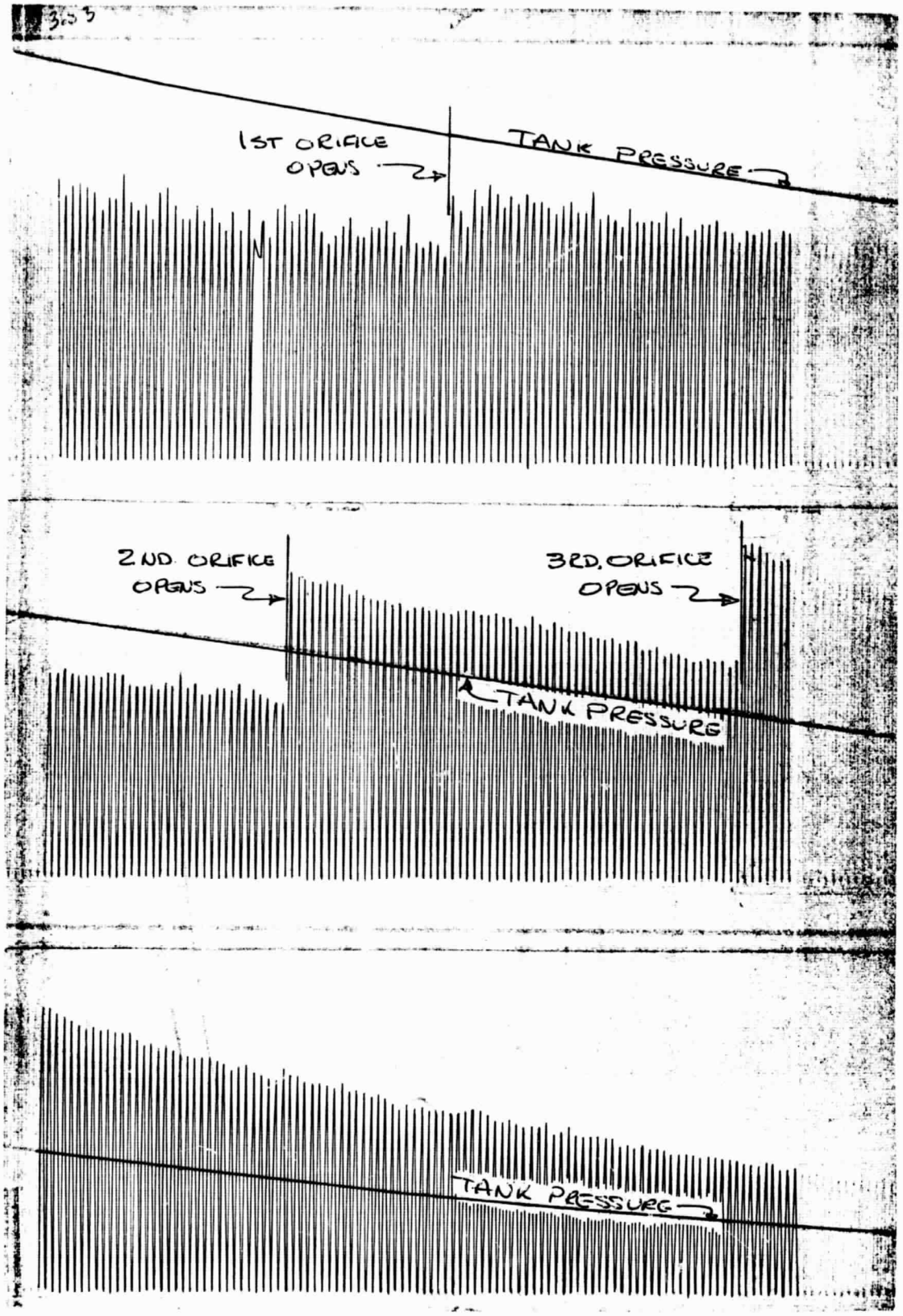

FIGURE 4-16. TYPICAL BLOWDOWN CURVE

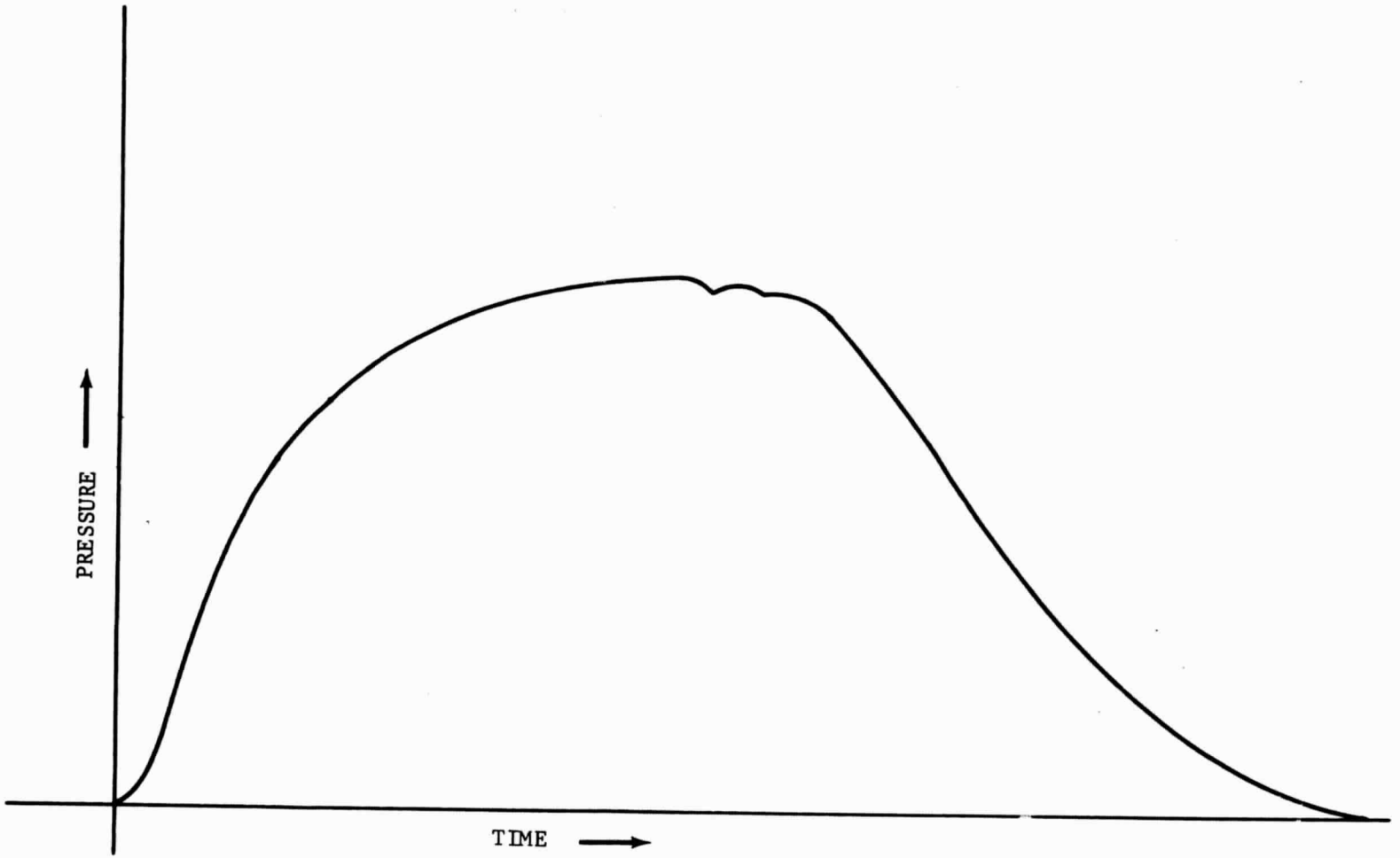

FIGURE 4-17. PRESSURE VERSUS TIME FOR ONE PULSE

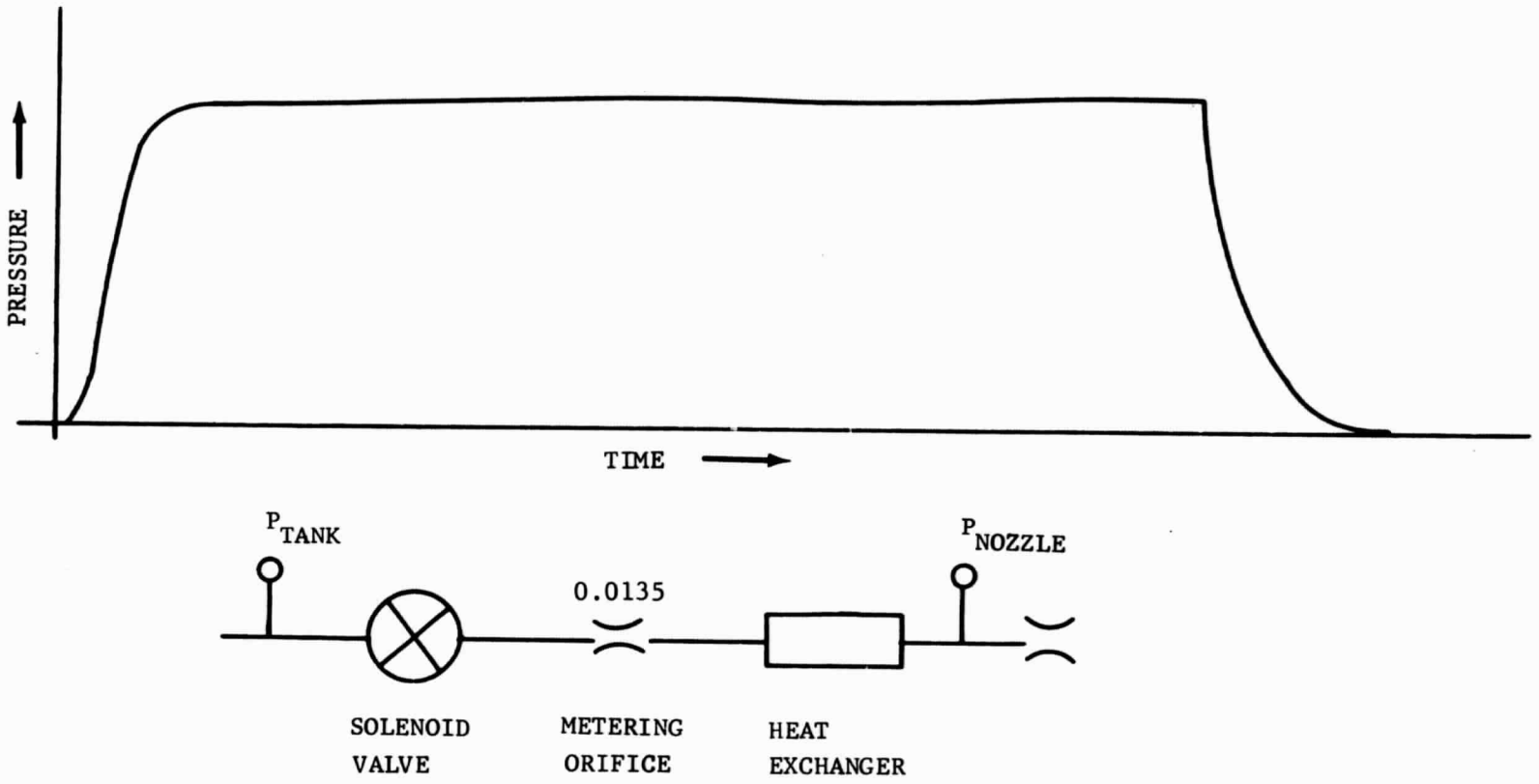

FIGURE 4-18. RESPONSE OF SYSTEM WITHOUT METERING ELEMENT

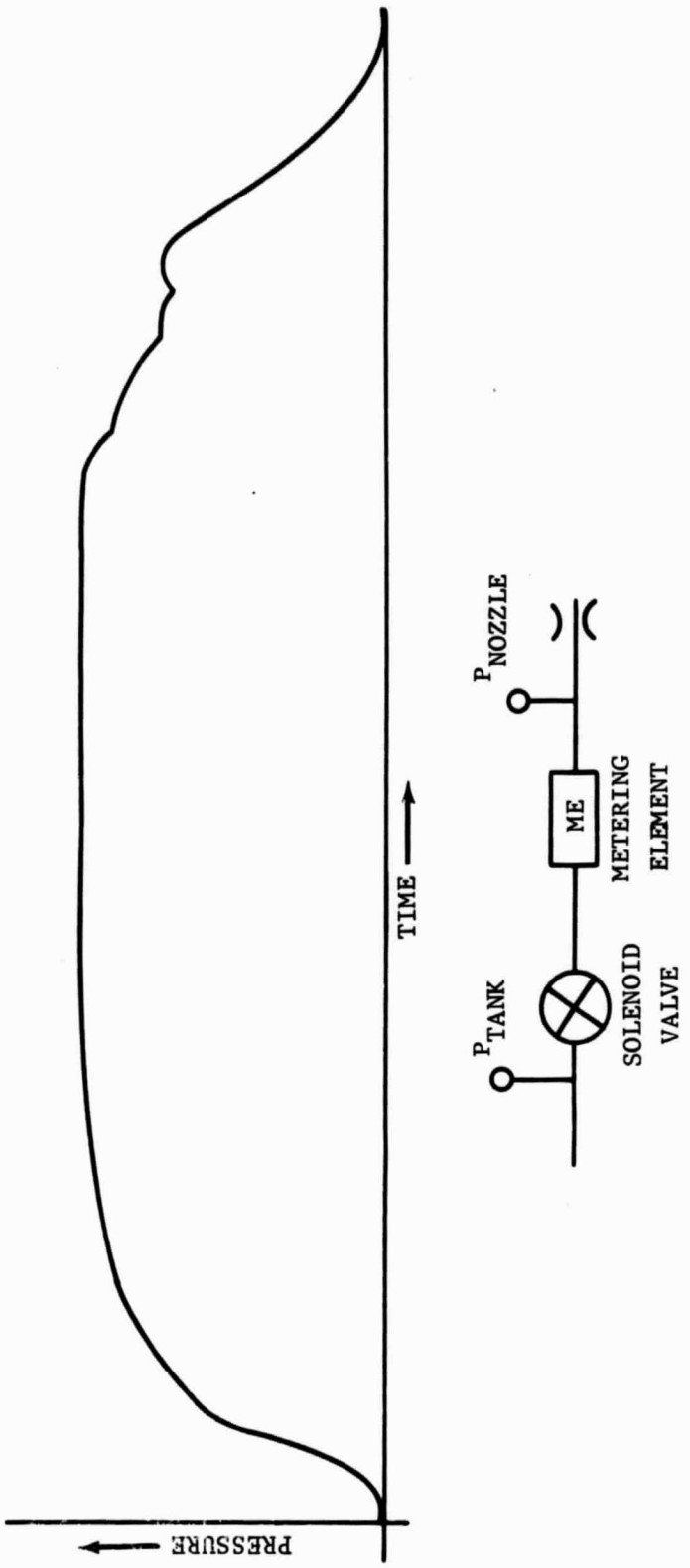

FIGURE 4-19. RESPONSE OF SYSTEM WITHOUT HEAT EXCHANGER

pieces for convenience of presentation on the page. The ordinate is pressure, the abscissa is time. The curve was made by pulsing the solenoid valve at 5 cycles per second with a square wave voltage signal adjusted to have 50% on time, 50% off time. The range of the curve labeled, "Tank Pressure" is from 800 psi to approximately 120 psi. The multi-spiked curve is the metered pressure measured just downstream of the metering element. The mean pressure level is about 50 psia. (The signal from the regulated pressure transducer has been considerably amplified so as to present it on the same graph with the tank pressure curve.) Variations in pressure from one pulse to the next are probably due to small differences in the closing times, from pulse to pulse, of the individual ports within the metering element. The curve does show the function of the metering element to be essentially as intended.

Figure 4-17 shows an expanded view of one cycle of the curve shown in Figure 4-16. As can be seen the response is very poor. In order to determine if one component was more principally responsible than another for the delay in rise and fall times, the system was operated first with the metering element removed, and then with the heat exchanger removed. The results are shown as Figures 4-18 and 4-19. It was apparent that improvement was needed on both of these components somewhat more so on the metering element. (The last two figures are not the improvement over Figure 4-17 that they at first appear because the on time for Figures 4-18 and 4-19 was approximately 400 to 500 milliseconds and about 100 milliseconds for Figure 4-17.) At this point in the program the attempt was made to reduce the volumes of heat exchanger and metering element as much as possible as described earlier. At the same time, actual volumes were measured and estimated and calculations of expected decay times were made on the basis of the mathematical model described in Section 4.1.2.

4.3.4 FINAL MEASUREMENTS OF SYSTEM RESPONSE

After fabricating the 2-inch heat exchanger and adding filler blocks to the metering element, further tests of the system response were made. Figure 4-20a shows a photograph of an oscilloscope trace of the system with the heat exchanger only. The decay time is approximately 10 milliseconds. Figure 4-20b shows a similar photograph for the metering element, the decay time is approximately 60 milliseconds. Although the heat exchanger was satisfactory, the metering element was not. Calculations of expected decay times indicated that volume of fittings, lines, and the pressure transducer itself would have to be reduced if the desired system rise and fall times of 20 and 50 milliseconds were to be realized.

The results after further rework are shown in Figure 4-21a. The trace is for the metering element only and only the fixed orifice is open, the others have been plugged. The decay time, as compared to Figure 4-20b, has been cut in half. Figure 4-21b shows the same thing, but with all four orifices functioning, the result, as expected, is even better. Figure 4-21c, for the complete system including heat exchanger, shows a rise time of approximately 20 milliseconds and a decay time of approximately 30 milliseconds, better than the goals initially established.

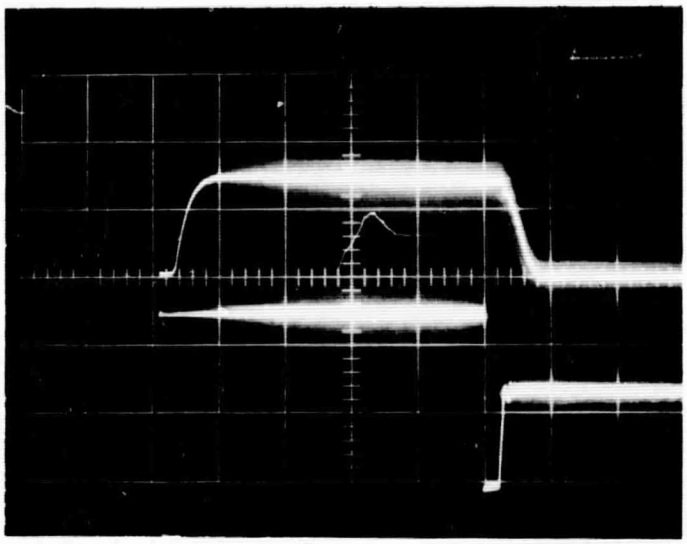

(20ms/cm)

(a) SYSTEM WITH HEAT EXCHANGER ONLY

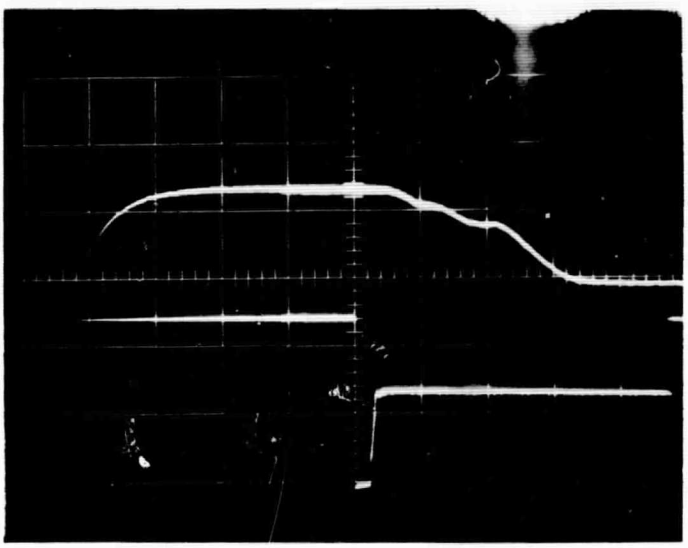

(20ms/cm)

(b) SYSTEM WITH METERING ELEMENT ONLY

FIGURE 4-20 DYNAMIC RESPONSE OF SYSTEM BEFORE FINAL REWORK

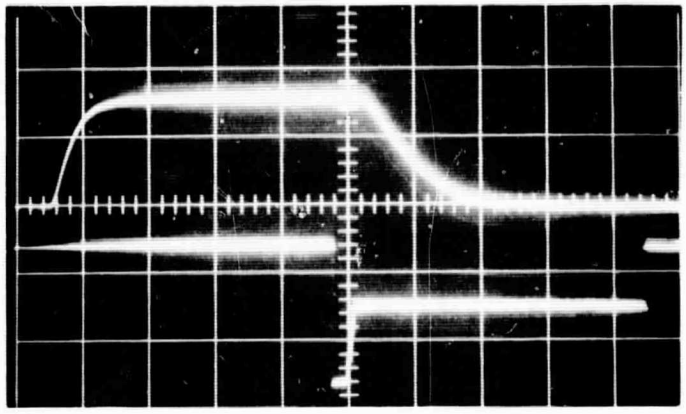

(a) AFTER REWORK OF METERING ELEMENT AND SYSTEM FITTINGS INCLUDING PRESSURE TRANSDUCER .0135 ORIFICE IN METERING ELEMENT, OTHERS PLUGGED

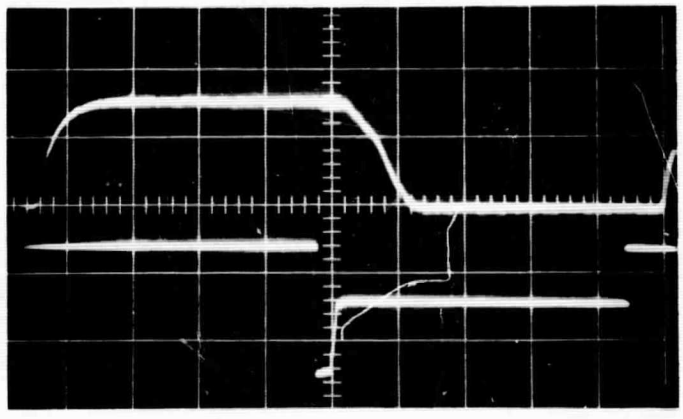

(b) SAME AS ABOVE BUT WITH ALL ORIFICES OF METERING ELEMENT FUNCTIONING AS INTENDED

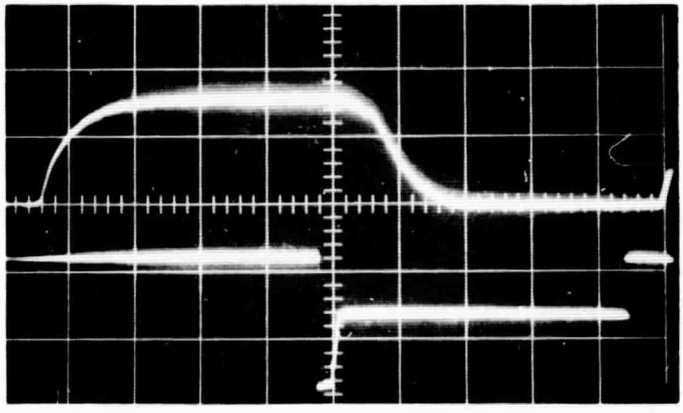

(c) COMPLETE SYSTEM WITH METERING ELEMENT AND HEAT EXCHANGER

FIGURE 4-21 DYNAMIC RESPONSE OF SYSTEM AFTER FINAL REWORK

4.4 TEST RESULT SUMMARY

The primary conclusion is that the system comprised of the solenoid valve, metering element, heat exchanger, pressure transducer and thruster nozzle has been demonstrated to operate as intended.

Some qualifications to the above statement should be made: (1) Pressure drop in the heat exchanger is higher than desirable and directly indicative of the fact that some of the passages have been partially obstructed with silver solder. However, it does not seem that this is a problem too difficult of solution. Also, since the pressure drop is due to orifice type blockage, rather than narrow tube restriction, a reduction in pressure drop would be expected to show a slight improvement in the heat transfer. (2) The metering element, though performing its function as intended, could obviously be reduced in weight and external volume by proper redesign paying particular attention to these variables. In doing this, it is quite probable that the internal volume would also be somewhat reduced making a further improvement in the system response time. It should be noted that the system response times measured have compared favorably with the vendor's reported response times of 20 and 22 milliseconds for the existing Pioneer system.

The work performed in Task IV was to demonstrate the operation of a simulated thruster system, and to this end, it is felt the objectives have been accomplished.

SECTION 5

CONCLUSIONS

A functional comparison study of valve designs showed that complete redundancy must be provided to protect against any single valve failure. The methods of providing redundancy for protection against any single valve failure are quad valves (series valves in parallel replacing each valve in the standard thruster layout) and the parallel redundant valve arrangement (one set of upstream parallel valves protecting several parallel thruster valves replacing each valve in the standard system). Since the minimum number of valves which can provide complete redundancy is $(2n + 2)$, where n is the number of control thrust vectors required, these solutions are costly in terms of weight, power and volume.

An intermediate solution to the problem is the flexure valve. This valve has flexure supported moving elements so that close fitting guides and wear are eliminated. Wear particles, which cause the majority of sticking, binding and leakage (damaged seat conditions) failures, are essentially eliminated. The probability of fail to close and leakage are improved considerably. Fail to open (coil failure, seat cold welding, material compatibility, etc.) is then the most likely thruster valve failure mode.

Multiple thrust control duplication (one control valve partially duplicates more than one control function) using valves which have a most-likely probability of fail to open can provide redundancy of control action without adding a complete set of redundant valves. For example, two canted jets on a spin stabilized vehicle can be substituted for the one precess jet. If one pure spin jet fails the appropriate canted jet will control the spin of the vehicle. The precess torque will integrate out to zero (nearly). If one precess jet fails the other will provide torque

but the time to accomplish the maneuver will be doubled. The spin induced may require corrective torque by a spin jet. In both failures the cost of the duplication is less efficient use of gas. However, protection against the most likely failure mode, fail to open, has been provided.

Feasibility of a new system approach to inert gas thruster systems was demonstrated which provided redundancy of all critical elements with no sacrifice in system weight. The system , for Pioneer type applications, is a multi-tank configuration utilizing burst discs for crude pressure regulation, a pressure sensitive bi-stable element metering device for finer flow control, a quad type valve arrangement and a solar impulse booster heater. A sawtooth variation of thrust output versus time is provided by the system. The probability of failure is insignificant for this system since burst disc reliability is high, the metering element has multiple elements (so that one element can fail without a catastrophic failure) and the valve elements are completely redundant. The basic system concept is also applicable to a ground command configuration for the Biosatellite.

REFERENCES

1. Design Data for Pressurized Gas Systems
   Prepared for NASA Contract NAS 7-105, Nov. 1963 Stanford Research Institute.

2. Design Guide for Pressurized Gas Systems
   Prepared for NASA Contract 7-388, March 1966
   ITT Research Institute, Chicago, Ill.

3. Valve Design, An Industry Survey
   Contract AF 04(611)-8392, Sept. 1962
   Rocketdyne Division of NAA - Report R-3819-3

4. Advanced Valve Technology for Spacecraft Engines
   Contract NAS 7-107, Report 8651-6016-RU-000
   Space Technology Lab, Redondo Beach, Calif.

5. Spacecraft Attitude Control Gas Systems Analysis
   Final Report Prepared for NASA, Contract NAS 7-100 April 1967
   Report SSD 70172 R, Hughes Aircraft Co., Space Systems Division
   El Segundo, Calif.

6. Spin Replenishment & Spin Axis Attitude Control for the Solrad IX Satellite. Prepared for U.S. Naval Res. Lab., Washington D.C. under Contract No. N 00173-67-C-0981. October 1967. Pub. No. UG4217 Philco Ford Corp., Space & Reentry Systems Div., Newport Beach, Calif.

7. Final Report, Hot Gas Bi-stable Jet Reaction Control Valve Program Prepared for Lockheed Missile and Space Co., Sunnyvale, Calif. under Contract NOW 63-0050GRC, September 1961, Publication U-2847 Philco Research Laboratories, Newport Beach, Calif.

8. Surface Tension Devices for Management of Space Propulsion System Propellants; SAE Conference Proceedings June 1967; S. C. DeBrock, Lockheed Missiles and Space Co.

References (Continued)

9. Space Vehicle Environment: Journal of the Aerospace Sciences, December, 1959.

10. Kay, J. M., "An Introduction to Fluid Mechanics and Heat Transfer," Cambridge University Press, Second Edition, 1963.

APPENDIX

TECHNICAL SUPPORT

This section contains a detail technical information on elements of the system mechanization design selected for evaluation in Task V of the subject contract not covered in Section 4. Technical data for the other systems mechanizations discussed in Section 3 can be found in Aeronutronic Report D530-67-624, Task IV Design Report.

A.1 MULTIPLE TANK GAS STORAGE SYSTEM

This section explains the analysis of a multiple volume, series arranged replacement to the pressure regulated system. A system schematic appears on Figure A-1 which shows the initial pressure condition of a representative 4 volume system. The first volume is stored at a pressure P_a which is less than the storage pressure of 3200 psi in the other 3 volumes. At the beginning of the mission the valve is opened and the cold nitrogen begins flowing at the pressure P_a. When this volume reaches a pressure of P_a/β, the first burst disc* BD_1 is ruptured and V_2, which is stored at high pressure, expands to P_a and refills V_1 to its initial storage pressure of P_a. This combined volume of V_1 and V_2 is then allowed to expand to P_a/β and the second burst disc is then ruptured. A similar process is then repeated until all the volumes reach a pressure of P_a/β. When this occurs, all the volumes are then allowed to expand to 50 psia which is the regulated system design pressure. Figure A-2 shows how the pressure varies with time.

A.1.1 PARAMETERIC COMPUTATIONS

The basic assumption is made that this system expels the same amount of gas above 50 psia as does the regulated system. The regulated system contains initially 104 cubic inches of gaseous nitrogen stored at 3200 psia.

*The burst disc can be replaced by either a squib valve or a thermal valve which will be explained in the next section.

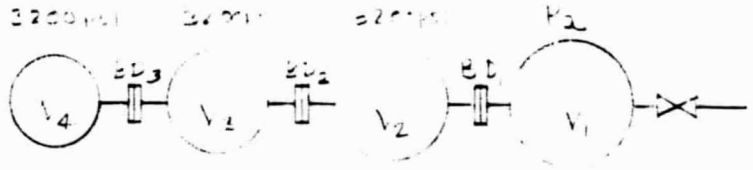

FIGURE A-1 MULTI-VOLUME GAS STORAGE SYSTEM

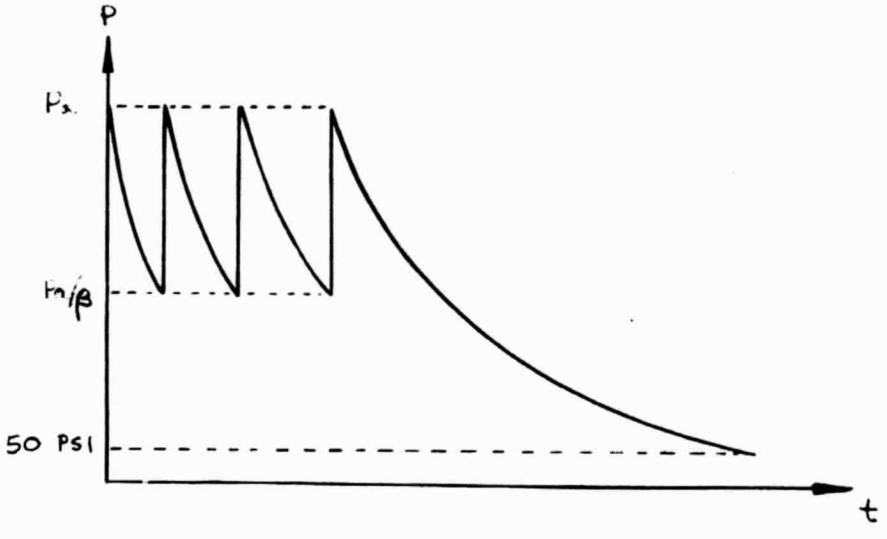

FIGURE A-2 MULTI-VOLUME SYSTEM PRESSURE HISTORY

It is also assumed that the total expansion occurs isothermally. This is certainly a good approximation before and after rupturing a burst disc and is good during the expansion because of an extremely low mass flow out of the system.

The mass of gas in a volume may be expressed by the equation of state:

$$M = \frac{PV}{RT} \qquad \text{A-(1)}$$

where:

M = mass of gas, lbs

P = pressure, psia

V = volume, $in.^3$

R = gas constant, in./°R

T = temperature, °R

the following subscripts are also defined

$( )_a$ -condition at high pressure storage of first volume

$( )_b$ -condition after initial expansion of first volume

$( )_c$ -initial condition (3200 psi)

$( )_d$ -condition at 50 psi

After the first disc is ruptured the following mass balance occurs:

$$M_{2c} + M_{1b} = M_{1a} + M_{2a} \qquad \text{A-(2)}$$

substituting from equation (1)

$$P_c V_2 + P_b V_1 = P_a(V_1 + V_2) \qquad \text{A-(3)}$$

but $P_b = P_a/\beta$

substituting in equation (3)

$$V_2 = V_1 \frac{P_a}{P_c - P_a} \left(1 - \frac{1}{\beta}\right) \qquad \text{A-(4)}$$

When the second disc is broken the following mass balance occurs:

$$M_{3c} + M_{2b} + M_{1b} = M_{3a} + M_{2a} + M_{1a} \qquad \text{A-(5)}$$

substituting the appropriate pressures and volumes equation (5) becomes:

$$V_3 = \frac{\frac{\beta - 1}{\beta} P_a}{P_c - P_a} (V_1 + V_2) = \alpha(V_1 + V_2) \qquad \text{A-(6)}$$

Similarly,

$$V_4 = \alpha(V_1 + V_2 + V_3) \qquad \text{A-(7)}$$

expressing all the volumes in terms of V_1:

$$V_2 = \alpha V_1$$

$$V_3 = \alpha (1 + \alpha) V_1$$

$$V_4 = \alpha (1 + \alpha)^2 V_1$$

In order to find the value of V_1, it is now assumed that the total mass of gas expelled from this system is equal to the total mass expelled from a regulated pressure system or:

$$M_{1a} + M_{2c} + M_{3c} + M_{4c} - (M_{1d} + M_{2d} + M_{3d} + M_{4d}) = \frac{(3200 - 50)}{RT} \qquad \text{A-(8)}$$

Solving for V_1 in terms of the regulated volume

$$\frac{V_1}{V_{reg}} = \frac{1}{(\alpha + 1)^3 - 1 + \frac{P_a - 50}{3150}} \qquad \text{A-(9)}$$

where

$$\alpha + 1 = \frac{3200 - \frac{P_a}{\beta}}{3200 - P_a} = \frac{P_c - \frac{P_a}{\beta}}{P_c - P_a}$$

The total volume is:

$$\frac{V_T}{V_1} = (\alpha + 1)^3$$

for an n bottle system these parameters are

$$\frac{V_1}{V_{reg}} = \frac{1}{(\alpha + 1)^{n-1} - 1 + \frac{P_a - 50}{3150}} \qquad \text{A-(10)}$$

$$\frac{V_T}{V_1} = (\alpha + 1)^{n-1} \qquad \text{A-(11)}$$

The total mass of gas of the system is:

$$\frac{M_T}{M_{reg}} = \frac{(\alpha + 1)^{n-1} - 1 + \frac{PP_a}{3200}}{(\alpha + 1)^{n-1} - 1 + \frac{P_a - 50}{3150}} \qquad \text{A-(12)}$$

and the total mass of gas expelled above the pressure P_b is:

$$\frac{M_e}{M_{reg}} = 1 - \frac{(1 - \frac{1}{\beta})P_a}{3200} \frac{V_T}{V_{reg}} \qquad \text{A-(13)}$$

The total volume of regulated volume can be obtained from the combination of Equations (10) and (11).

$$\frac{V_T}{V_{reg}} = \frac{V_T}{V_1} \frac{V_1}{V_{reg}} \qquad \text{A-(14)}$$

Equations (11) and (14) were plotted on Figures A-3, A-4 and A-5. Figure A-3 compares V_T/V_{reg} and V_1/V_T for n = 2, 3, 4, 5 and 10 and β = 3/2 and 2. Figure A-4 shows these parameters for n = 2, 3, 4, 5 and 10 and β = 3 and 4. Figure A-5 shows these parameters for n = 2 and 5, β = 3/2, 2, 3, 4. The figures show that V_T/V_{reg} decreases almost linearly with P_a, the initial storage pressure of the first volume, and approaches the regulated volume for P_a over 2000 psi. The total volume is also seen to decrease with an increase in the number of tanks. As expected, if β the expansion ratio increases then the total volume of the system decreases. The graphs also show that for low P_a, the volume of the first series volume occupies a larger fraction of the total volume. This trend decreases with increased number of tanks and increased expansion ratio.

Figure A-6 shows the mass ratios, the total mass to regulated mass and mass expelled above P_b over regulated mass. The total mass at worst reaches only 10 percent more mass than the regulated system and does not vary much with n or β. This ratio rapidly approaches unity for an increase of P_a. The expelled mass ratio is seen to be approximately constant with P_a especially for low expansion ratios. For n = 5 and β = 3/2 the respective mass ratios are 0.83 and 0.73. For larger values of β this ratio drops off with increased pressure.

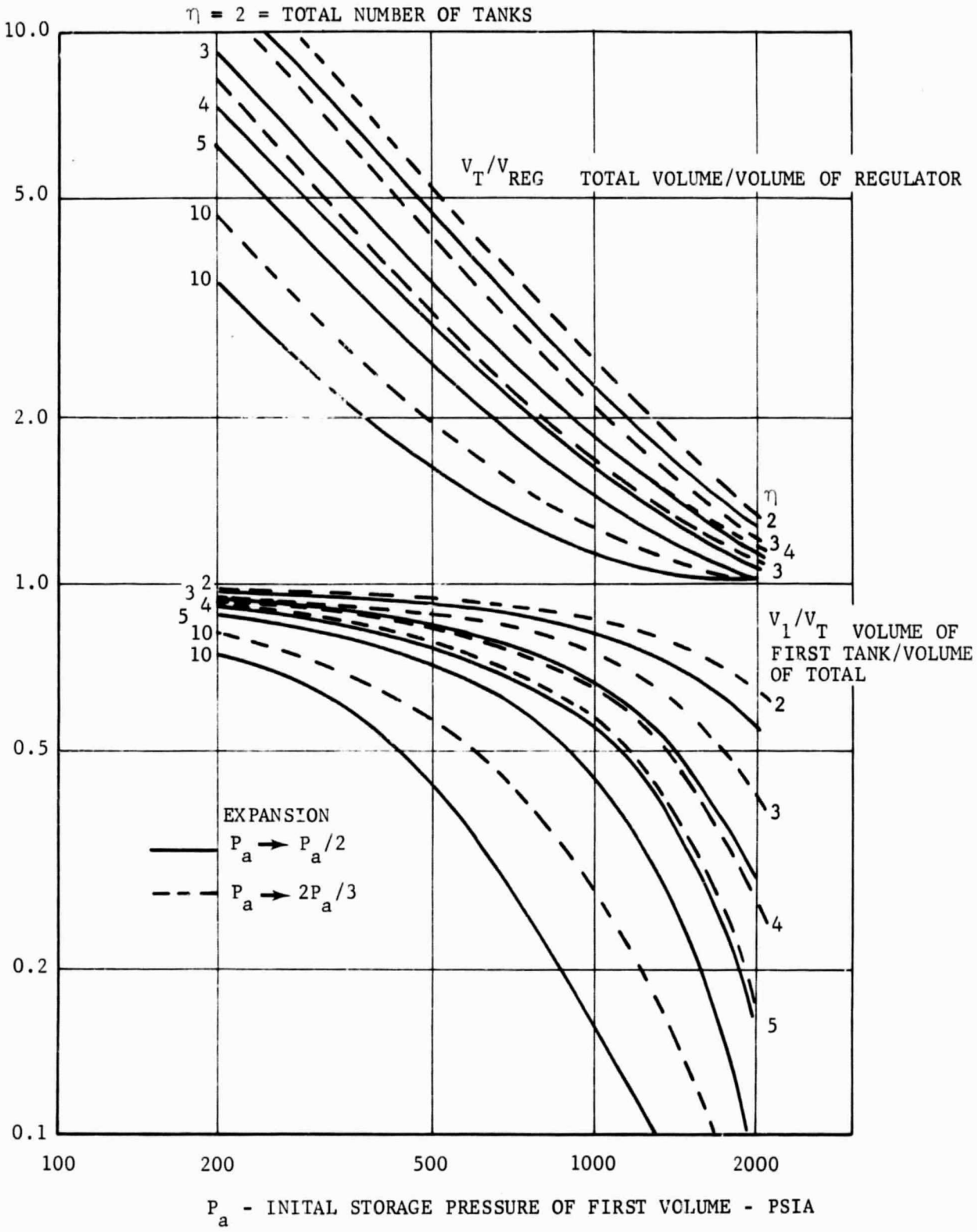

FIGURE A-3. VOLUME RATIO PARAMETERS FOR MULTI-VOLUME SYSTEMS

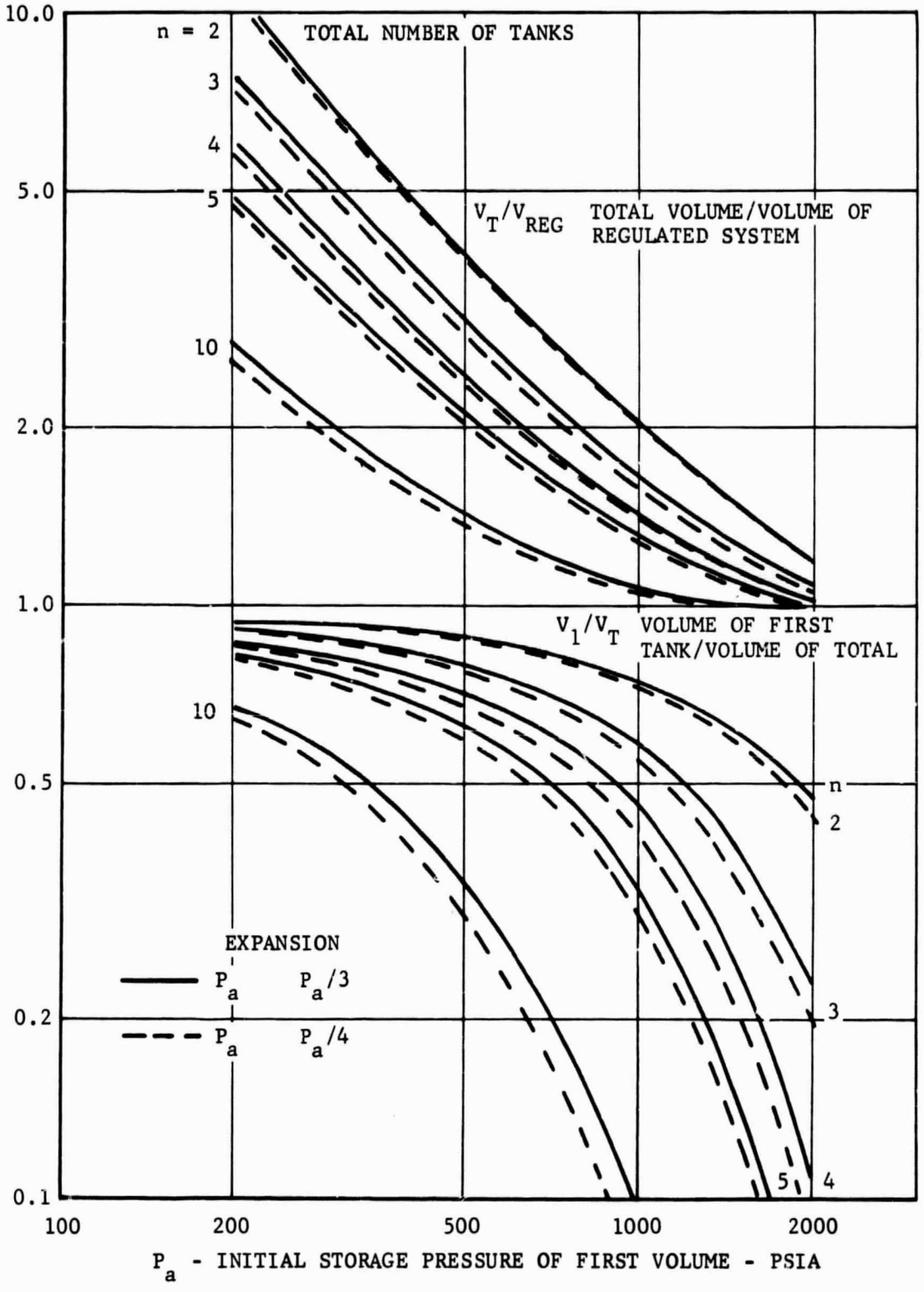

FIGURE A-4. VOLUME RATIO PARAMETERS FOR MULTI-VOLUME SYSTEMS

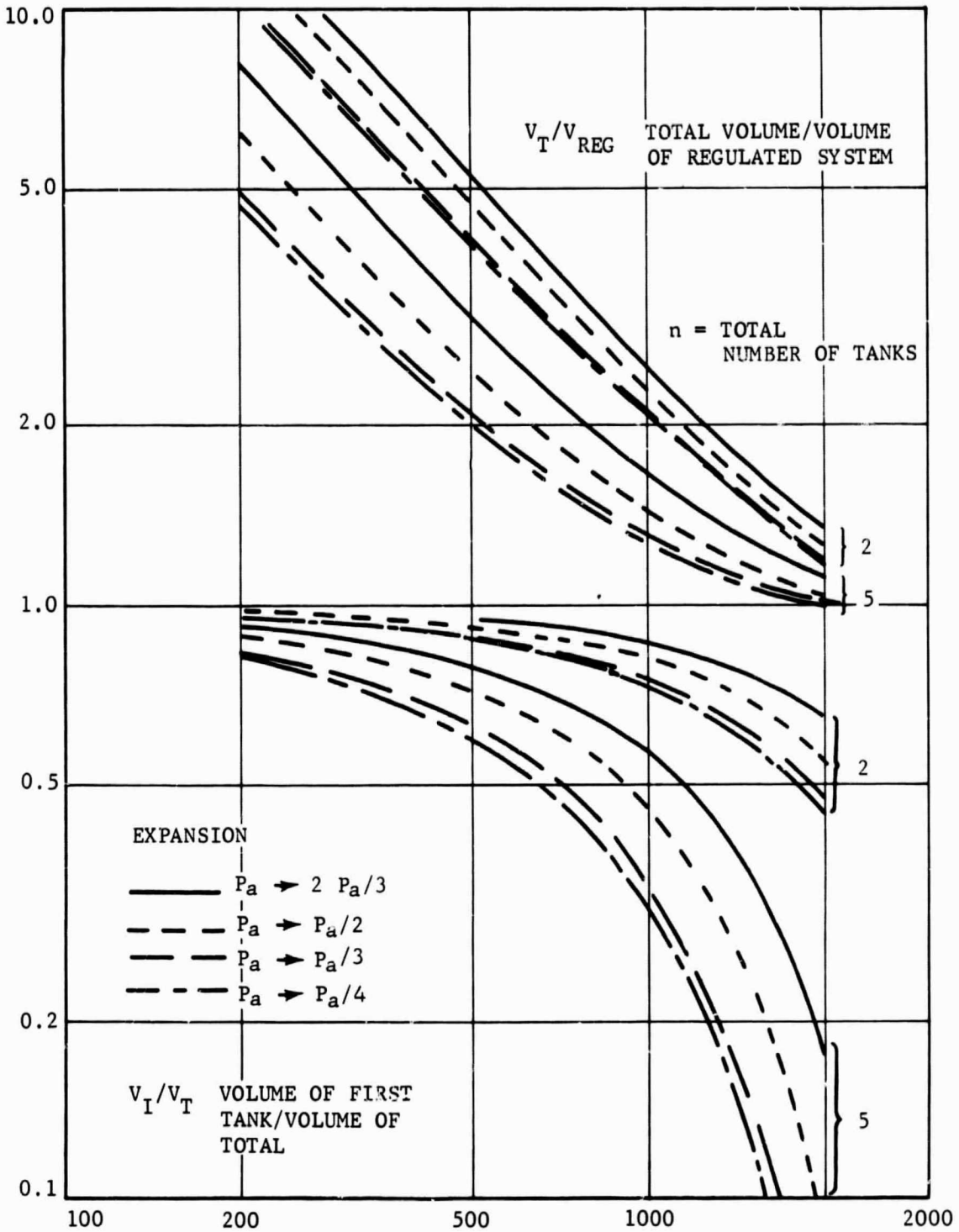

P_a - INITIAL STORAGE PRESSURE OF FIRST VOLUME - PSIA

FIGURE A-5. PRESSURE RATIO EFFECTS ON MULTI-VOLUME SYSTEMS

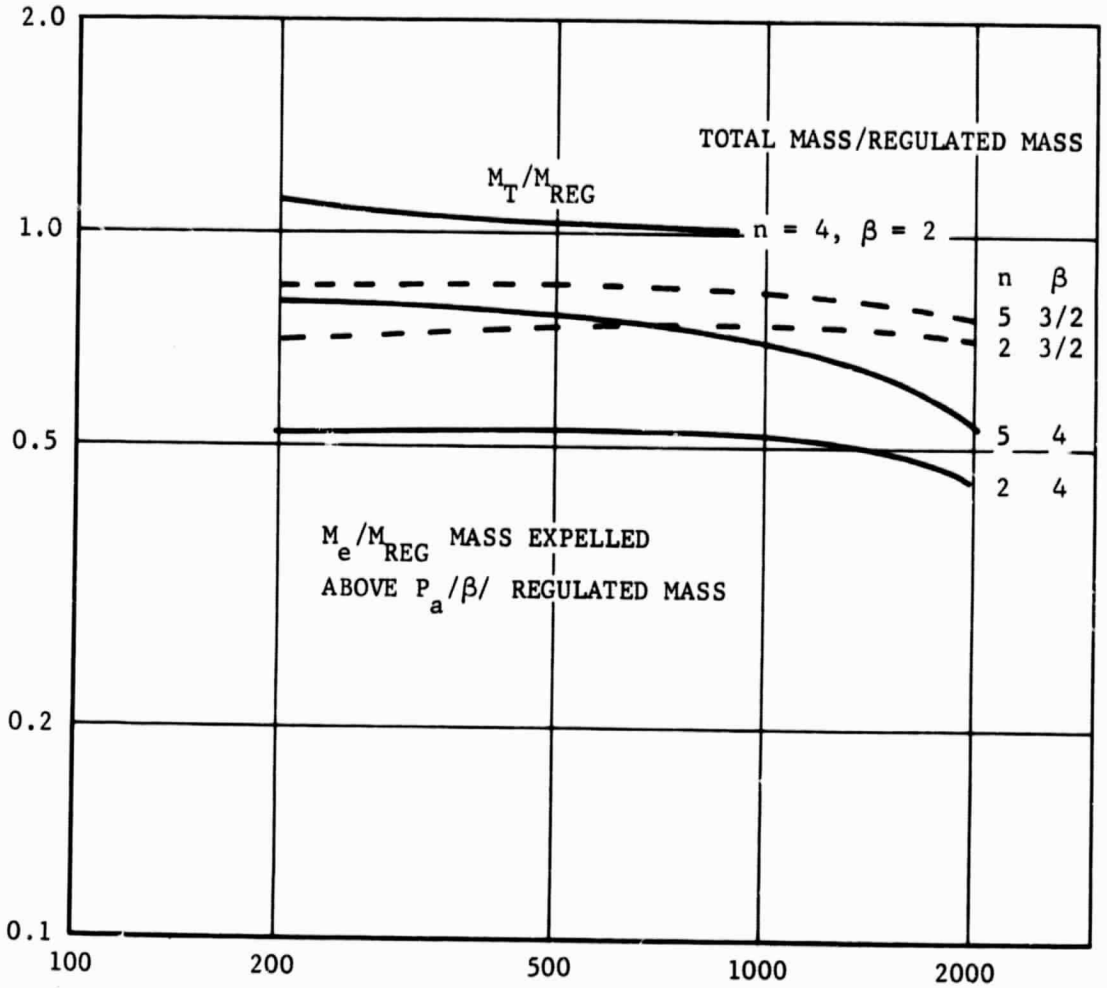

FIGURE A-6. MULTI-VOLUME SYSTEM MASS RATIO PARAMETERS

A.1.2 PIONEER TANK SIZING

The Pioneer satellite multitank system is based on four series arranged tanks with the first volume varying in pressure from 800 to 200 psia and with the subsequent tanks being stored at 3200 psia. The high pressure of 3200 was chosen to be identical to the existing system and a 4 to 1 variation of pressure was chosen to keep overall volume increase to a minimum. The low pressure of 200 psia assumes that the burst discs will rupture at 3000 psi pressure differential. An increase in static temperature causes the burst disc to rupture at a slightly higher first tank pressure. A decrease of temperature causes the opposite. The system is designed to perform its mission over a change of $\pm 20^{\circ}F$ of ambient temperature and with an accuracy of disc rupture of ± 0.5 percent on pressure differential.

From Figure A-4 it is seen that the total volume to regulated system volume is 1.62. With the use of the equations as developed the volumes of all the tanks can be calculated. The weights of tanks are similarly calculated from thin wall stress relations for a tank using titanium alloy of 150,000 psi yield strength with a safety factor of 1.5. A minimum tank thickness of 1/32 inch was chosen for ease of handling.

The thermal I_{sp} booster heats the gas and increases the delivered I_{sp} from 75 seconds to 91 seconds. Hence the volume ratio decreases to 1.34. Table A.1 summarizes the tank weights and inside diameters. All the tanks came out to be 1/32 inch thick. The parameters of the analysis of Section A.1 are also summarized in the table.

TABLE A.1

PIONEER MULTITANK PARAMETERS

Tank	Inside Diameter (Inches)	Weight (lbs)
1	4.84	0.368
2	3.05	0.146
3	3.28	0.169
4	3.52	0.194
	TOTAL	0.878

Volume Ratios

Parameter	Value
$\frac{V_1}{V_T}$	0.51
$\frac{V_T}{V_{reg}}$	1.35
V_T	140 $in.^3$

NASA TN D-4925

A RADIOMETER FOR USE IN THERMAL STUDIES OF SPACECRAFT

By George E. Sweet and Howard B. Miller

Langley Research Center
Langley Station, Hampton, Va.

NATIONAL AERONAUTICS AND SPACE ADMINISTRATION

For sale by the Clearinghouse for Federal Scientific and Technical Information
Springfield, Virginia 22151 – CFSTI price $3.00

A RADIOMETER FOR USE IN THERMAL STUDIES OF SPACECRAFT

By George E. Sweet and Howard B. Miller
Langley Research Center

SUMMARY

A new disk radiometer that is essentially a modification of a loss-measuring slug transducer has been designed for space vacuum-thermal environmental studies. The device is operable in vacuums less than 1.3×10^{-3} N/m^2 at ambient temperature levels from 80° K to 450° K. Both steady-state and time-varying total irradiances with magnitudes between 200 and 1500 W/m^2 can be measured with an error of about 10 percent. Once the radiometer is calibrated by using an extended black-body reference source, it can be used in a variety of thermal study situations without recalibration. Because it is small in size (2.3-cm diameter by 0.5-cm height) and external-cooling or constant-temperature references are not required, it effects a minimal thermal disturbance to the test surface. The major feature of this radiometer is a shield which is located between the sensor and mounting surface. This shield is instrumented so that an empirical correction can be applied to the radiometer measurements to compensate for unwanted heat transfer between the sensor and mounting surface. Criteria are presented for designing the sensor so that it will remain in temperature equilibrium with relevant heat sources and thus simplify data reduction. Example applications of the radiometer to a thermal-control balloon model are also presented.

INTRODUCTION

A radiometer was required to measure steady-state and time-varying total irradiances in the range of 200 to 1500 W/m^2 at the surfaces of spacecraft and models of spacecraft under vacuum conditions (pressures less than 1.3×10^{-3} N/m^2). When the radiative and conductive components of heating can be separated at the test surfaces, the results of thermal tests can be more rapidly evaluated. This separation is particularly beneficial for complex configurations where multiple reflections and emissions occur. For such applications a radiometer with the following characteristics is desirable:

(1) Small physical dimensions to minimize shadowing effects

(2) Low thermal mass to minimize thermal disturbances to the test surfaces

(3) Capability of indicating irradiances when the mounting-surface temperature is appreciably different from that of the radiometer

(4) Capability of maintaining a constant calibration irrespective of the mounting method

(5) Good constancy of calibration between radiometers

A radiometer meeting all these requirements could not be found. Some slug radiometers are described in references 1 and 2. Radiometers of this type generally have large thermal masses and are subject to error for measurements of steady-state irradiances. Gradient radiometers, although capable of measuring time-varying irradiances, require massive heat sinks (ref. 1). The radiometer described in reference 3 overcomes many of the disadvantages of other designs but is impractical for use in irradiance mapping because of its thermal mass and sophisticated electronics.

The present paper presents design parameters for constructing what is essentially a total loss-measuring slug transducer. The loss-measuring principle is based upon the fact that signal errors are proportional to temperature differences between the sensing element and radiometer case. In the present radiometer an instrumented shield located between the sensor and the mounting surface is analogous to the case of a conventional loss-measuring device. This radiometer is different from most slug transducers in that it is small (2.3-cm diameter by 0.5-cm height) and its components have a low thermal mass. As a result, for many applications the sensor remains in thermal equilibrium with the relevant heat sources, and data reduction is simplified.

Calibration data are included herein for several prototype radiometers for two simulated mounting conditions. Tests for response to time-varying irradiance, angular sensitivity, and the application of this radiometer to a passive thermal-control balloon model are also presented.

SYMBOLS

C	radiometer correction, $k\left(T_d - T_b\right) + C'$
C'	displacement of correction curve from coordinate axis
c	specific heat
E	energy
$F_{a,d}$	source-sensor view factor

$F_{b,d}$	shield-sensor view factor
H	irradiance
H_e	equivalent black-body irradiance of heat sources
k	slope of the radiometer correction curve C, $\frac{T_e - T_d}{T_d - T_b}$
M	constant, $\frac{c\gamma\tau}{\epsilon}$
S	surface area
T	temperature
T_e	equivalent black-body temperature of heat sources, $\left(\frac{H_a}{\sigma}\right)^{1/4}$
t	time
$\frac{dT}{dt}$	slope of time-temperature curve
α	absorptance
γ	density
ϵ	emittance
θ	angle between radiation source and normal to radiometer
σ	Stefan-Boltzmann constant
τ	thickness

Subscripts:

a	heat source
B	bottom
b	radiometer shield

d	radiometer sensor
m	mounting surface
T	top
w	wall

RADIOMETER DESCRIPTION

The signal output of a loss-measuring radiometer is dependent on the case temperature, that is, the signal is affected by heat transfer between the case and the sensing element. The case of the loss-measuring slug transducer is instrumented to measure temperature differences between the case and the sensor. These temperature differences are proportional to the signal error induced by the unwanted heat transfer between these elements. In the present device an instrumented shield, analogous to a radiometer case, is used to provide this information. In the following sections an empirical correction for radiometer errors is introduced, an error analysis is presented, and the sensor temperature response described.

Principle of Operation

The principle of operation of the present radiometer is similar to that of a slug radiometer (ref. 1). The following sketch shows a representative radiometer installation with temperature notation as indicated.

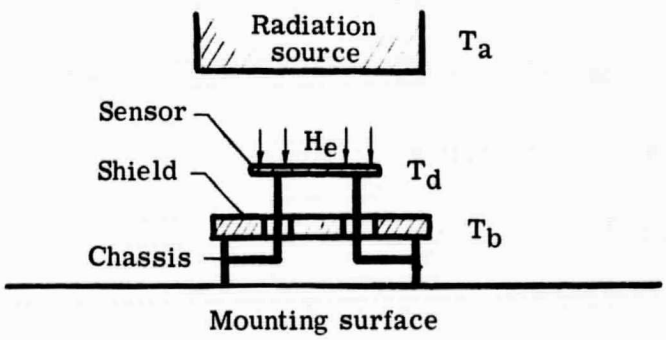

The irradiance at the sensor H_e is $S_a\epsilon_a F_{a,d}\sigma T_a^4$. In many instances the analysis of test data is simplified by considering the source radiation to be originating from an infinite black body. The equivalent irradiance at the sensor is then σT_e^4 where T_e is the temperature of this black body. The general equation for the irradiance at sensor is obtained from the following energy balance:

$$\sum E = 0 = \alpha_d S_d H_e - \epsilon_d S_d \sigma T_d^4 - (c\gamma\tau S)_d \left(\frac{dT}{dt}\right)_d + \text{Net radiative and conductive heat transfer between sensor and shield} \quad (1)$$

The principal feature of the present radiometer is the shield which is interspaced between the sensor and the mounting surface. This shield intercepts most of the radiant and conductive heat transfer between the sensor and the mounting surface. The magnitude of this unwanted heat transfer is then proportional to $T_d - T_b$, the temperature difference between the sensor and the shield. For convenience the last term in equation (1) is introduced as an empirical temperature correction C which is added to the sensor temperature T_d. Hence,

$$H_e = \left(\frac{\epsilon}{\alpha}\right)_d \sigma(T_d + C)^4 + \left(\frac{c\gamma\tau}{\alpha}\right)_d \left(\frac{dT}{dt}\right)_d$$

If the sensor is assumed to be gray (absorptance α_d is equal to emittance ϵ_d), the equivalent black-body irradiance at the sensor is

$$H_e = \sigma(T_d + C)^4 + M_d \left(\frac{dT}{dt}\right)_d \quad (2)$$

where M_d is a constant for the radiometer sensor. At solar wavelengths the assumption of a gray sensor will introduce small errors of about 2 percent. Separate calibrations should be carried out at these wavelengths and optical-property measurements should not be depended on. Equation (2) is similar to that of the slug-radiometer equation given in reference 1. The present radiometer is different in that the sensor constant M_d is much smaller than that of some slug designs (ref. 2). This difference causes the present device to attain thermal equilibrium with radiant sources more quickly than other slug designs. As a result, the sensor will remain essentially in equilibrium with the slowly changing radiance of spacecraft surfaces. Equation (2) then simplifies to

$$H_e = \sigma(T_d + C)^4 \quad (3)$$

The black-body temperature of the source is

$$T_e = \left(\frac{H_e}{\sigma}\right)^{1/4} = T_d + C \quad (4)$$

The empirical correction C is obtained by correlating calibration data with sensor-shield temperature differences.

Error Analysis

Expressions for determining the radiometer error as a function of thermocouple measuring accuracy and of k the slope of the correction curve are presented. The error in measuring an irradiance H_e is

$$\text{Percent error } H_e = \frac{\Delta H_e}{H_e} \times 100 \tag{5}$$

The approximate error ΔH_e for transient irradiances may be obtained from equation (2) by substituting $k(T_d - T_b) + C'$ for C and taking increments. By substituting this result into equation (5), the error is obtained as

$$\text{Percent error } H_e = \frac{4\sigma(T_d + C)^3\left[\Delta T_d + k(\Delta T_d + \Delta T_b) + \Delta C + \Delta C'\right] + M\Delta\left(\frac{dT}{dt}\right)_d}{H_e} \times 100 \tag{6}$$

where ΔC and $\Delta C'$ are the errors in C attributable to calibrations and ΔT is the practical uncertainty of the radiometer temperature detectors. Noting that $H_e = \sigma T_e^4$ and substituting this equality into equation (6) yields

$$\text{Percent error } H_e = \frac{4(T_d + C)^3\left[\Delta T_d + k(\Delta T_d + \Delta T_b) + \Delta C + \Delta C'\right] + \frac{M}{\sigma}\Delta\left(\frac{dT}{dt}\right)_d}{T_e^4} \times 100 \tag{7}$$

For steady-state irradiances the thermal-mass term is dropped and $T_d + C$ becomes equal to T_e (eq. (4)). The error is

$$\text{Percent error } H_e = \frac{4\left[\Delta T_d + k(\Delta T_d + \Delta T_b) + \Delta C + \Delta C'\right]}{T_e} \times 100 \tag{8}$$

The percent error, expressed in equivalent black-body temperature, may be found by noting that the numerator in equation (8) is $4\Delta T_e$. Then

$$\text{Percent error } T_e = \frac{\text{Percent error } H_e}{4} \tag{9}$$

Sensor Temperature Response

For an isolated sensor that exceeds the source temperature by a small amount $T_d - T_e$, the time required to cool from $T_{d,1}$ to $T_{d,2}$ can be determined by

linearizing equation (2). By substituting σT_e^4 for H_e and considering the correction C small, equation (2) may be written as

$$0 = -\sigma\left(T_e^4 - T_d^4\right) + M_d\left(\frac{dT}{dt}\right)_d \tag{10}$$

For small temperature differences, $T_e^4 - T_d^4$ is approximately equal to $4T_e^3\left(T_e - T_d\right)$. Substituting this relation into equation (10) and solving for dt_d yields

$$dt_d = -\frac{M_d}{4\sigma}\frac{dT_d}{T_e^3\left(T_d - T_e\right)} \tag{11}$$

By integrating equation (11) the time required for the sensor to cool from $T_{d,1}$ to $T_{d,2}$ is obtained.

$$t = \frac{M_d}{4\sigma T_e^3}\log_e\frac{T_{d,1} - T_e}{T_{d,2} - T_e} \tag{12}$$

For an equivalent black-body temperature of 400° K, a radiometer sensor representative of the present design $\left(M_d = 350\ J/m^2\text{-}K^\circ\right)$ would require about 55 seconds to cool from 410° K to 401° K. For $T_e = 300^\circ$ K, the time to cool the same amount would be $\left(\frac{400}{300}\right)^3 \times 55$ or 130 seconds. The time required for the temperature to decay 1/e of a small increment $T_d - T_e$ is $\frac{M_d}{4\sigma T_e^3}$. For $T_e = 400^\circ$ K, this decay would take about 24 seconds and for $T_e = 300^\circ$ K, about 57 seconds. Although these response rates are slow, many radiation sources encountered in spacecraft testing also change temperature slowly. Criteria for determining whether the sensor response rate is sufficiently rapid to ignore the thermal-mass term in equation (2) are presented in the appendix. In order that the correction C not be influenced by mass effects, the temperature response for the sensor and shield should be made equal.

DESIGN AND CONSTRUCTION

In this section the method used to construct the prototype radiometers for operation in an environment ranging from 80° K to 450° K is described. Figure 1 shows the radiometer components which include a plastic chassis and thermocouple-instrumented sensor and shield. The assembled radiometers were 0.5 cm in height and 2.3 cm in diameter with mounting lugs included. The results of tests and calibrations indicated several construction refinements that could be incorporated in future models. These refinements are discussed in a later section.

Sensor

The sensor was made from a 0.0076-cm-thick (3-mil) silver disk which was 1.27 cm in diameter. The side of the sensor facing the shield was gold-plated to minimize radiant heat transfer between these two components. The disk was embossed to increase its rigidity. A thermocouple fabricated from No. 40 chromel-alumel wire was welded to an indentation in the center of the disk. Electron-beam welding was chosen to insure a good electrical connection at the thermocouple junction and good thermal contact. To increase response with respect to the relevant heat sources, the top surface of the sensor was painted with 3M 401-C 10 flat black epoxy paint. Reflectance measurements indicate that in the spectral region between 1 and 25 μm, this coating had an emittance of 0.95. The solar absorptance-emittance ratio was about 1.02. To minimize error by conduction loss, the thermocouple leads were routed across and close to the top surface where they would be warmed by the source radiation and would be essentially the same temperature as the sensor.

Shield

The shield was made from a 0.0051-cm-thick (2-mil) stainless-steel disk which was 1.9 cm in diameter. The optical coatings and method of thermocouple attachment were the same as those for the sensor. This disk was mounted on the chassis 0.24 cm beneath the sensor.

The shield, which is larger than the sensor, serves several important functions. Primarily, it blocks most of the radiant heat transfer between the sensor and the mounting surface. It also receives part of the irradiance to be measured and seeks to attain temperature equilibrium with the source. As a result, error-producing thermal gradients between the sensor and shield are small. Perhaps the most important function of the shield is to provide temperature information indicative of the magnitude of unwanted heat transfer between the sensor and mounting surface. An empirical correction C (eq. (3)) is determined by correlating radiometer calibration data with the temperature differences between the sensor and shield.

For the measurement of time-varying irradiance, both the sensor and the shield should be designed to cool or heat at the same rate. Because the sensor shadows part of the shield from the source radiation, the shield constant M_b must be less than M_d for the sensor. Thus, for equal cooling rates

$$M_b = M_d\left(1 - F_{b,d}\right)$$

The prototype radiometers were not intended to measure rapid transient irradiances, and M_b was about twice $M_d\left(1 - F_{b,d}\right)$.

Chassis

The chassis (see fig. 1) was injection molded from a polytetrafluorethylene plastic. This material was chosen because of its low thermal conductivity, good dimensional stability, and low outgassing between 100° K and 500° K. The chassis was designed to provide a long thermal path between the sensor attachment point and the mounting feet. The parts of the chassis facing the mounting surface were vapor deposited with gold to minimize radiant heat transfer between the chassis and the mounting surface. The remaining parts were left uncoated to promote rapid cooling or heating. The low-temperature emittance of the uncoated parts was about 0.8.

The sensor and shield were attached to the chassis by mushrooming the ends of the locating pins with a warm soldering iron. The No. 40 chromel-alumel thermocouple wires leading from the sensor and shield were attached to No. 36 chromel-alumel extension wires. These, in turn, were secured to the radiometer by lead-wire supports molded onto the chassis.

APPARATUS AND PROCEDURES

The radiometers were calibrated to determine the radiometer correction C. They were also tested to determine their accuracy in measuring time-varying irradiances and angular sensitivity with respect to a collimated heat source. These calibrations and tests were conducted at a pressure less than 1.3×10^{-3} N/m^2 in the 5-foot-diameter, 5-foot-long vacuum system at the Langley Research Center. Strip-chart recorders were used for all temperature measurements.

Calibration Apparatus

The calibration apparatus as installed in the vacuum chamber is shown in figure 2. A heated plate of known radiant power was used as the calibration source. A temperature-controlled mounting surface was used as a second heat source to simulate unwanted heat transfer between the radiometer and its supporting surface. This second heat source was used in a different way for each of the two sets of calibrations. First, the radiometer was mounted directly on the heat source to simulate conductive heat transfer between the radiometer and a mounting surface. Second, the radiometer was suspended slightly above this heat source to simulate radiant heat transfer. In order to minimize the effect of heat-source radiation reflected from the chamber walls to the radiometer, the entire wall area surrounding the test apparatus was cooled with liquid nitrogen.

The calibration source was made from a 0.63-cm-thick copper disk, 25.4 cm in diameter. Its temperature was controlled by passing heated or cooled nitrogen vapors through a copper coil attached to the rear surface of the disk. In an attempt to increase

the effective emittance, the side of the source facing the radiometer was machined to produce a surface covered with miniature pyramids. To determine the uniformity of temperature distribution, the peak of one pyramid and the base of each of five pyramids located in a radial pattern were instrumented with thermocouples made of No. 40 chromel-alumel wire. This surface was then coated with 3M 401-C 10 flat black epoxy paint.

The reflectance of the calibration surface was measured by using two samples, which were prepared at the same time. The results of these measurements indicated an emittance of 0.96 for one sample whereas an emittance of 0.935 was indicated for the other sample. An examination of the samples indicated that these differences were probably due to a nonuniform application of the paint. Flat samples, also coated with the 3M paint, indicated an emittance of 0.95. For the present tests, the average emittance of the calibration source was assumed to be 0.95.

The temperature-controlled mounting surface was built to simulate conditions which might be experienced by a radiometer mounted on a variable-temperature surface. This surface consisted of a 2.54-cm-diameter copper disk attached to a soldering iron. Energy transfer to the radiometer was controlled by operating the mounting surface at various temperature levels. The two mounting positions of the radiometer with respect to the mounting surface are shown in figure 3. For the suspended-mounting tests, the mounting surface was painted black to make the background heat transfer radiative. For the surface-mounting tests, the paint was removed and the exposed copper substrate caused the heat transfer to be predominantly conductive. In both cases a clearance of 1 cm was maintained between the sensor and calibration source.

Method of Calibration

A series of calibration-source and radiometer-shield temperatures were recorded with the sensor temperature T_d held constant at 250° K, 300° K, 350° K, and 400° K. These constant temperatures were maintained by manipulating the heat controls for the calibration source and mounting surface to elevate successively the background radiation while lowering the calibration-source temperature. The temperature difference between T_e and T_d is equal to the correction C in equation (2) and $T_e = T_a\left(\epsilon_a \times F_{a,d}\right)^{1/4}$. The view factor for these calibrations was 0.998 ± 0.001. This correction C was plotted against the temperature difference between the sensor and shield to form curves of constant sensor temperature. (See fig. 4.) For a given sensor temperature and known temperature difference between the sensor and shield, the correction C is obtained as indicated by the dashed lines. When this correction is added to the sensor temperature, the equivalent black-body temperature T_e of the irradiance at the radiometer sensor, as indicated by equation (3), is obtained. Although these data were recorded while the

calibration source was cooling by radiation to the liquid-nitrogen-cooled walls, the radiometer constant M_d was much less than $(c\gamma\tau)_a$ of the calibration source; therefore, the thermal-mass term in equation (2) is negligible, and the cooling effect can be neglected. (See appendix.) The accuracy of the corrections ΔC is $\Delta\left[\left(\epsilon_a F_{a,d}\right)^{1/4} T_a\right] + \Delta T_d$. For the present calibrations ΔC was primarily dependent on temperature-measurement accuracy which was about $\pm 2^\circ$ K. The error in ΔC was therefore about $\pm 4^\circ$ K.

Time-Varying-Irradiance Test

The object of the time-varying-irradiance test was to compare and evaluate the two methods of data reduction (eqs. (2) and (3)). The apparatus and method of supporting the radiometer are shown in figure 2. The radiometer and calibration source were first cooled to about 190° K. Then heated nitrogen gas was used to raise the temperature of the calibration source rapidly to about 400° K. Heat was not applied to the mounting surface for these tests.

Angular-Sensitivity Test

A radiometer, mounted on the center of a 30-cm-square plate, was placed inside a vacuum chamber with an effective black-body wall temperature of 180° K. Simulated solar energy produced by a carbon arc was allowed to pass through a chamber window and strike the radiometer as it was progressively rotated from 0° to 90°. For comparative purposes, two mounting surfaces with different optical properties were used. All measurements were recorded as a function of angular displacement from the simulator axis. For these tests a second radiometer, similar to the one being tested, was mounted normal to the radiation source and used to monitor the constancy of the solar-simulator radiation.

DISCUSSION OF RESULTS

Calibrations

Figure 5 shows calibration results for both suspended- and surface-mounted radiometers for a constant sensor temperature of 300° K. Within the accuracy of the present calibrations, these results indicate that some basic design objectives were met; that is, a good constancy of calibration existed between individual radiometers, and the mounting method produced a negligible effect on the calibrations. For these tests the mounting-surface temperatures ranged from 260° K to 640° K. Figure 6 shows that the radiometer response is relatively insensitive to simulated mounting-surface temperatures over a wide temperature range. For example, for a mounting-surface temperature 160° K greater than that of the sensor, the correction was only -4° K.

At a sensor temperature of 300° K, the average calibration curve passed about 1.5° K above the intersection of the coordinate axes. (See fig. 5.) This trend was more predominant at the higher sensor temperatures (2° K at 350° K, and 2.5° K at 400° K). Ideally, when the sensor and shield temperatures are equal, no correction should be needed because there would be no net heat transfer between the elements. In actuality, the sensor-shield view factor was less than one, about 0.9, and some heat transfer did occur between the sensor bottom and the liquid-nitrogen-cooled walls. Also, the calculated T_e may have been too large because the exact emittance of the calibration source was unknown.

Because these conditions did not fully account for the measured displacements, several of the test radiometers were dismantled. A microscopic examination of the gold-plated surfaces revealed that in numerous places the embossing dies had exposed the silver substrate, and it was now tarnished. Reflectance measurements indicated emittances between 0.2 and 0.3, an order of magnitude greater than expected. Thus, radiant heat transfer from the underside of the sensor to the nitrogen-cooled walls $\left(0.1\epsilon_{dB}\sigma T_d^4\right)$ was about ten times greater than anticipated.

Calibration curves calculated from the measured emittance and with only radiant heat transfer considered are compared with the measured curve for a sensor temperature of 300° K in figure 7. The calculated curves indicate that a vertical displacement would increase as the emittance of the underside of the sensor increased. To minimize this displacement, one of the test radiometers was modified by bonding a 0.0076-cm-thick (0.3-mil) gold disk to the underside of the sensor $\left(\epsilon_{dB} \approx 0.03\right)$. In figure 8 the calculated and measured calibration curves are compared for this modified radiometer for a constant sensor temperature of 300° K. This figure indicates that both the displacement and the magnitude of the correction C were reduced.

Differences between the measured and calculated curves are indicative of the part of the correction that is due to conduction and approximations in analysis. Calibration curves for this radiometer at other temperatures are compared in figure 9. The upward displacement of these curves from the intersection of the coordinate axes is still present at the higher temperatures. These displacement errors, although small, can be reduced by increasing the sensor-shield view factor.

By using the slopes of the calibration curves presented in figure 9 and an assumed thermocouple uncertainty of ±2° K, the expected radiometer error was calculated from equations (8) and (9). The results are summarized in the table at the top of page 13. Calibration uncertainties contributed to more than half of the errors listed in this table. These errors could be significantly reduced by employing precision potentiometers during calibrations.

Incident irradiance, H_e, W/m^2	Equivalent black-body temperature, T_e, ^oK	Percent error in –	
		H_e	T_e
220	250	10.7	2.7
460	300	9.7	2.4
850	350	8.3	2.1
1450	400	7.0	1.7

Time-Varying Irradiance

The object of the time-varying-irradiance test was to show the applicability of equation (3). Figure 10 presents a comparison of the temperature response of the radiometer sensor and shield to a rapid rise in the equivalent black-body temperature of the calibration source. The maximum rate of source temperature change was 34^o K per minute and occurred at 3 minutes after the start of the test. This rate diminished to about 3^o K per minute after 14 minutes. Although these rates of change are arbitrary, they are believed to encompass most of the irradiances and rates of change of irradiances that would be encountered in spacecraft testing. One exception was that the radiometer would not respond rapidly enough to measure the transient radiance from a solar simulator that was suddenly turned on.

The sensor and shield constants M_d and M_b were not equal for the radiometer tested. The sensor constant M_d was calculated to be 350 J/m^2-^{o}K, and the shield constant M_b was 630 J/m^2-^{o}K. After 5 minutes, however, the rates of heating for these elements became essentially equal and the differences between the constants probably did not significantly affect the reduced data. Compare the slopes of the sensor and shield curves in figure 10.

Figure 11 shows the differences between equivalent calibration-source temperatures T_e and corrected radiometer readings. The radiometer readings were corrected in two ways: first, by merely adding the correction C to T_d (eq. (3)); and second, by adding C to T_d and including the thermal-mass term (eq. (2)). The fact that the corrected radiometer data do not eventually equal the equivalent black-body temperature of the source T_e (14 minutes and beyond) is attributed to experimental error and is within the accuracy of the device. Of greater importance is a comparison between the two methods of data reduction. At 11 minutes the error resulting from the use of equation (3) rather than the use of equation (2) is only about 1^o K (about 1.5-percent difference in energy). Here the rate of change of the equivalent temperature of the calibration source was about 4^o K per minute. When the source rate of change of temperature is greater than 4^o K per minute, the thermal-mass term should be included.

Angular Sensitivity

Figure 12 presents differences between corrected radiometer readings and the effective black-body temperature of the incident irradiance T_e for several angular positions with respect to a solar simulator. For these tests a second radiometer, similar to the one being tested, was mounted normal to the radiation source and used to monitor the constancy of the solar-simulator radiation. The effective black-body temperature of the source is expressed as

$$T_{e,source} = \left\{\left[\left(T_d + C\right)_{monitor}^4 - T_{e,w}^4\right]\cos\theta + T_{e,w}^4\right\}^{1/4}$$

where $T_{e,w}$ was the effective black-body temperature of the vacuum-chamber walls.

These tests were made with the test radiometer mounted on both black and aluminum surfaces. Neither the temperatures of nor the reflections coming from the mounting surfaces had an appreciable effect on these results. (See fig. 12.) At angles approaching 90^o, the radiometer indicated appreciably greater irradiance than the source. This difference was believed to be due to heating of the sensor support posts by the simulator. A small cylindrical guard ring was then placed around the radiometer to prevent direct simulator radiation from striking these posts. The outside of the ring was painted black. To minimize the radiant heat transfer from the guard ring to the sensor, the inside of the ring was made shiny ($\epsilon = 0.03$). Unfortunately, the guard ring was taller than necessary and the sensor was partially shielded from the simulator radiation. This shielding caused the radiometer to indicate a lower than actual irradiance, particularly between 50^o and 80^o. (See fig. 12.) Despite this occurrence, the guard ring improved the radiometer performance, particularly near 90^o.

Improved Radiometer Design

In considering the design and construction of prototype radiometers, two of the most difficult problems would be to construct a sensor with a rapid response and to minimize the effects of strong side radiation on the sensor support posts without increasing the physical dimensions. Turning up the edges of the shield to prevent side radiation from warming the sensor support posts and to increase the sensor-shield view factor was considered. This alteration, however, would have the effect of decreasing the shield temperature response since the mass would be increased and the effective radiating area decreased. Perhaps a better approach would be to space the sensor-shield elements closer together to minimize side radiation effects and to thus increase the view factor.

In the present radiometer the cooling rates of the sensor and shield were not equal, that is, M_b was about twice M_d. To equalize these rates and retain a desirable temperature response the thermal mass of the shield should be decreased. Because the

minimum practical thickness of the shield is believed to be between 0.0051 and 0.0076 cm (2 and 3 mils), the only recourse would be to decrease the thermal mass of the optical coatings on the shield. The black shield coating on the prototype radiometers was about 0.0051 cm thick (2 mils) and accounted for nearly one-half of the shield constant M_b. A newly developed space-stable coating with optical properties comparable to the 3M 401-C 10 flat black epoxy paint is described in reference 4. It is an anodized aluminum blackened by a nickel-sulfide dye which does not significantly increase the thermal mass of the base material. Several sample shields with this coating have been successfully fabricated from 0.0076-cm-thick (3-mil) aluminum. The bottoms of the shields were brush-plated with gold, and the thermocouples were soft-soldered to the gold plating. By using these techniques the sensor and shield could be designed to give equal temperature responses and perhaps improve the radiometer response rate.

RADIOMETER APPLICATIONS TO BALLOON STUDY

The uses and mounting of these radiometers as applied to thermal-vacuum tests of balloon thermal-control enclosures for spacecraft are shown in figure 13. Figure 13(a) shows the opaque balloon model and a radiometer located beside it to monitor the solar-simulator radiance. The purpose of this investigation was to measure the irradiance in areas where a payload would be located within the balloon. A heater was suspended within the balloon to simulate the heat dissipated by the payload. Figure 13(b) shows radiometers mounted along a support bar which was mounted across the balloon diameter. Figure 13(c), an enlargement of part of this bar, shows the radiometers attached to auxiliary mounting annuli which were spot-welded to the bar. Three wire prongs, spot-welded to the annuli, were used to hold the radiometer by its mounting lugs. These auxiliary mounts permit easy radiometer installation on a variety of surfaces. For example, a radiometer for measuring the average balloon α/ϵ ratio was mounted to the inside balloon wall (0.0019 cm (0.75 mil) thick) by this method.

Figure 14 presents representative irradiance measurements along the balloon diameter. Both corrected and uncorrected radiometer data are shown. The high irradiance near the sun-heated side of the balloon is due to the high balloon-wall temperatures in this area. The high irradiance measured at the 70-percent diameter is due to the focusing of heater energy by the balloon walls. The low reading at the 90-percent diameter is due to the opening in the balloon. In most of these data, the radiometer corrections were well within the accuracy of the radiometer, and, therefore, they were not applied.

CONCLUDING REMARKS

Governing parameters for designing a radiometer for use in spacecraft thermal studies are presented. Since this radiometer effects a minimal thermal disturbance on the test surface, a large number may be used to map the irradiance distribution of complex configurations. The feasibility of fabricating these radiometers from materials that are compatible with a space environment has been demonstrated. Representative calibration and performance data show that calibration corrections are relatively insensitive to the method of mounting and to the optical properties and temperature of the mounting surface. In a study of a thermal-control balloon model, application of corrections to the radiometer measurements was found to be unnecessary.

Langley Research Center,
National Aeronautics and Space Administration,
Langley Station, Hampton, Va., July 26, 1968,
124-09-18-06-23.

APPENDIX

RADIOMETER DESIGN CRITERIA FOR SIMPLIFIED DATA REDUCTION

Since radiating surfaces cool or warm cyclically at relatively slow rates in normal spacecraft or model testing, it is possible to design a radiometer that will remain essentially in temperature equilibrium with these surfaces. For such a radiometer, the thermal-mass term $M_d\left(\frac{dT}{dt}\right)_d$ in equation (2) would be negligible, and equation (3) could be used. To determine whether the simplified form is applicable, consideration must be given to the accuracy of the temperature detectors, the anticipated rate of change of the source radiation, and the sensor constant M_d. The following analysis provides a basis for determining when the thermal-mass term of equation (2) can be ignored.

The energy-balance equation for a cooling object is

$$\sum E = 0 = -\epsilon_a \sigma S_a T_a^4 - (c\gamma S\tau)_a \frac{dT_a}{dt}$$

or

$$\frac{dT_a}{dt} = -\left(\frac{\epsilon}{c\gamma\tau}\right)_a \sigma T_a^4 \tag{A1}$$

Similarly, the energy-balance equation for a gray sensor with a view factor of 1 located on a cooling object is

$$\sum E = 0 = \epsilon \sigma S T_e^4 - \epsilon \sigma S T_d^4 - c\gamma S\tau \frac{dT_d}{dt} \tag{A2}$$

The equivalent black-body irradiance from the source and incident to the sensor is σT_e^4; that is, $\sigma T_e^4 = \epsilon_a \sigma T_a^4$.

Multiplying both sides of equation (A2) by dT_a, dividing by ϵ and S, and solving for $\sigma T_d^4\, dT_a$ yields

$$\sigma T_d^4\, dT_a = \sigma T_e^4\, dT_a - \left(\frac{c\gamma\tau}{\epsilon}\right)_d \frac{dT_d\, dT_a}{dt} \tag{A3}$$

By substituting equation (A1) into equation (A3)

$$\sigma T_d^4\, dT_a = \sigma T_e^4\, dT_a + \left(\frac{c\gamma\tau}{\epsilon}\right)_d \left(\frac{\epsilon}{c\gamma\tau}\right)_a \sigma T_a^4\, dT_d$$

is obtained.

Note that the irradiance indicated by the radiometer is $\sigma T_d^4 = H_d$, and that the actual incident irradiance is $\sigma T_e^4 = \epsilon_a \sigma T_a^4 = H_e$. Solving for the indicated irradiance H yields

$$\left.\begin{aligned} H_d\, dT_a &= \left[H_e\, dT_a + H_e\left(\frac{c\gamma\tau}{\epsilon}\right)_d \left(\frac{1}{c\gamma\tau}\right)_a dT_d\right] \\ H_d &= H_e\left[1 + \left(\frac{c\gamma\tau}{\epsilon}\right)_d \left(\frac{1}{c\gamma\tau}\right)_a \frac{dT_d}{dT_a}\right] \\ H_d &= H_e\left[1 + \frac{M_d}{(c\gamma\tau)_a}\frac{dT_d}{dT_a}\right] \end{aligned}\right\} \quad \text{(A4)}$$

When the source is cooling, the rate of sensor cooling will approach that of the source and $\frac{dT_d}{dT_a}$ will approach 1. Thus, for small ratios of $\frac{M_d}{(c\gamma\tau)_a}$, the irradiance as indicated by the radiometer is approximately $H_d \approx H_e$. For many thermal model and spacecraft tests, H_d as indicated by the radiometer will be equal to H_e within the accuracy of the temperature-detecting devices. For accurate measurement by thermocouples, the radiometer constant M_d should be about one twenty-fifth of $(c\gamma\tau)_a$. When rapid transient irradiances, such as the irradiance from a rapid-rise electric heater, must be measured, equation (2) must be used.

REFERENCES

1. Stempel, F. C.; and Rall, D. L.: Direct Heat Transfer Measurements. ISA J., vol. 11, no. 4, Apr. 1964, pp. 68-73.

2. Gilcrest, A. S.; and Mon, G. R.: A Calorimeter for Determining Thermal Radiation Fluxes in Space Simulation Chambers. Annu. Tech. Meeting Proc., Inst. Environ. Sci., 1963, pp. 369-376.

3. Kendall, James M., Sr.; and Plamondon, Joseph A.: An Absolute Cavity Radiometer for the Measurement of Thermal Radiation. AIAA/IES/ASTM Space Simulation Conference, Sept. 1966, pp. 179-184.

4. Wade, William R.; and Progar, Donald J.: (With appendix by Donald H. Humes): Effects of a Simulated Space Environment on Thermal Radiation Characteristics of Selected Black Coatings. NASA TN D-4116, 1967.

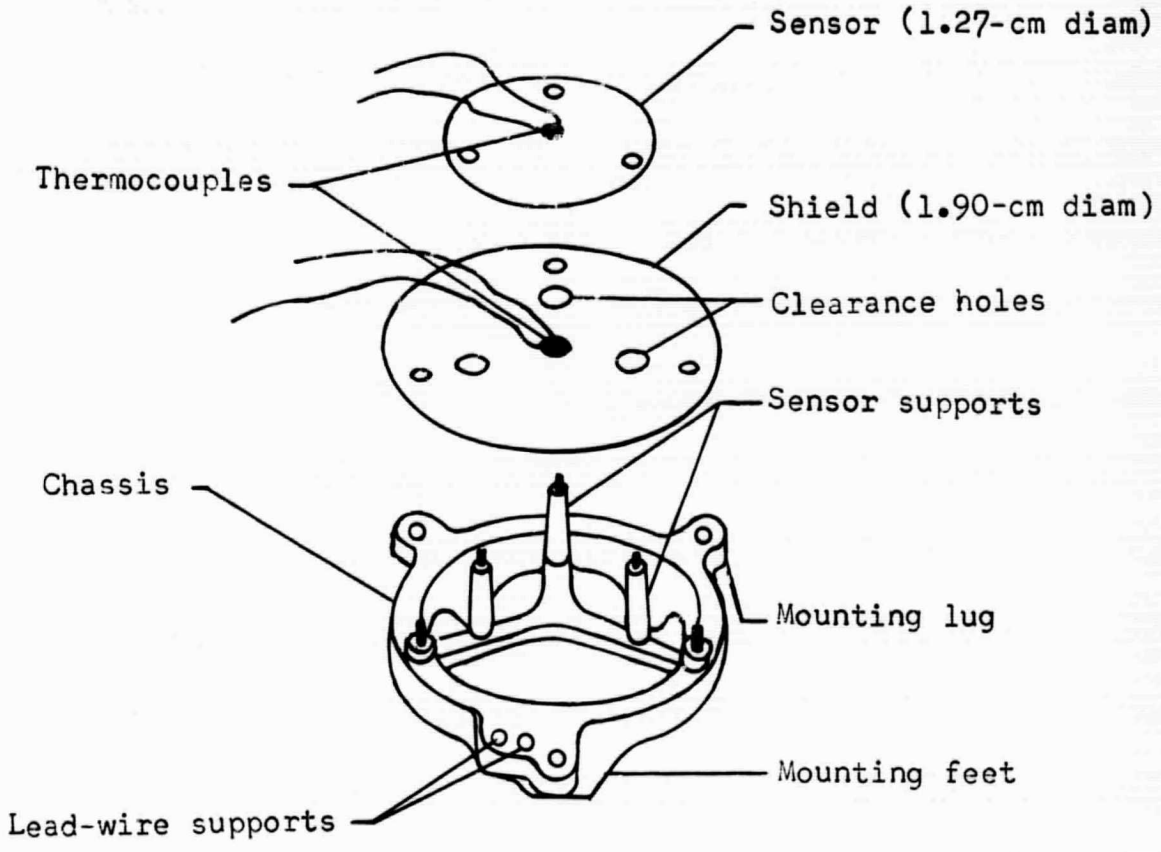

Figure 1.- Details of radiometer components.

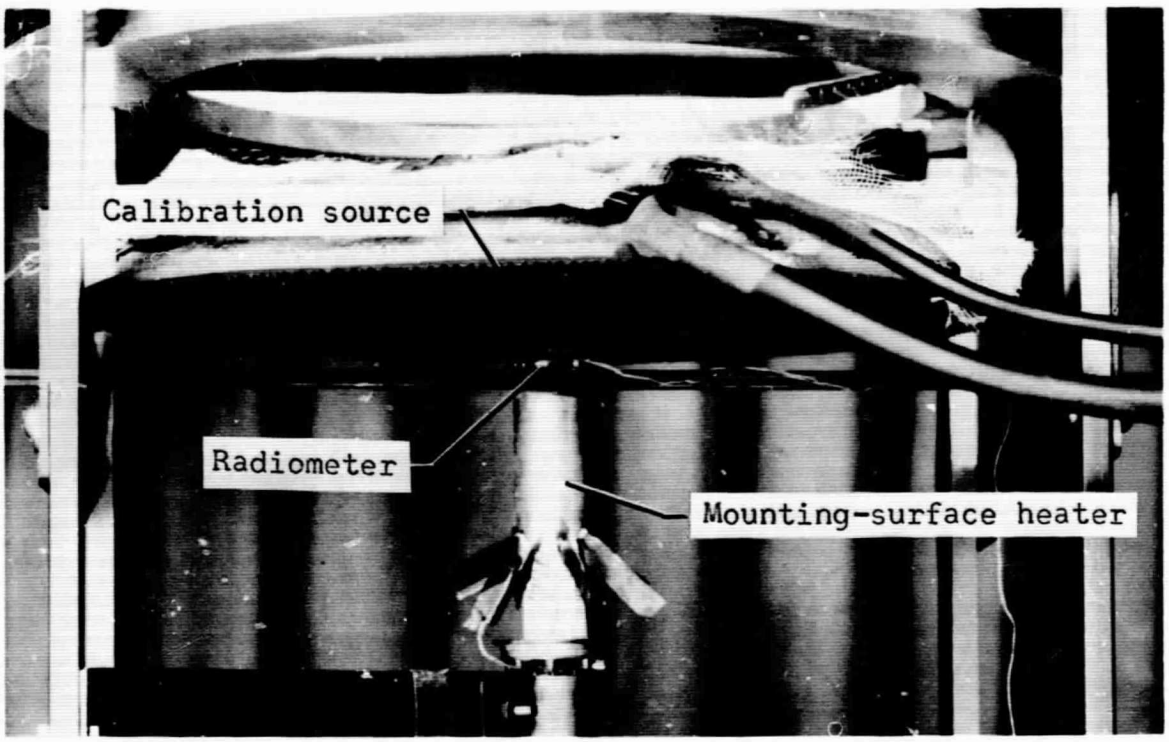

L-68-8536

Figure 2.- Calibration apparatus installed in 5-foot-diameter, 5-foot-long vacuum system at the Langley Research Center.

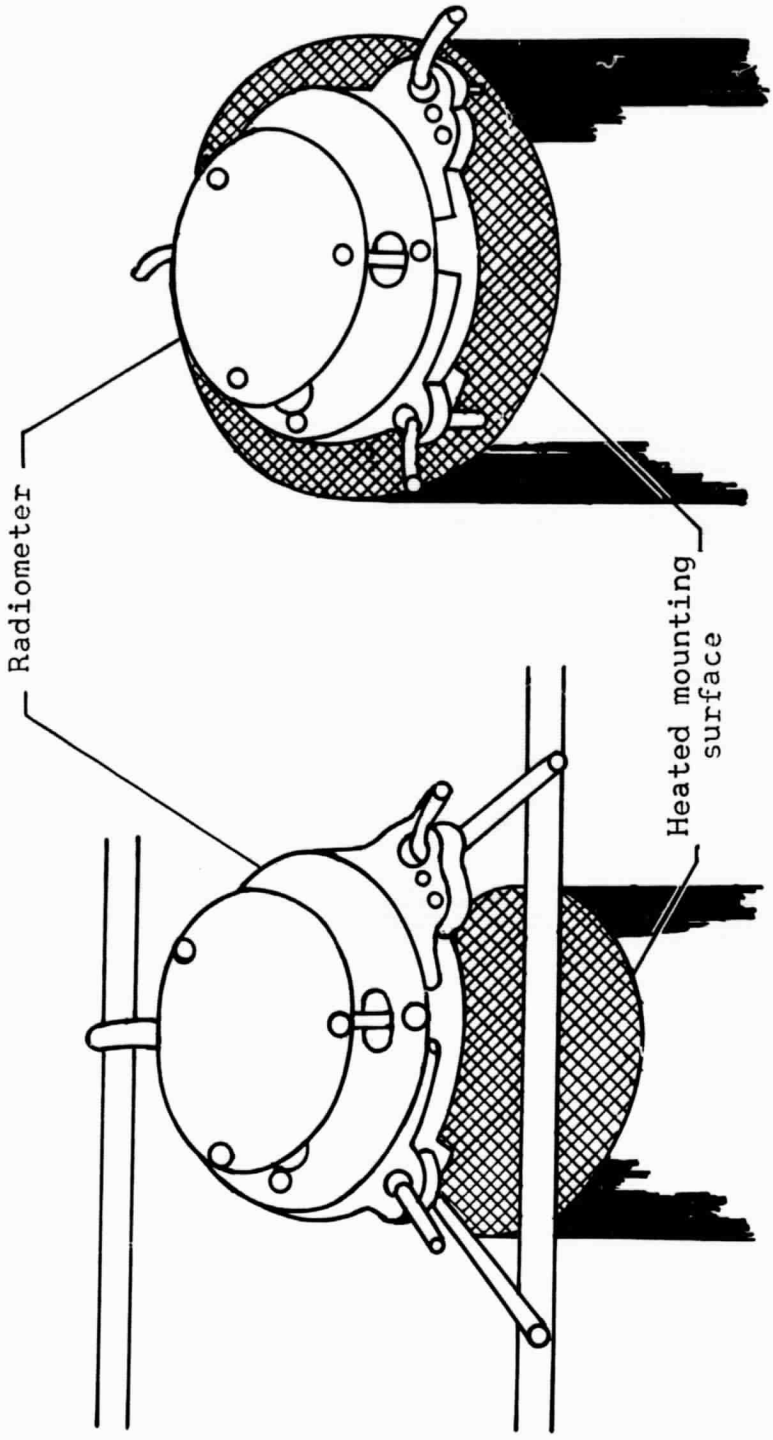

(a) Suspended mounting.

(b) Surface mounting.

Figure 3.- Radiometer mountings used for calibrations.

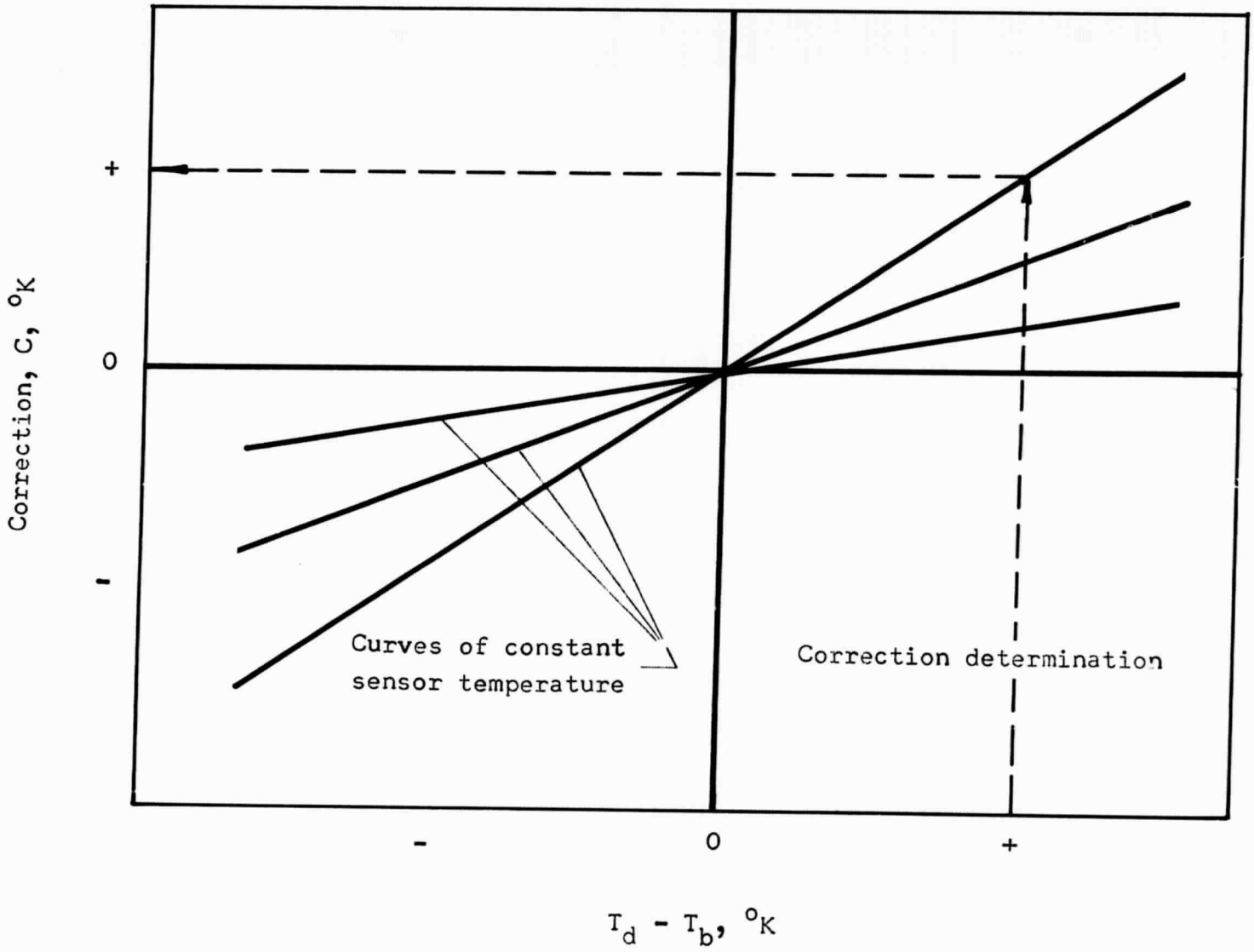

Figure 4.- Method of presenting calibration data.

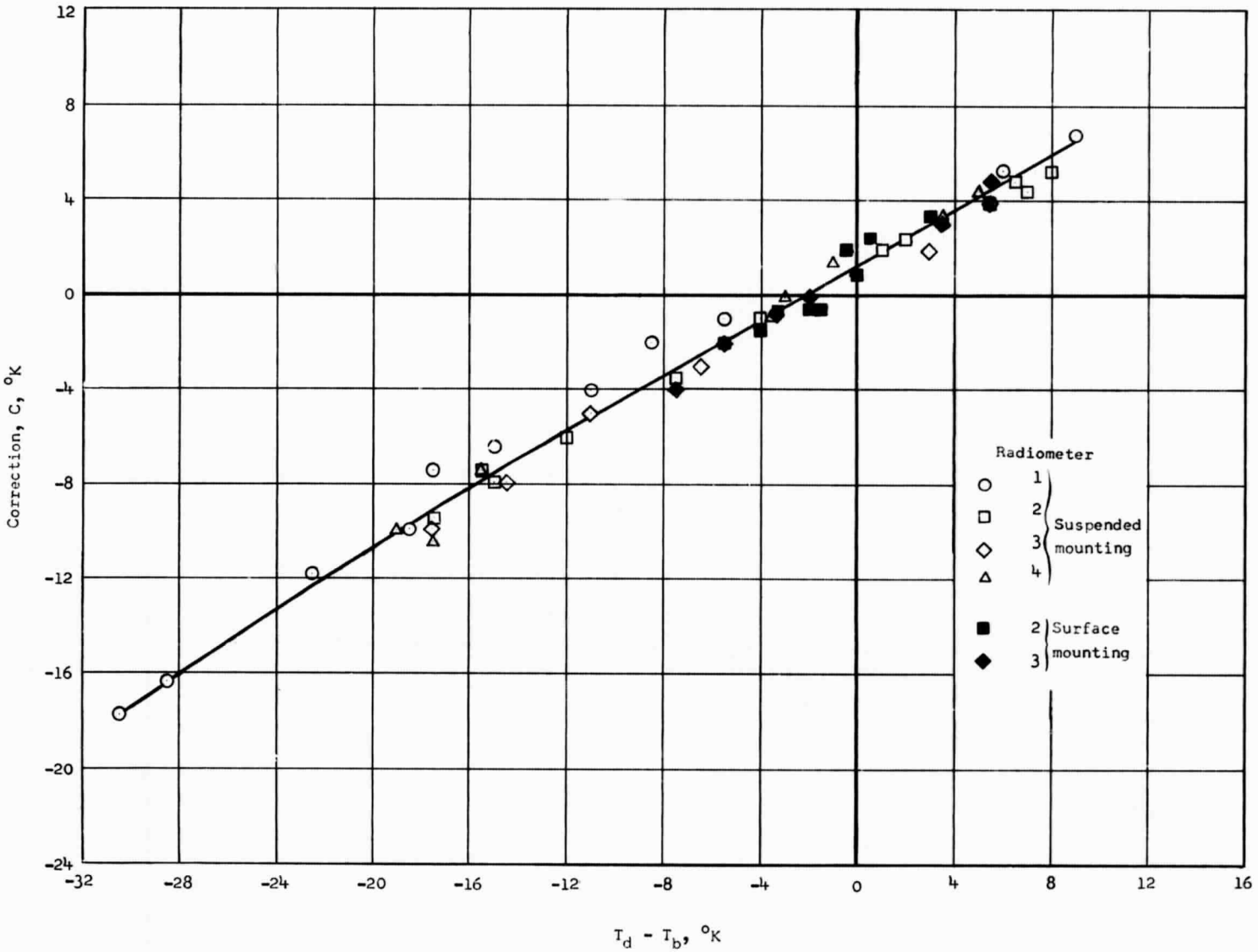

Figure 5.- Comparison of calibration results for suspended- and surface-mounted radiometers for a constant sensor temperature of 300° K.

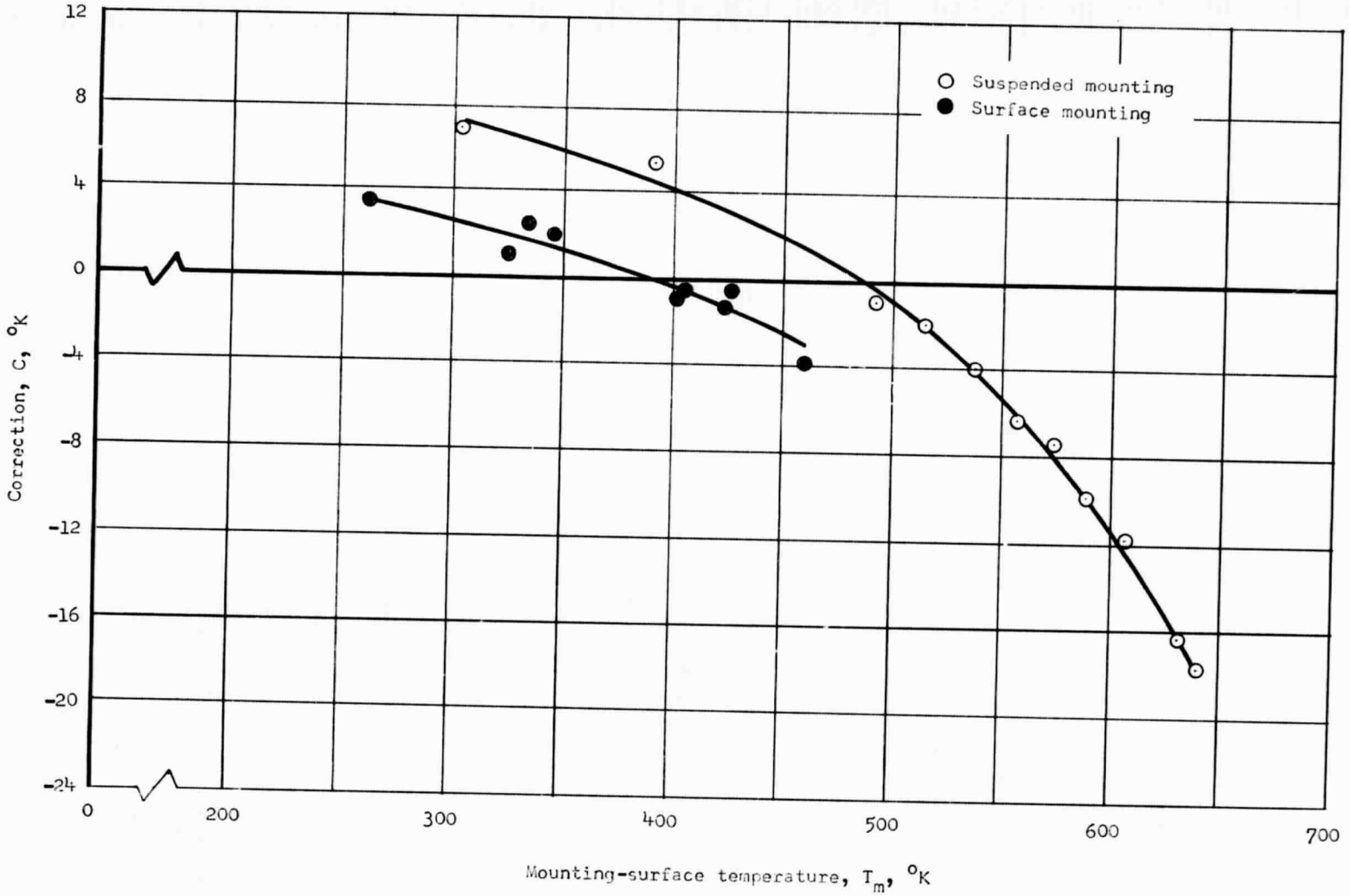

Figure 6.- Correlation of radiometer correction for test radiometer 1 with mounting-surface temperatures for a constant sensor temperature of 300° K.

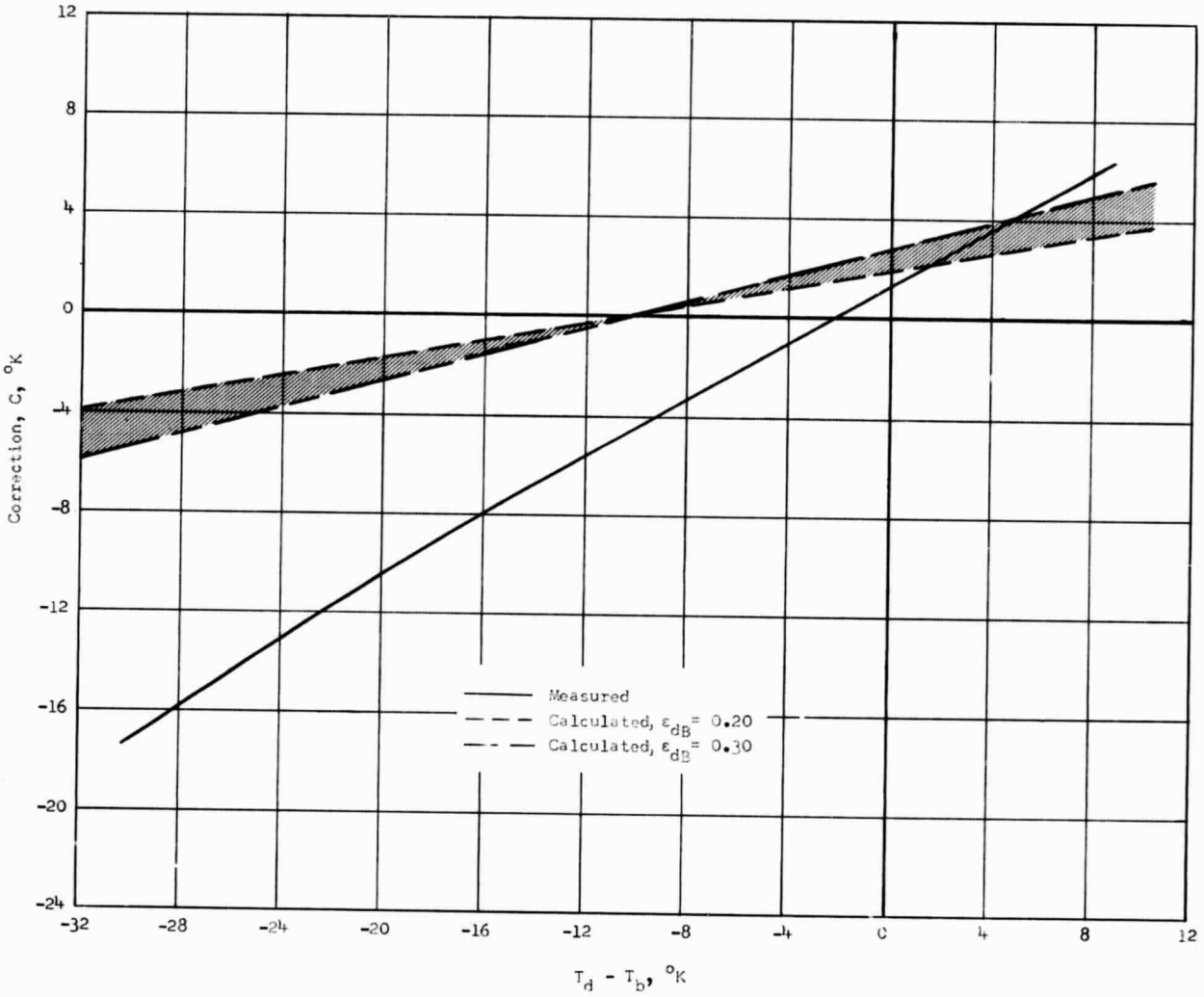

Figure 7.- Comparison of calculated calibration data, with only radiant heat transfer considered, with measured calibration data for a constant sensor temperature of 300° K.

$$C = \left[\left(1 + \frac{\epsilon_{dB}}{\epsilon_{dT}}\right) T_d^4 - \frac{\epsilon_{bT} S_b}{\epsilon_{dT} S_d} \epsilon_{dB} F_{b,d} T_b^4\right]^{1/4} - T_d.$$

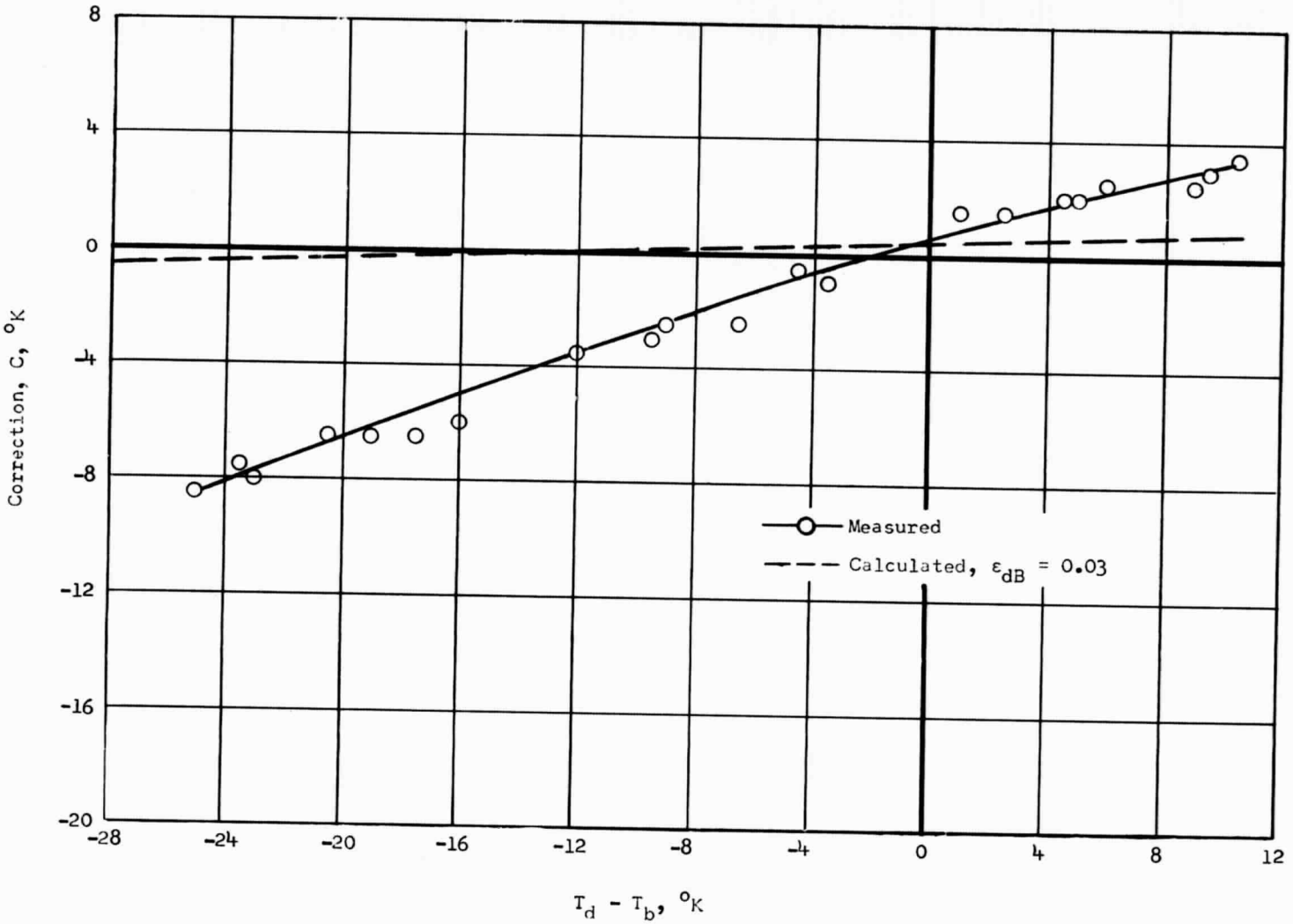

Figure 8.- Comparison of calculated calibration data, with only radiant heat transfer considered, with measured calibration data for a radiometer sensor with a low-emittance undersurface at constant sensor temperature of 300° K. $C = \left[\left(1 + \frac{\varepsilon_{dB}}{\varepsilon_{dT}}\right) T_d^4 - \frac{\varepsilon_{bT} S_b}{\varepsilon_{dT} S_d} \varepsilon_{dB} F_{B,d} T_b^4\right]^{1/4} - T_d$.

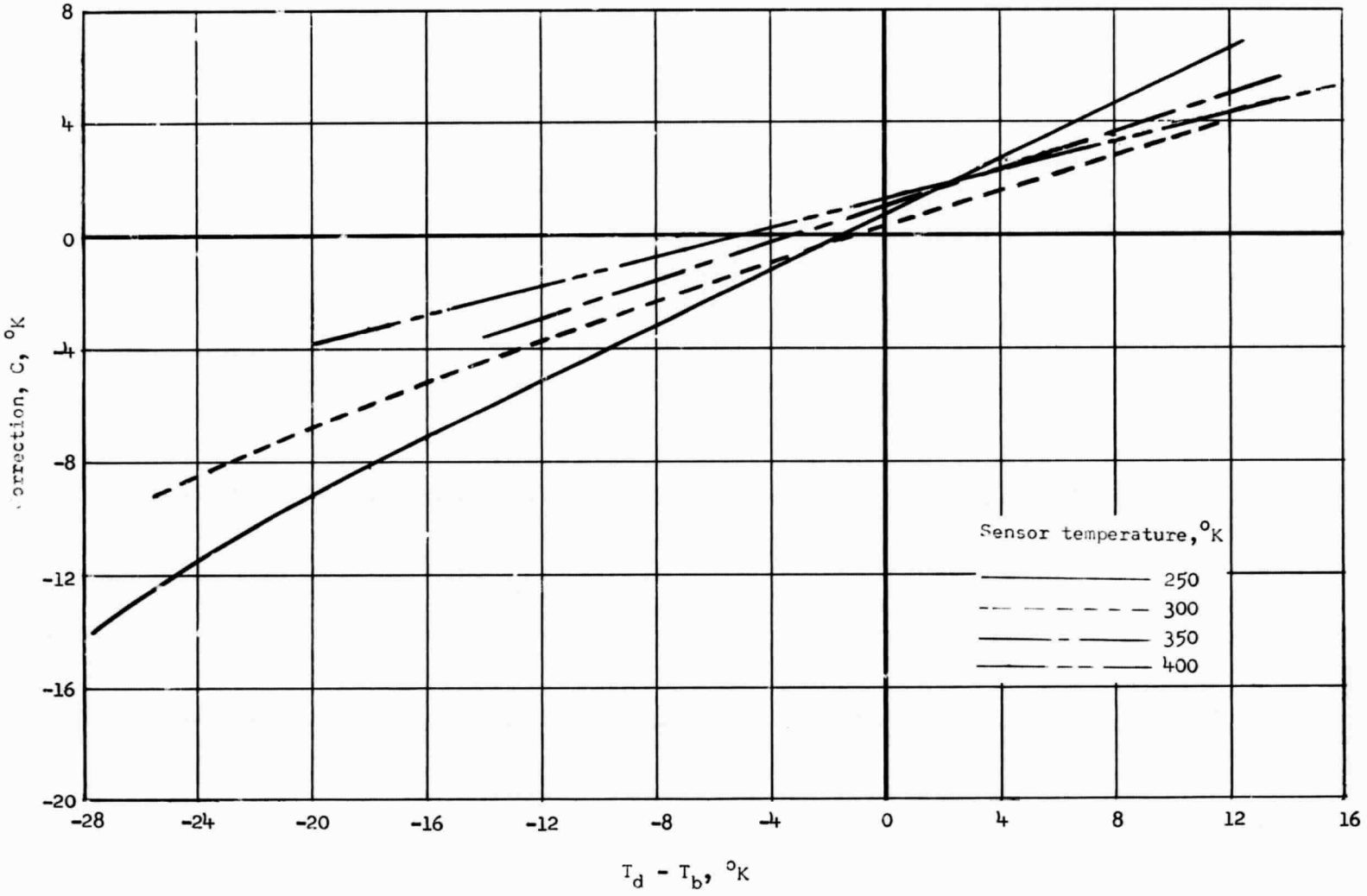

Figure 9.- Summary of measured calibration data.

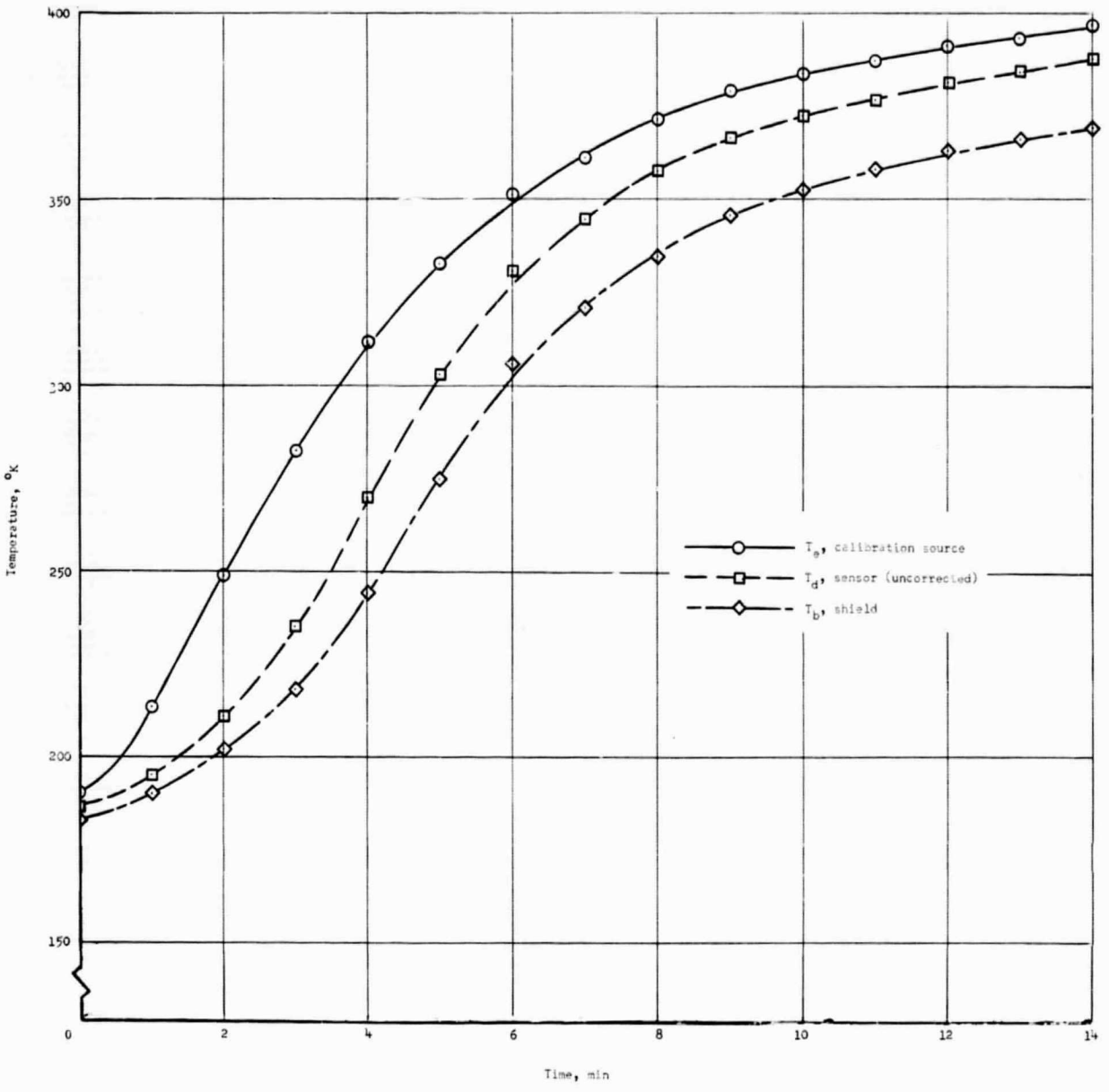

Figure 10.- Comparison of the temperature response of the radiometer sensor and shield to a rapid rise in the equivalent black-body temperature of the calibration source.

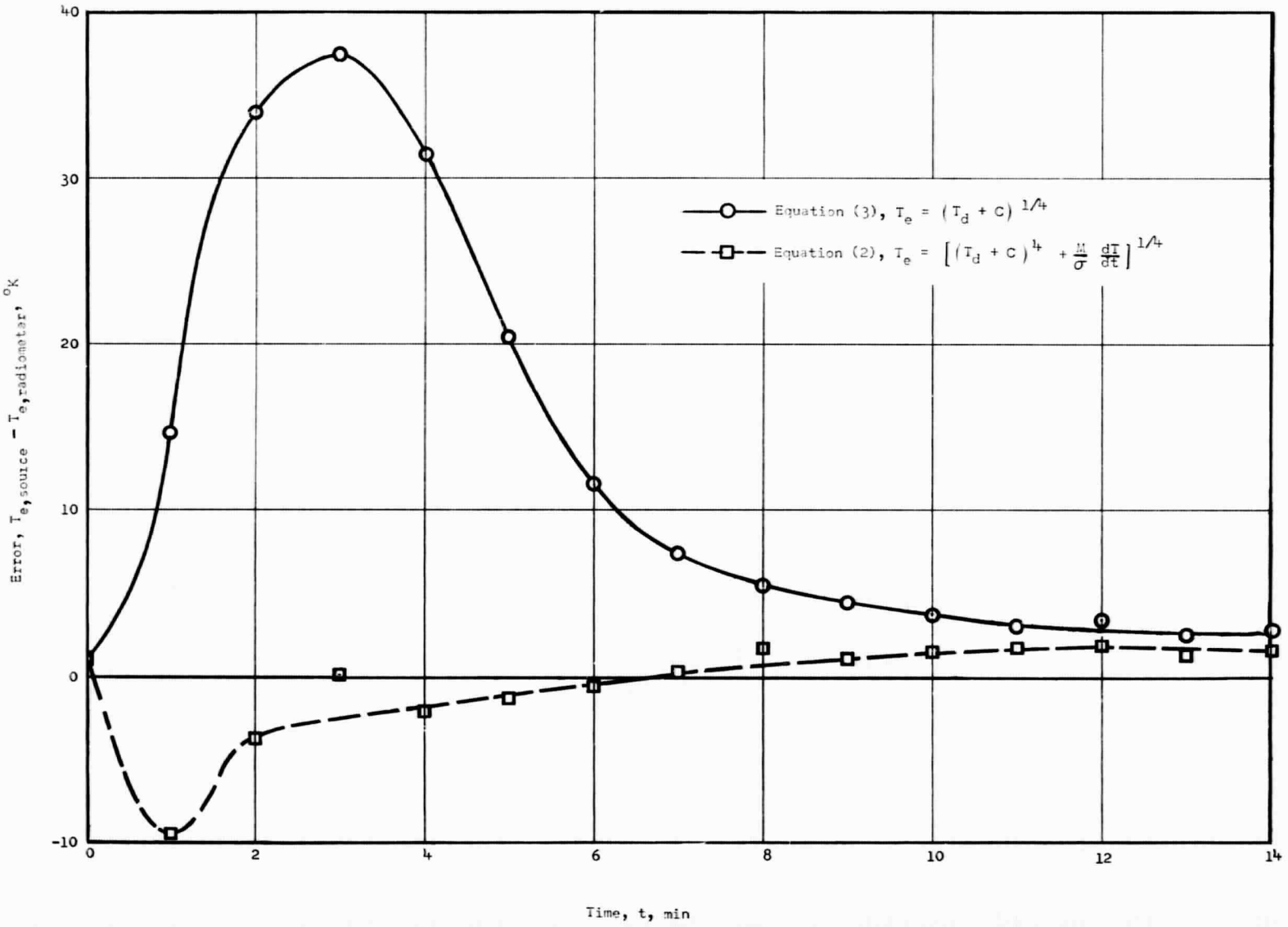

Figure 11.- Comparison of temperature differences between radiometer and calibration source for approximate (eq. (3)) and exact (eq. (2)) methods of data reduction.

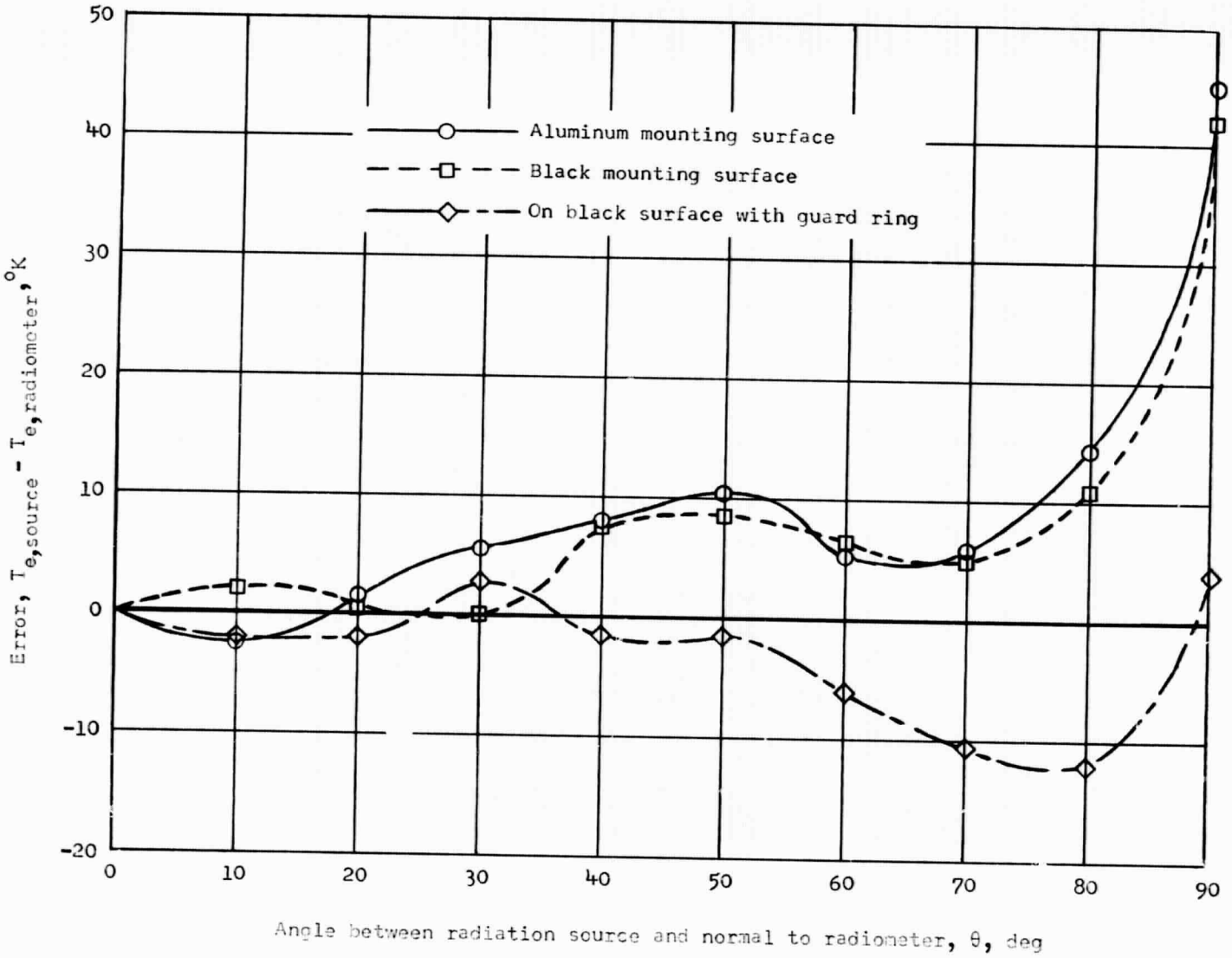

Figure 12.- Corrected radiometer readings compared with effective black-body temperature of incident irradiance for several angular positions with respect to a solar simulator and for variations in mounting surface.

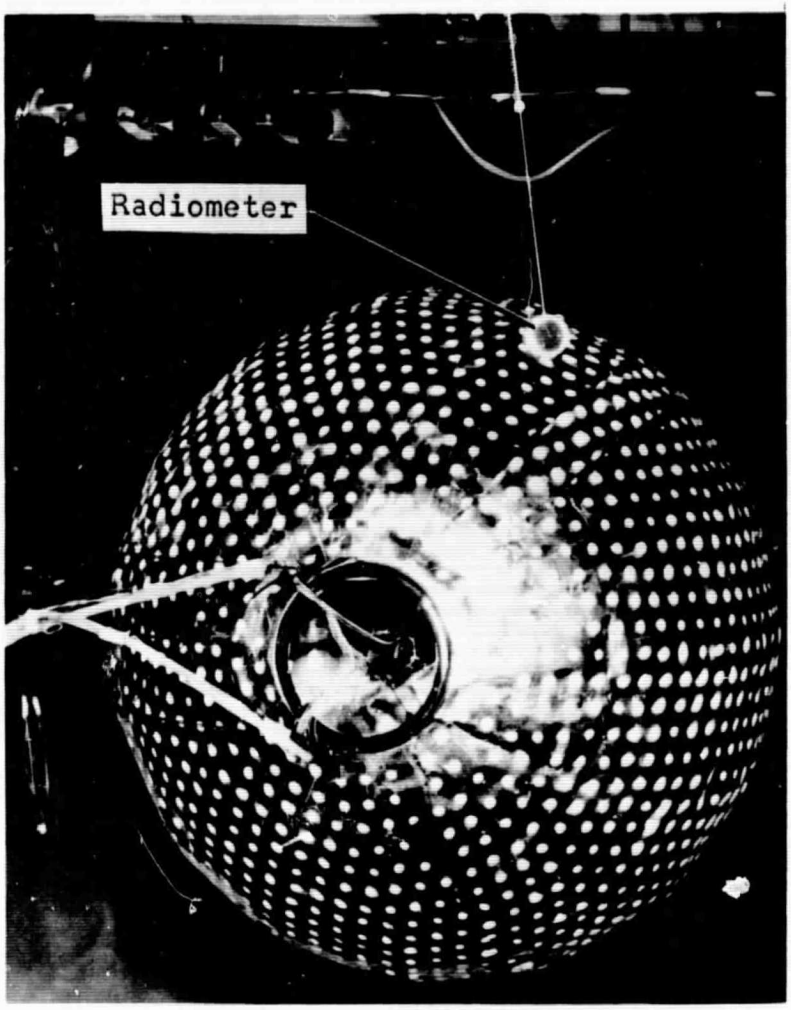

(a) Balloon model and radiometer for monitoring simulator radiance. L-68-5673

Figure 13.- Apparatus used in model balloon tests.

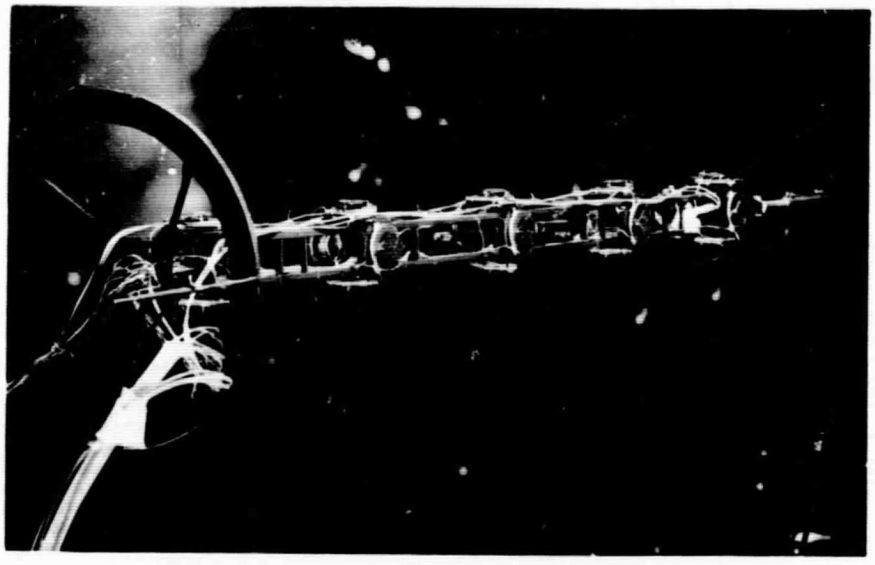

(b) Radiometer support bar.

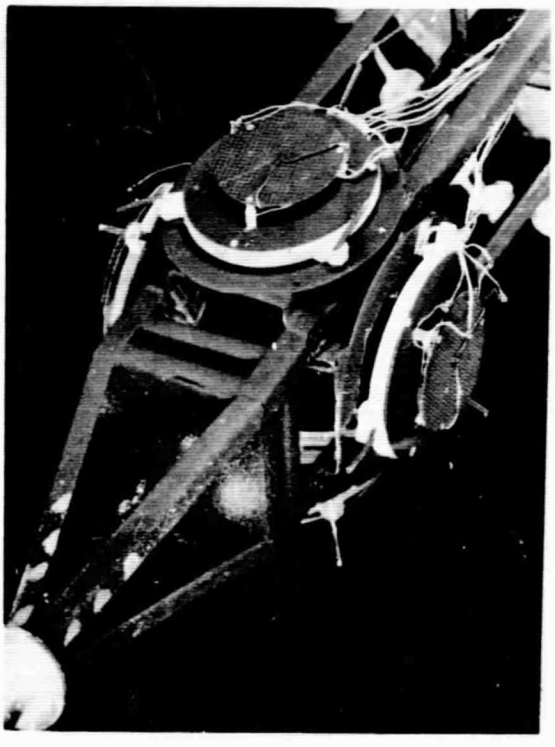

(c) Radiometer mounting detail. L-68-5674

Figure 13.- Concluded.

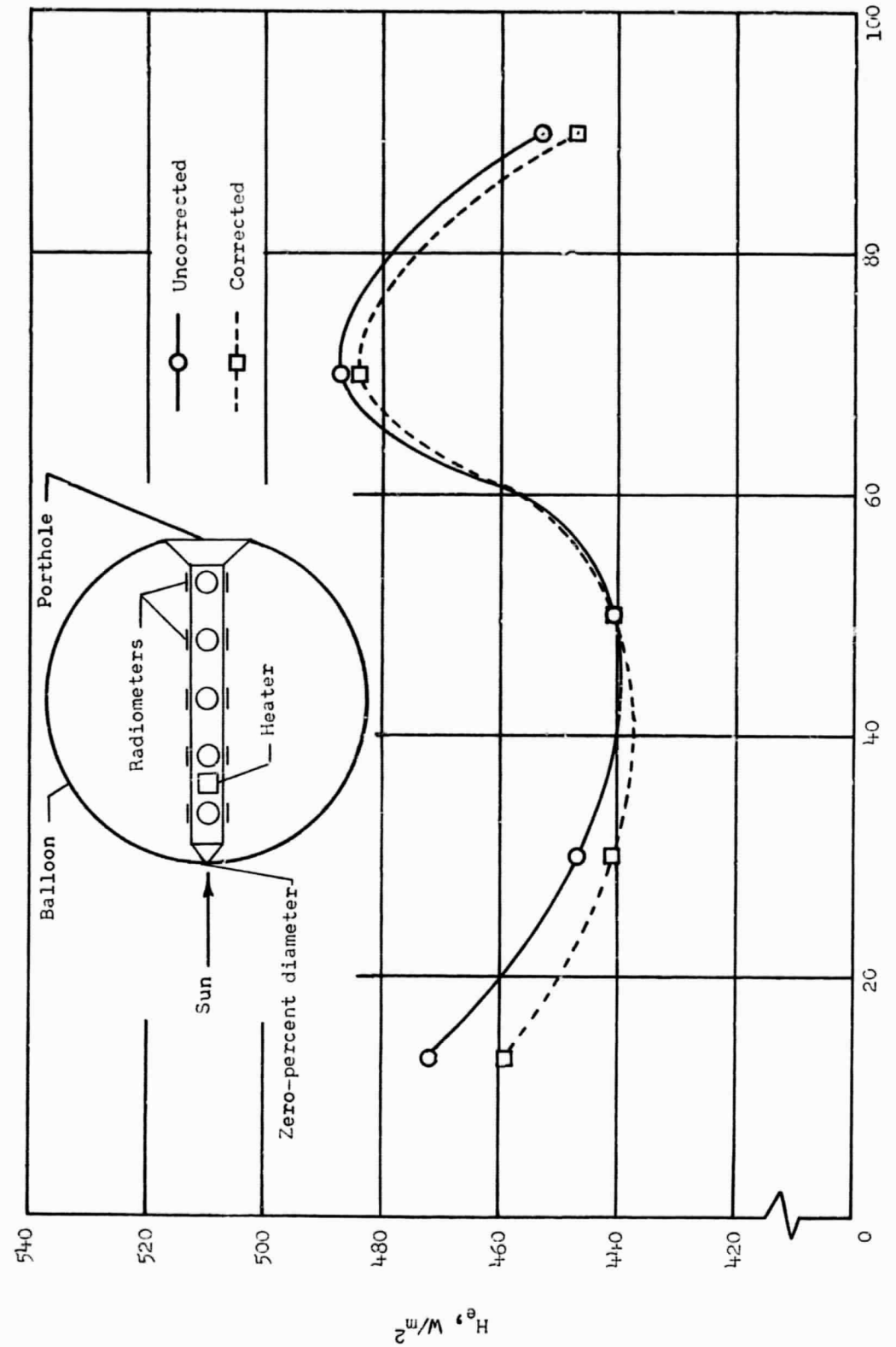

Figure 14.- Comparison of corrected and uncorrected irradiance measurements along balloon diameter.

NASA-Langley, 1968 — 14 L-5643